

UC Irvine

UC Irvine Electronic Theses and Dissertations

Title

Pthlha and mechanical force control spatial-temporal aspects of hypertrophic cartilage development in the zebrafish craniofacial skeleton

Permalink

<https://escholarship.org/uc/item/4rf3z4sj>

Author

Hoyle, Diego Jose

Publication Date

2019

Peer reviewed|Thesis/dissertation

UNIVERSITY OF CALIFORNIA
IRVINE

Pthlha and mechanical force control spatial-temporal aspects of hypertrophic cartilage development in the zebrafish craniofacial skeleton

DISSERTATION

submitted in partial satisfaction of the requirements
for the degree of

DOCTOR OF PHILOSOPHY

**in Biological Sciences,
with a concentration in Developmental and Cell Biology**

by

Diego Jose Hoyle

Dissertation Committee:

Dr. Thomas F. Schilling, Chair

Dr. Bogi Andersen

Dr. Ken Cho

Dr. Michael Parsons

Dr. Maksim Plikus

Dr. Marian Waterman

2019

DEDICATION

To
my mother, Carola,
for her unconditional love and protection,
and for making me the person that I am

TABLE OF CONTENTS

	Page
LIST OF FIGURES	iv
ACKNOWLEDGEMENTS	vi
CURICULUM VITAE	vii
ABSTRACT OF THE DISSERTATION	viii
CHAPTER I: Introduction	1
CHAPTER II: Patterning of the hypertrophic zone in embryonic zebrafish cartilages requires <i>pthlha</i>	
Introduction	28
Materials and Methods	32
Results	36
Discussion	49
CHAPTER III: Initiation of hypertrophic differentiation in embryonic zebrafish cartilages requires mechanical force	
Introduction	57
Materials and Methods	60
Results	62
Discussion	72
CHAPTER IV: Characterization of embryonic perichondrium	
Introduction	76
Materials and Methods	79
Results	85

	Page
	101
CHAPTER V:	109
Discussion	113
Correlations between chondrocyte polarity and ossification patterning	117
Introduction	128
Materials and Methods	135
Results	150
Discussion	150
CHAPTER V:	135
Conclusions	150
REFERENCES	150

LIST OF FIGURES

	Page
Figure 1.1: Morphogen Gradients versus Reaction Diffusion models	5
Figure 1.2: Cartilages form via convergent extension	12
Figure 1.3: Long bones ossify first in the middle then on their distal ends	16
Figure 1.4: GP function requires that chondrocytes transition through multiple layers	18
Figure 1.5: GP homeostasis is controlled by negative feedback mechanisms	21
Figure 1.6: Could interactions between Ihh and Pthlh in ossifying cartilages fit the RD Model?	23
Figure 2.1: Ceratohyal chondrocytes express hypertrophic zone markers soon after embryonic differentiation	37
Figure 2.2: <i>pthlha</i> is expressed at the distal ends of ch	41
Figure 2.3: <i>pthlha</i> restricts dorsal expansion of the ch primary HZ	43
Figure 2.4: Mosaic <i>pthlha</i> expression disrupts bone collar as a function of proximity and number of expressing cells	45
Figure 2.5: Mosaic <i>pthlha</i> expression disrupts HZ patterning	48
Figure 3.1: Paralysis between 68-96 hpf prevents HZ formation	63
Figure 3.2: HZ loss during paralysis is not due to developmental delay	67

	Page
Figure 3.3: Paralysis between 72-120 hpf leads to loss of chondrocyte proliferation	70
Figure 4.1: Neither <i>col14a1a</i> , <i>lgals2b</i> , <i>dkk3b</i> , or <i>thbs2</i> are expressed in the perichondrium	86
Figure 4.2: <i>gdf5</i> is expressed in the perichondrium	88
Figure 4.3: <i>crabp2b</i> is expressed in the perichondrium	90
Figure 4.4: <i>gdf5</i> upstream sequence yielded no expression	92
Figure 4.5: Identification of two genomic regions within the <i>crabp2b</i> locus that drive perichondrial expression	95
Figure 4.6: Two <i>crabp2b</i> regulatory regions drive expression in the perichondrium	97
Figure 4.7: Tendon attachment zones colocalize with <i>crabp2b</i> regulatory region-driven expression	100
Figure 5.1: Laser ablations locally disrupt cartilage intercalation and polarity	118
Figure 5.2: Laser ablations in the ventral section of the ch do not affect cell polarity in the dorsal ceratohyal	123
Figure 5.3: The effects of laser ablations in the ventral ch assayed by <i>in situ</i> hybridizations and live imaging are incongruent	125

Figure 5.4: The difference in length between ablated and non-ablated ch cartilages in live imaged embryos is negligible 127

Figure 6.1: Model for the integration of mechanical force and Pthlh signaling in GPs 139

Figure 6.2: Tentative model for the formation of tendon attachment zones in developing cartilages 142

ACKNOWLEDGEMENTS

This work would not have been possible without the support of several people. First, I would like to thank my thesis advisor Tom for welcoming me in his lab and providing a good environment for my scientific development. During my graduate years, Tom's advice was crucial in various projects I undertook in his lab and for my development as a scientist. I would also like to thank the members of my committee, Ken Cho, Max Plikus, Mike Parsons, Marian Waterman, and Bogi Andersen, for their support and for their scientific and career advice. I also thank former and current members of my lab, Pierre, Arul, Danny, Praveer, Lauren, David, Lianna, Pavan, Irene, Aranud, Courtney, Adam, Julian, and Ines for all their help and support. Especially, I would like to thank Pierre since he was my mentor in the lab, and many of the techniques used in this work, I learned from him. I would also like to thank my friends for their support and for all the times they made me laugh. Among them, I would like to thank Raul for all the drinks we had, Soledad for reminding me to have fun, Jin and Vaishali for all those delicious breakfasts we had, and Lily for her company on some of the days I stayed at the microscope overnight. Finally, I would like to thank my parents and sisters, Carola, Elio, Erika, and Brenda for always listening to the science I was doing. Especially, I would like to thank my mother Carola for creating the opportunity for me to come to study in the US. Her courage and resilience gave me strength to keep going through all the difficulties and obstacles I have faced up to this point and taught me to never give up on who I am and my goals in life.

CURRICULUM VITAE

Diego Jose Hoyle

EDUCATION

- 2001-2003 Universidad Nacional Agraria La Molina, Lima, Peru
- 2004-2007 College of Marin, Kentfield, CA
- 2007-2009 University of California, Los Angeles, CA
B.S. in Molecular, Cell, and Developmental Biology
- 2009 Santa Monica College, Santa Monica, CA
- 2012-2019 University of California, Irvine, CA
Doctor of Philosophy in Biological Sciences, with a concentration in
Developmental and Cell Biology

RESEARCH EXPERIENCE

- 2009 Undergraduate Research Assistant
University of California, Irvine, CA
- 2011-2012 Junior Specialist
University of California, San Francisco, CA
- 2012-2019 Graduate Student Researcher
University of California, Irvine, CA

MEETINGS

- 2018 International Zebrafish Conference-Poster Presentation
- 2019 West Coast Society for Developmental Biology Conference-Poster Presentation

PUBLICATIONS

Cheli VT, Daniels RW, Godoy R, Hoyle DJ, Kandachar V, Starcevic M, Martinez-Agosto JA, Poole S, DiAntonio A, Lloyd VK, Chang HC, Krantz DE, Dell'Angelica EC (2010). Genetic modifiers of abnormal organelle biogenesis in a Drosophila model of BLOC-1 deficiency. Human Molecular Genetics 19(5), 861–878.

Hoyle DJ, Rodriguez-Fernandez IA, Dell'Angelica EC (2011). Functional interactions between OCA2 and the protein complexes BLOC-1, BLOC-2, and AP-3 inferred from epistatic analyses of mouse coat pigmentation. Pigment Cell and Melanoma Research 24(2), 275-281.

ABSTRACT OF THE DISSERTATION

Pthlha and mechanical force control spatial-temporal aspects of hypertrophic cartilage development in the zebrafish craniofacial skeleton

By

Diego Jose Hoyle

Doctor of Philosophy in Biological Sciences,
with a concentration in Developmental and Cell Biology

University of California, Irvine, 2019

Professor Thomas F. Schilling, Chair

Tissue patterning in any developmental system requires well-coordinated signaling events that result in the formation of distinct cell types in the appropriate locations. While many of these signaling mechanisms are known, how they are initially established during development is less understood. Endochondral ossification involves cartilage replacement by bone in sites within the cartilage where chondrocytes become hypertrophic. In long bones, this occurs first in the mid-region of the cartilage, then on the distal ends. This process results in the formation of growth plates (GP), segments of cartilage in between these ossification zones that drive bone elongation via a combination of chondrocyte proliferation and endochondral ossification of GP cartilage. Two signals, Indian Hedgehog (Ihh), which promotes the process of ossification by inducing hypertrophic differentiation of chondrocytes near the mid-region ossification zone, and Parathyroid Hormone-Like Hormone (Pthlh), which represses hypertrophic differentiation of chondrocytes via a gradient that originates near the distal ossification

zones, control the rate and direction of bone growth. In addition to these, mechanical force plays important roles in tissue maintenance, as illustrated by the effects that zero gravity has on the bones and muscles of astronauts in orbit at the International Space Station. While *Ihh* is essential for the formation of hypertrophic zones (HZ) in embryonic cartilages, it is not expressed at the initial stages of HZ formation, suggesting that alternative signaling components are needed to begin the ossification process. Similarly, whether or not *Pthlh* plays a role in initial patterning of HZs and ossification remains unclear. In my thesis, I study the role of *Pthlh* signaling in the early patterning of HZs and explore the role of mechanical force in the process of endochondral ossification using the zebrafish jaw cartilages as a model.

Using a transgenic reporter line for the *entpd5a* gene, I show that HZs develop earlier than previously reported in zebrafish cartilages. Using this result as a base, I look at the expression pattern of *pthlha* and find expression domains of *pthlha* that inversely correlate with HZ patterns. Knockout of *pthlha* leads to an expanded HZ and increased ossification rates, results congruent with the known role of *Pthlh* in GPs. Mosaic misexpression of *pthlha* in chondrocytes results in disruption of HZs and bone formation as a function of the number and proximity of *pthlha*-expressing cells to the site of bone formation. In addition, mosaic misexpression of *pthlha* in chondrocytes leads to the mispatterning of the HZ such that it forms ectopically. These results suggest that *Pthlh* signaling is necessary and sufficient to pattern the initial HZs in embryonic cartilages and suggest that *Pthlh* signaling also helps establish the *Ihh/Pthlh* negative feedback loop that regulates GP homeostasis. In addition to these findings, I show that mechanical force is specifically required for chondrocyte hypertrophic differentiation in

developing HZs and for chondrocyte proliferation in zones of the cartilage that do not initially become hypertrophic. This result suggests that an additional signal may modulate the effects of mechanical force on chondrocytes, and we speculate that this signal is *Pthlh*. Therefore, this work establishes Pthlh as the early patterning signal of endochondral ossification and reveals a role for mechanical force in initiating the process.

CHAPTER I

Introduction

Overview

A fundamental question in developmental biology is how cell identities are defined depending on their position within organs and tissues. Previous studies suggest that this often involves combinations of secreted signals, such as two graded signals that are differentially expressed across the patterning axis forming integrated negative feedback loops (Bastida et al., 2009; Nakamura et al., 2006). This is likely a recurrent theme in development. The activating signal promotes its own expression and that of the inhibitory signal. In turn, the inhibitory signal represses the activator signal expression as a function of proximity to the source of the inhibitory signal. This interplay results in gradients of signaling activity that define stable cellular identities along body axes. This type of patterning, known as the Turing Pattern, was proposed by Alan Turing as part of his Reaction-Diffusion (RD) model in 1953, which sought to explain how systems can generate various patterns autonomously (Turing, 1990). Since then, the RD model has become one of the standard models to represent interactions between morphogens (graded signals that specify multiple cell fates in a concentration-dependent manner). However, how these signaling feedback loops are initially established is largely unknown in many cases.

Growth plates (GP), which drive long bone elongation, are maintained by similar feedback mechanisms. Most bones initially form as cartilage that is replaced by bone in

specific locations as development proceeds. In long bones, ossification first occurs in the mid-region, then on the distal ends. The cartilage remaining in between forms the GP, which produces more cartilage via cell proliferation in the direction of the central ossification zone, which continues to be replaced by bone throughout the life of the organism. This directional bone growth is maintained by a negative feedback loop formed by Indian Hedgehog (*Ihh*) and Parathyroid Hormone-Like Hormone (*Pthlh*) (Vortkamp et al., 1996). *Ihh*, the activator of hypertrophic differentiation, induces its own expression and that of *Pthlh*. In turn, *Pthlh* cannot induce its own expression but represses *Ihh*. The interplay between these two signals maintains GPs. Despite extensive research on this signaling network in the established GP, how these signaling centers are initially established and why cartilages begin ossifying where they do are still unanswered questions.

Understanding feedback mechanisms in signaling networks in GPs can lead to treatments for human diseases. While *Ihh* promotes chondrocyte proliferation in GPs, Fibroblast Growth Factor (*Fgf*) signaling represses chondrocyte proliferation to balance the effects of *Ihh* (Hinoi et al., 2006; Ohbayashi et al., 2002). Diseases that disrupt this balance can lead to defective GP function, thereby impairing bone growth.

Achondroplasia, an autosomal dominant disease that produces short stature and short limbs, is one such disease caused by mutations in Fgf Receptor 3 (*Fgfr3*) that stabilize its binding to Fgf18, leading to decreased chondrocyte proliferation (Monsonneg-Orran et al., 2000; Rousseau et al., 1994). Therefore, potential treatments for this disease would need to disrupt the interaction between *Fgf18* and *Fgfr3*, which would allow chondrocytes to proliferate normally. Following this reasoning, ongoing efforts to

develop a treatment to this disease via use of a soluble Fgfr3 recombinant protein to act as a decoy for Fgf18 illustrate how basic understanding of the processes controlling bone elongation has the potential to improve the lives of people living with these diseases (Garcia et al., 2013).

In my thesis, I use development of the zebrafish jaw to study how cartilage ossification patterns and their feedback mechanisms are initially established. The ceratohyal (ch), which supports the jaw, is a rod-like cartilage that begins ossifying in its mid-region, develops secondary ossification zones at its distal ends, and eventually forms growth zones in between, much like GPs of long bones. However, the ch cartilage contains several orders of magnitude fewer cells than a mammalian long bone, making it an ideal model to manipulate the feedback mechanisms controlling GPs. Hence, I use the ch cartilage for most of my studies. In Chapter II, I show evidence that *Pthlh* determines where cartilages initially ossify and suggest that *Pthlh* also establishes the direction of the feedback mechanisms in GPs. In Chapter III, I show that mechanical force is required for the onset of cartilage ossification. In chapter IV, I show preliminary data on the initial formation of the perichondrium, a thin cell layer that insulates and provides important regulatory cues to cartilages, and I identify Cellular Retinoic Acid Binding Protein 2B (*crabp2b*) as an early perichondrial marker. Finally, in Chapter V, I describe preliminary attempts using 2-photon laser ablation to test mechanisms of propagation of cartilage polarity, a process that is critical for cartilage morphogenesis.

Morphogen Gradient versus Reaction-Diffusion Models in Pattern Formation

One of the most fundamental questions in developmental biology is how cells acquire distinct fates depending on their location. In 1924, Spemann and Mangold found that the dorsal edge of a gastrulating amphibian embryo, also known as the Spemann Organizer, induced dorsal fates and formed a new embryonic axis if transplanted to the ventral side of a host embryo (Spemann and Mangold, 1924; Wolpert et al., 2006). Hence, a small group of cells determines the fates of others throughout the early embryo, prompting the question of how this small group of cells could transmit this information to others. Through various other sets of experiments, a consensus model for morphogen gradients was established. The key premises of this model are diffusion of a signal, which forms a gradient, and which induces different cell fates at different thresholds (Figure 1.1A). First, a localized group of cells secretes a signal that diffuses through tissues creating a concentration gradient such that cells closer to the source have more exposure to the signal than cells that are farther away. Neighboring cells receiving the signal have threshold sensitivities to this signal such that different cell fates are acquired as a function of local signal concentration (Wolpert, 1969; Wolpert et al., 2006). Therefore, according to this model, a morphogen was secreted from the Spemann Organizer that determined dorsal to ventral cell fates.

However, the Morphogen Gradient model fails to explain how systems self-regulate. Since the formation of a signal gradient through diffusion is a critical component of the model, this would suggest that the range and shape of the signal gradient are critical parameters for tissue patterning. When a Spemann Organizer is transplanted into the ventral side of an embryo, a prediction would be that two partially

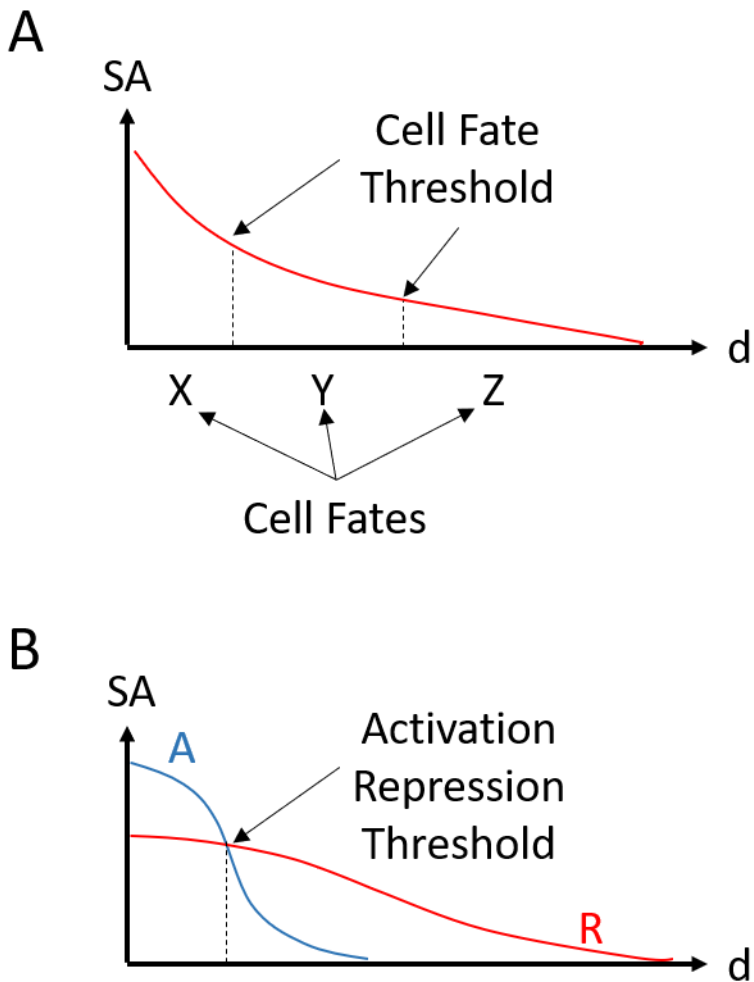


Figure 1.1: Morphogen Gradients versus Reaction Diffusion models. (A) Graphical representation of the Morphogen Gradient Model. A morphogen is secreted from a source on the left of the curve and diffuses to the right, generating a concentration gradient that creates a gradient of signaling activity (represented by the red curve) that induces different cell fates at different signaling thresholds. (B) A graphical representation of a Turing Pattern from the Reaction Diffusion Model. An activator signal is secreted to the left of the curve, creating a gradient of signaling activity (blue). The activator signal induces its own expression and that of a Repressor (red). The repressor functions to repress the activity of the activator and is more diffusible than the activator, so the signaling activity of the repressor prevents signaling of the activator at longer ranges. This results in the morphogenetic activity of the activator remaining restricted to a certain range and introduces a feedback mechanism for the repressor to modulate its own activity range. SA=signaling activity, d=distance, A=activator, R=repressor.

overlapping gradients, one from the dorsal side, and one from the ventral side (ectopic) would form, yet ventral fates are still specified in embryos with an ectopic Spemann Organizer. Therefore, a pertinent question would be whether the introduction of an ectopic Spemann Organizer somehow redefines the range and shape of the endogenous gradient, which would suggest the presence of a feedback mechanism. The current model for gastrula dorsal-ventral patterning proposes two signaling centers that interact with each other (De Robertis, 2006; De Robertis and Kuroda, 2004). Bone Morphogenetic Protein 4 (BMP4) is secreted from the ventral side of the gastrula and induces ventral fates (Gawantka et al., 1995; Joly et al., 1993; Kawahara et al., 2000), while Chordin and Noggin, which antagonize BMP ligands and prevent them from binding to their receptors, are secreted from the Spemann Organizer (Piccolo et al., 1996; Zimmerman et al., 1996). Although the feedback mechanisms between these signaling centers are not completely understood, BMP signaling promotes ventral expression of Sizzled, an inhibitor of Tolloid-related proteases that degrade Chordin (Bijakowski et al., 2012; Lee et al., 2006; Ploper et al., 2011). Depletion of Sizzled leads to BMP signaling upregulation and ventralization of the embryo (Collavin and Kirschner, 2003). Therefore, the ventral signaling center can modulate the shape and range of the Chordin gradient generated by the Spemann Organizer.

Such an example illustrates the need to include feedback into models of morphogenetic events. The RD model has been very useful in understanding various morphogenetic events in embryogenesis. As previously mentioned, the RD model was formulated by Alan Turing to explain how a pair of diffusible molecules interact and produce steady states. The Turing Pattern is one of these steady states and is

represented as a non-linear wave in which wavelength is determined by interactions between the two hypothetical molecules and their diffusion rates (Turing, 1990). Gierer and Meinhardt postulated that RD systems required a short-range activator signal that induces both itself and a long-range signal that represses the activator (Gierer and Meinhardt, 1972), essentially forming a negative feedback loop between two diffusible signals (Figure 1.1B).

The feedback mechanism between Nodal and Lefty in left-right (LR) asymmetry of the vertebrate body axis is a good example of RD. In this case, Nodal is the activator signal for left identity, and Lefty acts as an inhibitory signal for Nodal. Apparently due to ciliary motion in the embryo, Nodal accumulates on the left side of the embryo (Nonaka et al., 1998). Nodal induces its own expression and that of Lefty (Nakamura et al., 2006; Saijoh et al., 2000). Since Lefty is more diffusible than Nodal, despite both signals originating on the left side, Lefty's gradient has longer range, which ensures that Nodal is unable to target the right side of the embryo (Muller et al., 2012; Nakamura et al., 2006; Sakuma et al., 2002). In this example, Nodal, the activator signal, defines left side identities and where Lefty is to be expressed. Hence, the activator signal source defines the position and direction of the negative feedback loop. However, is this a requirement in all negative feedback loops regardless of how well they fit the RD model? Despite understanding how various negative feedback mechanisms such as BMP-Chordin or Nodal-Lefty work throughout development, how they initially form is less understood.

The anterior-posterior patterning of limbs is another example of a patterning system involving a signaling network that includes a negative feedback loop, the origin of which is not well understood. In the limb, the Zone of Polarizing Activity (ZPA) is

responsible for this patterning, which forms in the ventral side of the limb bud and expresses Shh (Riddle et al., 1993). Here, Shh induces its own expression and that of BMP. In turn, BMP represses Shh expression (Bastida et al., 2009). This negative feedback loop, which maintains the ZPA, does not fit the RD model. Despite this, how this system is initially established is unknown. Just as in LR asymmetry, one possibility is that Shh, the activator, is expressed first, which in turn induces BMP expression. In this scenario, Shh determines the position and direction of the morphogenetic wave. However, it is also possible that a BMP gradient initially forms such that BMP signaling is low on the ventral side of the limb bud, allowing the ZPA to form. Next, the ZPA would induce BMP expression and change the shape of the BMP gradient accordingly. In this scenario, BMP, not Shh, determines the position and direction of the morphogenetic wave. Could negative feedback loops form as described by the second scenario? Would this also apply to RD models? For my thesis work, I have used endochondral ossification patterning in the zebrafish jaw cartilage to test if the inhibitory signal in the negative feedback loop operating in GPs can determine how the loop forms. This is in contrast to LR asymmetry, for example, where the activator signal determines the direction of the negative feedback loop.

Cartilage Differentiation

Before discussing how bones form from cartilages, we must first understand how cartilages form. Cartilages start from mesenchymal progenitors that begin differentiating into chondrocytes when they receive a BMP signaling pathway (Buckland et al., 1998; Healy et al., 1999; Pizette and Niswander, 2000). This was inferred from the observation that BMP4-coated beads strongly induced chondrogenesis in the 5-day

chick limb bud (Buckland et al., 1998). However, chondrogenesis occurs in two stages. First, BMP signaling initiates the formation of mesenchymal precartilaginous condensations, a process in which mesenchymal cells tightly pack and condense due to upregulation of N-Cadherin (Oberlender and Tuan, 1994; Pizette and Niswander, 2000; Widelitz et al., 1993). Monoclonal antibodies against N-Cadherin can inhibit condensation formation in micromass cultures in a dose-dependent manner (Oberlender and Tuan, 1994). Next, BMP signaling leads to activation of SRY-Box Transcription Factor 9 (*Sox9*), which is necessary and sufficient to induce chondrocyte differentiation (Bi et al., 1999; Healy et al., 1999). In addition to its role in sex determination (Kent et al., 1996; Morais da Silva et al., 1996; Wagner et al., 1994), *Sox9* is considered the “master regulator” of cartilage differentiation because it is required cell autonomously in mesenchymal cells to differentiate into chondrocytes (Bi et al., 1999), and because its misexpression is sufficient to induce cartilage differentiation ectopically (Healy et al., 1999). This requirement for *Sox9* is conserved in all vertebrates in which it has been examined (Bi et al., 1999; Foster et al., 1994; Healy et al., 1999; Wagner et al., 1994; Yan et al., 2002). Thus, BMP signaling and *Sox9* are two major factors that initiate and control chondrocyte differentiation.

One of the consequences of *Sox9* activation in differentiating chondrocytes is the secretion of cartilage-specific extracellular matrix (ECM). One of the main components of this ECM is Type-II Collagen. Encoded by the Collagen Type II Alpha 1 Chain (*Col2a1*) gene, Type-II Collagen is only expressed in cartilage, and it is required for normal differentiation and maintenance of chondrocytes (Barbieri et al., 2003; Zhao et al., 1997). Mutations in the *Col2a1* gene can lead to Achondrogenesis Type II,

Osteoarthritis, Achondroplasias, Chondrodysplasias, and dwarfism (Ala-Kokko et al., 1990; Chan et al., 1995; Korkko et al., 2000; Vissing et al., 1989). *Sox9* directly binds an enhancer in the *Col2a1* locus and activates its expression in chondrocytes (Bell et al., 1997; Ng et al., 1997; Zhao et al., 1997). However, how does *Sox9* activate *Col2a1* expression in chondrocytes and not in other tissues? It turns out that *Sox9* alone is insufficient to drive *Col2a1* expression to the high levels detected in chondrocytes. *Sox9* must first be phosphorylated by Cyclic AMP-Dependent Protein Kinase A (PKA) in two of its residues in order for it to bind and activate the *Col2a1* locus (Huang et al., 2001; Huang et al., 2000). *Pthlh*, which plays an important role in GP maintenance, is one of the factors secreted by cartilage driving the phosphorylation of *Sox9* via PKA (Huang et al., 2001), which plays important roles in the maintenance of GPs.

Finally, recent reports suggest that mechanotransduction may play a role in cartilage differentiation and GP maintenance. Mechanotransduction is a term that encompasses multiple signaling pathways by which cells sense mechanical force. It includes the release of Transforming Growth Factor β ligands from the extracellular matrix (ECM) of tendons by muscle contraction to signal tenocytes to mature (Subramanian et al., 2018), as well as mechanical load sensing in bones via Integrins for osteocyte survival (Aguirre et al., 2006; Noble et al., 2003; Plotkin et al., 2005). In cartilage, it was noticed that paralysis in chick led to smaller skeletal elements (Hall and Herring, 1990). Closer examination of paralyzed chick embryos showed that mechanical force via muscle contraction is required for chondrocyte proliferation (Germiller and Goldstein, 1997). In addition, *Sox9* and *Col2a1* expression requires the activity of Transient Receptor Potential Vanilloid 4 (*Trpv4*), which is a $\text{Ca}^{+2}/\text{Na}^{+}$ channel that is

activated by both mechanical forces and hypotonic stress (Muramatsu et al., 2007; Nilius et al., 2004; O'Connor et al., 2014). This implicates mechanical force in chondrocyte differentiation. While other studies have suggested roles for mechanical force in ossification and bone growth (Hosseini and Hogg, 1991; Hu and Albertson, 2017), it is unclear whether these are related to the effects of mechanical force on cartilage differentiation or separate effects.

Cartilage Morphogenesis

The fact that *Sox9* mutant cells are excluded from precartilaginous condensations in chimeric mice suggests that *Sox9* also plays some role in the movements of differentiating chondrocytes (Bi et al., 1999). As it turns out, *Sox9* also initiates the process of cartilage morphogenesis, which consists of differentiating chondrocytes intercalating perpendicular to the long axis of the cartilage element (Le Pabic et al., 2014; Sisson et al., 2015). This process is remarkably similar to convergent extension (CE), the process that elongates the anterior-posterior axis of vertebrate embryos during gastrulation (Huebner and Wallingford, 2018) (Figure 1.2).

While failure to express N-Cadherin contributes to *Sox9* mutant cells being excluded from cartilages, it was eventually found that cartilage elongation requires assistance from Planar Cell Polarity (PCP) signaling (Le Pabic et al., 2014). PCP is the polarity of cells in the plane of a tissue, a phenomenon that has been best studied in epithelia. Examples of PCP are the orientation of hairs and ommatidia in the fruit fly wings or eyes, respectively, as well as the orientation of hairs in our skin and hair cells in the inner ear (Goodrich and Strutt, 2011; Sienknecht, 2015). However, PCP signaling

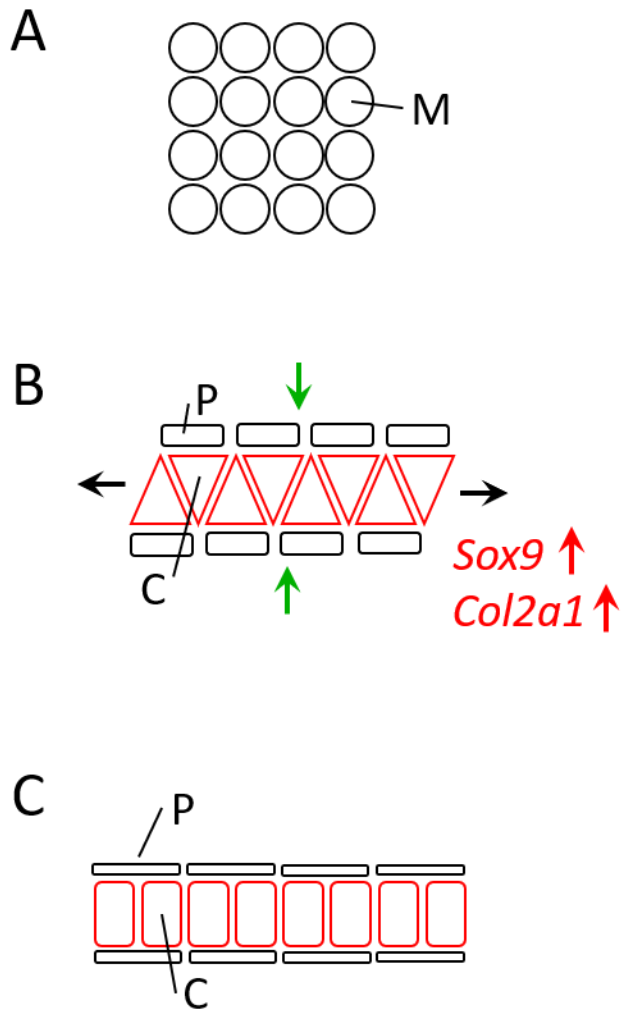


Figure 1.2: Cartilages form via convergent extension. (A) Representation of mesenchymal cells prior to cartilage differentiation. (B) Representation of convergent extension of differentiating cartilage. Chondrocyte differentiation begins with *Sox9* and *Col2a1* upregulation (red arrows) in the middle of the mesenchyme, which intercalate with each other (convergence, green arrows) to elongate the forming cartilage in the perpendicular direction (extension, black arrows). (C) Representation of a cartilage after convergent extension. Chondrocytes have swollen and are stacked as coins along the long axis of the cartilage. The cells in the periphery of the mesenchyme that do not upregulate *Sox9* remain outside the chondrocyte stack and become the perichondrium. M=mesenchymal cell, P=perichondrium, C=chondrocyte.

was later found to be involved in other processes such as directional cell migration, axon guidance, and CE movements such as those seen in cartilage morphogenesis (Davey and Moens, 2017; Le Pabic et al., 2014; Sisson et al., 2015).

PCP signaling involves at least two distinct pathways that have been most extensively studied in *Drosophila melanogaster*: the core pathway, and the Fat (*Ft*)/Dachsous (*Ds*) Pathway. The core pathway depends on the intracellular asymmetrical distribution of six core PCP proteins. The transmembrane components Frizzled (*Fz*), Vang Gogh (*Vang*), and Flamingo (*Fmi*) are required for PCP propagation from cell to cell (Chen et al., 2008; Strutt and Strutt, 2008; Wu and Mlodzik, 2008). On the other hand, cytosolic components Dishevelled (*Dsh*), Prickle (*Pk*), and Diego (*Dgo*) interact with the intracellular domains of *Fz*, *Vang*, and *Fmi* and form a complex that is required for their intracellular asymmetric distribution (Axelrod, 2001; Das et al., 2004; Feiguin et al., 2001; Shimada et al., 2001). The mechanism leading to the asymmetrical distribution of these components is not well understood, but there is evidence to suggest, at least in some cases, that distribution of core pathway components depends on the activity of the *Ft/Ds* pathway (Olofsson et al., 2014; Sharp and Axelrod, 2016; Yang et al., 2002). Mutations in any of these 6 components leads to complete PCP loss (Wong and Adler, 1993). Wingless (*Wg*), a Wnt signaling ligand, was previously proposed to serve as an upstream signal generating asymmetry (Adler et al., 1997), but this idea fell out of favor since mutations in several fruit fly Wnt ligands had no PCP phenotypes (Chen et al., 2008; Lawrence et al., 2002). This idea remains controversial in cartilage morphogenesis since *Wnt5a* is required for the asymmetric subcellular localization of the vertebrate *Vang* ortholog *Vangl2* and cartilage CE (Gao et al., 2011;

Qian et al., 2007). Hence, the core pathway is also known in vertebrates as a type of non-canonical Wnt signaling, sometimes referred to as Wnt-PCP. The Tyrosine Kinase Orphan Receptor 2 (*Ror2*) acts downstream of *Wnt5a* to activate the JNK pathway (Oishi et al., 2003). Mutations in *Wnt5a* and *Ror2* cause Robinow Syndrome, characterized by limb shortening, spine segmental defects, brachydactyly, and facial dysmorphism (Afzal et al., 2000; Person et al., 2010; van Bokhoven et al., 2000). Additionally, the *Wnt5a* paralog, *wnt5b*, and Wnt signaling coreceptor Glypican 4 (*gpc4*) are required for zebrafish cartilage morphogenesis (LeClair et al., 2009; Sisson et al., 2015), but how these two genes relate to PCP in mammalian cartilages is unclear.

In contrast, the *Ft/Ds* pathway relies on heterotypic binding of protocadherins *Ft* and *Ds* (Matakatsu and Blair, 2004). The Golgi resident protein Four-jointed (*Fj*) constitutes a third component. In *Drosophila* imaginal discs both *Ds* and *Fj* are expressed in opposing gradients, which modulates *Ft* and *Ds* interactions and their asymmetric distribution at the plasma membrane via *Fj*-dependent phosphorylation of *Ds* extracellular domains (Simon, 2004; Strutt et al., 2004; Yang et al., 2002; Zeidler et al., 1999). These interactions modulate the activity of intracellular effectors such as Dachs (*D*) and Atrophin (*Atro*) (Fanto et al., 2003; Mao et al., 2011). Hence, the *Ft/Ds* pathway relies on expression gradients to generate asymmetry. In cartilage, *fat3*, *dchs2*, and Arginine-Glutamic Acid Dipeptide (RE) Repeats A (*rerea*), which are orthologs for fruit fly *Ft*, *Ds*, and *Atro*, respectively, are all required for chondrocyte intercalation in zebrafish jaw cartilage morphogenesis. In addition, *fat3*, *dchs2*, and *rerea* form a positive feedback loop with *sox9a*, the zebrafish *Sox9* ortholog, through an unknown mechanism. Absence of either *fat3* or *dchs2* prevents *sox9a* expression and vice versa.

In contrast, *rere* mutations lead to increased chondrocyte differentiation (Le Pabic et al., 2014). Given the role of *rere* in recruiting nuclear deacetylases for gene inactivation (Fanto et al., 2003), the opposite phenotypes of *fat3/dchs2* and *rere* have led to the speculation that *fat3/dchs2* signaling serves, at least in part, to recruit *rere* to the intracellular domain of *fat3* at the plasma membrane to prevent DNA deacetylation and allow *sox9a* to be expressed in chondrocytes (Le Pabic et al., 2014). The mechanism by which *rere* modulates PCP or chondrocyte intercalation is not known. Furthermore, functional interactions between Wnt-PCP and Fat/Dchs signaling pathways have not been studied in cartilage.

Cartilage Ossification

Following cartilage morphogenesis, most cartilages undergo endochondral ossification, a process where cartilage is replaced by bone. Morphologically, hypertrophic chondrocytes (HC) are swollen and round due to the presence of large vacuoles. As they swell, HCs secrete ECM that prepares the cartilage for the transition to bone. When HCs finish their maturation process, they undergo apoptosis, leaving large ECM deposits that serve as a scaffold for osteoblasts forming in the perichondrium surrounding HZs. In the long bones of mice and chickens, this process begins in the mid region of the cartilage and is often referred to as the primary ossification center (OC) (Figure 1.3A). During development, the primary OC expands in both directions of the long axis of the cartilage via endochondral ossification. As this process continues, two secondary OCs form at the distal ends of the cartilage (Figure 1.3B). As the primary OC continues to expand, the remaining cartilage between OCs forms GPs (Figure 1.3C). These GPs direct longitudinal bone growth by transitioning chondrocytes through three

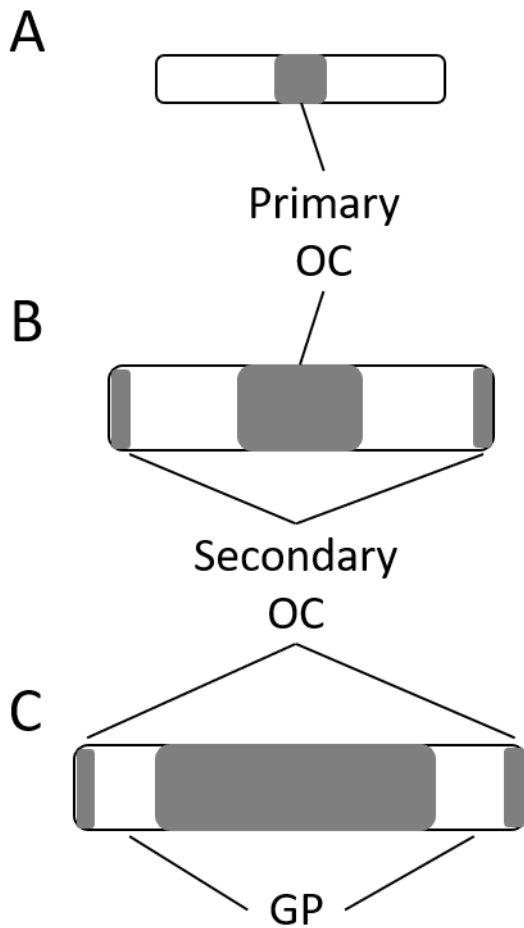


Figure 1.3: Long bones ossify first in the middle then on their distal ends. (A) Representation of a long bone cartilage as it begins to ossify. Ossification initially begins in the mid region of the cartilage, forming the primary ossification center (OC). (B) Representation of an ossifying long bone cartilage. As the primary OC expands along the long axis of the cartilage, secondary OCs appear on the distal ends of the cartilage. (C) Representation of a long bone. The primary OC continues to expand along the length of the cartilage until the remaining cartilages between the primary and secondary OCs form growth plates (GP), which constantly produce new cartilage for the primary OC via chondrocyte proliferation while preventing their own ossification.

zones: the resting zone (RZ), the proliferation zone (PZ), and the HZ (Figure 1.4A). While, the RZ is located adjacent to secondary OCs, the HZ is located adjacent to the primary OC. The PZ is located between the RZ and the HZ. The RZ contains resting chondrocytes (RCs) that are slow proliferating chondrocytes that serve as a reserve population. These zones can be recognized by the expression of marker genes (Figure 1.4B). The distal tip of the RZ is characterized by *Pthlh* expression. Chondrocytes in both the RZ and PZ express *Sox9* and *Col2a1*, which are required for chondrocyte maintenance. Finally, chondrocytes in the HZ express both Indian Hedgehog (*Ihh*) and *Col10a1*, which are needed for the ossification process. Chondrocytes at the RZ slowly transition into the PZ in which proliferating chondrocytes (PCs) divide rapidly. Finally, PCs transition in the HZ to become hypertrophic and make more bone (Figure 1.4C). In short, GPs ensure that bones continue growing via a combination of proliferation and hypertrophic differentiation (Kronenberg, 2003). In humans, GPs gradually ossify and disappear by the beginning of adulthood. Thus, both spatial and temporal control of GPs is critical for achieving an adult bone of the appropriate size and shape.

Several signaling pathways are involved in controlling different aspects of GP biology. However, interactions between *Ihh* and *Pthlh* signaling pathways constitute the main regulatory mechanism regulating GP (Figure 1.5). *Ihh* is the main signal directing HZ maturation. *Ihh* is expressed in hypertrophic chondrocytes (HCs), and it has multiple targets in the GP. First, *Ihh* targets HCs and PCs adjacent to the HZ to induce hypertrophic differentiation and feed the HZ with new chondrocytes (Mak et al., 2008). In addition, *Ihh* targets the PZ to promote chondrocyte proliferation, ensuring production of chondrocytes to transition into the HZ (Karp et al., 2000; St-Jacques et al., 1999). *Ihh*

Figure 1.4: GPs function requires that chondrocytes transition through multiple layers. (A) Representation of a long bone GP. The GP is made of multiple layers. To the left is the resting zone (RZ), which is made of resting chondrocytes (RC) that divide slowly. Next is the proliferative zone (PZ), composed of rapidly dividing proliferative chondrocytes (PC) that drive elongation of the cartilage. The pre-hypertrophic zone (PHZ) is a transition zone where PCs stop dividing and begin the hypertrophic differentiation process, becoming pre-hypertrophic chondrocytes (PHC). As these mature, they enter the hypertrophic zone (HZ) and become hypertrophic chondrocytes (HC) themselves by swelling and secreting extracellular matrix required for the ossification process. HCs eventually undergo apoptosis and leave a porous matrix that is used by osteoblasts (O) from the primary OC to produce more bone. Meanwhile, the perichondrium (P, blue), which is made of flat cells in the peripheries of the RZ and PZ, become periosteum (Po, green) as adjacent cartilage ossifies and contribute to the production of new osteoblasts. (B) Representation of the expression of GP markers. *Pthlh* is expressed in the distal tip of the RZ. *Sox9* and *Col2a1* are markers for differentiating chondrocytes and are actively expressed in the RZ and PZ. *Ihh* and *Col10a1* are mainly expressed in the PHZ and HZ. (C) Representation of the direction in which chondrocytes transition through the different zones in GPs.

also induces osteoblast differentiation in the perichondrium adjacent to the HZ to begin the ossification process (Felber et al., 2011; St-Jacques et al., 1999). Mutations in *Ihh* lead to short cartilages with severely delayed ossification (St-Jacques et al., 1999). Finally, *Ihh* induces expression of *Pthlh* in the perichondrium and distal tip of the RZ. This generates a gradient of Pthlh protein that delays hypertrophic differentiation in a subset of cells in the HZ called prehypertrophic chondrocytes (PHCs), which are the transition between the PZ and the HZ (Vortkamp et al., 1996). However, *Pthlh* also targets the PZ to prevent premature hypertrophic differentiation (Chung et al., 1998; Weir et al., 1996). *Pthlh* accomplishes this by repressing expression of Runt-Related Transcription Factor 2 (*Runx2*), which is required for *Ihh* expression (Li et al., 2004; Yoshida et al., 2004). Mutations in *Pthlh* lead to severe skeletal dysplasia and accelerated ossification (Karaplis et al., 1994). In addition to the *Ihh/Pthlh* negative feedback loop, another mechanism acting through the perichondrium modulates the proliferative effect of *Ihh* in chondrocytes (Figure 1.5). *Ihh*-dependent induction of osteoblasts in the perichondrium leads to upregulation of *Runx2* in these cells (Eames et al., 2011), which promotes *Fgf18* expression in perichondrial cells to restrict chondrocyte proliferation, thereby checking the proliferative influence of *Ihh* in the PZ (Hinoi et al., 2006; Ohbayashi et al., 2002). Hence, these functional interactions between *Ihh* and *Pthlh*, as well as between *Ihh* and *Fgf*, form a negative feedback loop that maintains the distinct zones within the GP and governs how chondrocytes transition through these zones.

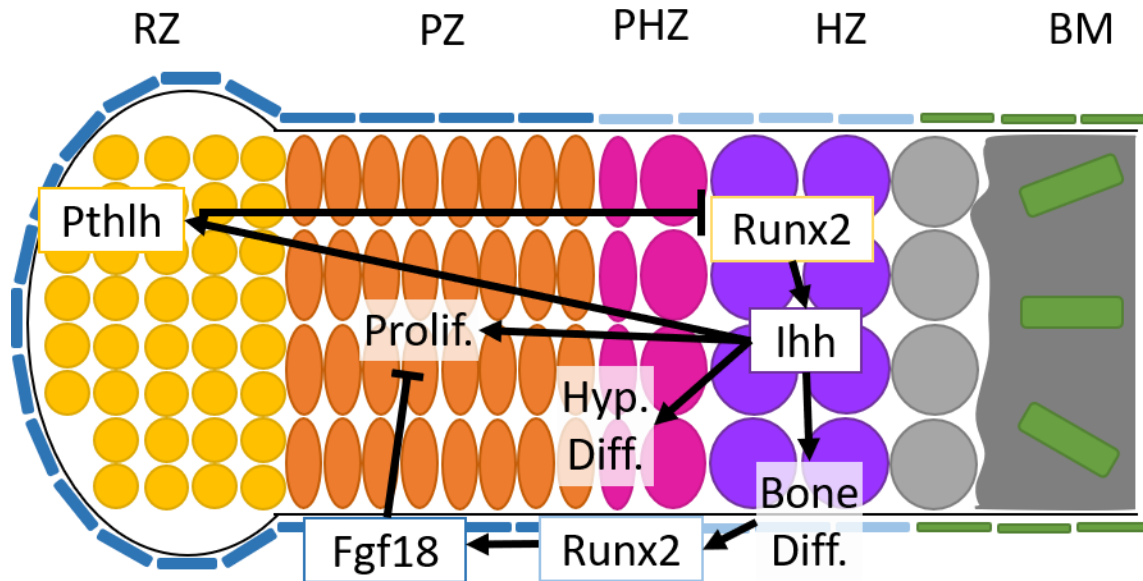


Figure 1.5: GP homeostasis is controlled by negative feedback mechanisms. *Ihh* is expressed in the HZ and promotes hypertrophic differentiation in adjacent cells, inducing its own expression. *Ihh* also induces expression of *Pthlh* on the distal end of the RZ. From this location, *Pthlh* forms a gradient of decreasing concentration towards the HZ. *Pthlh* signaling represses *Runx2*, which is required for *Ihh* expression, in the RZ and PZ, effectively maintaining these zones free of hypertrophic differentiation. In addition, *Ihh* also promotes chondrocyte proliferation in the PZ. However, this activity is modulated from the perichondrium by *Runx2*, which is also induced by *Ihh* as perichondrial cells become osteoblasts. *Runx2* expression in the perichondrium leads to *Fgf18* upregulation in perichondrial cells, which signals to PCs to repress proliferation.

Ossification Patterning

Despite our understanding of how GPs and OCs are maintained, the mechanisms that determine where HZs form are not understood. In zebrafish, *Ihh*, which induces its own expression and promotes hypertrophic differentiation, is not expressed at the site of HZs prior to the onset of chondrocyte hypertrophic differentiation (Eames et al., 2011).

Therefore, we hypothesize that *Pthlh*, a repressor of hypertrophy induced by *Ihh*, could determine HZ position and negative feedback loop direction within cartilages by restricting where *Ihh* is initially expressed. In support of this hypothesis, *in situ* hybridization for *pthlha*, the zebrafish ortholog for *Pthlh*, has shown that it is expressed in domains in the cartilage primordium well before the onset of hypertrophic differentiation, though the precise expression pattern has not been closely examined (Yan et al., 2012). However, previous manipulations of Pthlh signaling in mice and chicks failed to change the ossification pattern of long bones. Expression of *Pthlh* throughout the cartilage inverted the order in which primary and secondary OCs formed but did not change their location (Weir et al., 1996). A different study made chimeric mice that had chondrocytes lacking a functional *Pthlh* receptor, *Pthr1*, embedded within wild-type (WT) cells in the PZ. As expected, mutant cells became hypertrophic prematurely. In addition, PZs with mutant cells were enlarged, likely due to increased *Pthlh* expression around the clones, and small ectopic OCs formed in some cases, but the locations of the primary and secondary OCs were still unchanged (Chung et al., 1998). It is possible that these manipulations failed to change basic ossification patterns because of the size of chick and mouse long bone cartilages, such that signals were diluted. In addition, none of the previously mentioned studies addressed the roles of

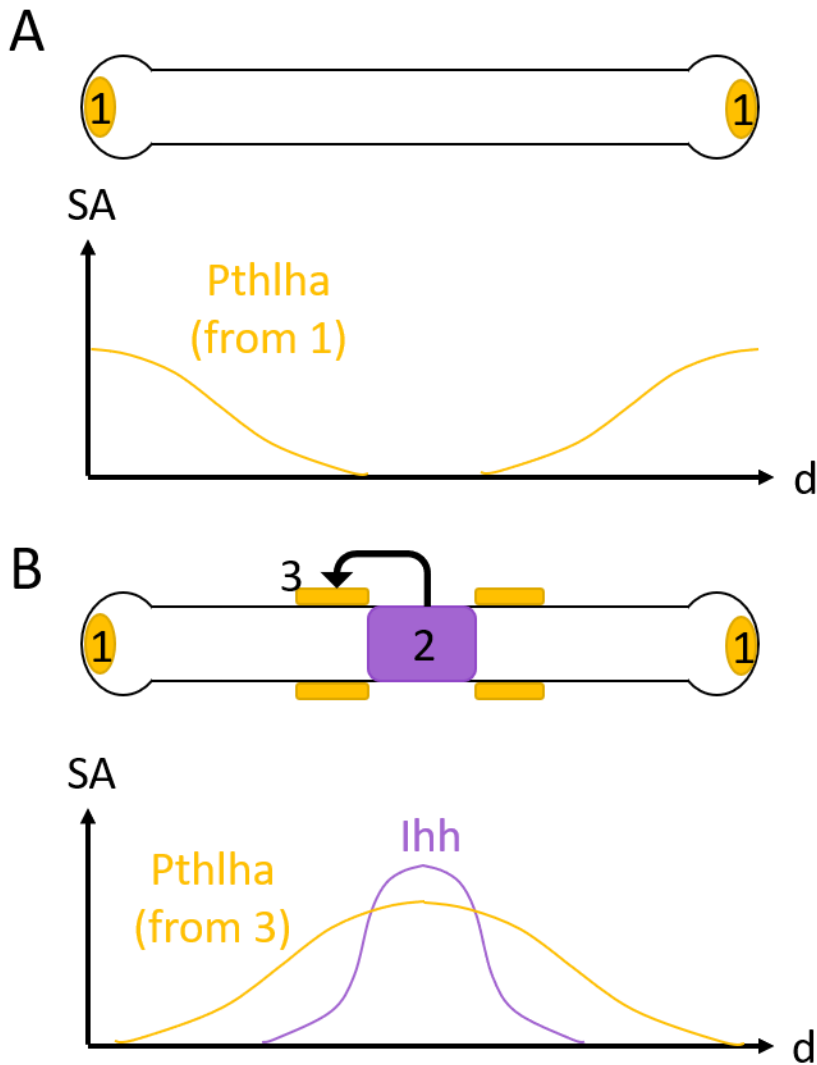


Figure 1.6: Could interactions between *Ihh* and *Pthlh* in ossifying cartilages fit the RD Model? Representation of our hypothesis for the induction of *pthlha* expression near the HZ by *Ihh* from the developing HZ. (A) First, *pthlha* is expressed in the distal ends of the cartilage prior to chondrocyte hypertrophic differentiation (1), generating gradients of *Pthlh* signaling activity that restrict formation of HZs to the mid region of the cartilage. (B) As the HZ develops (2), it expresses *Ihh* that forms a sharp gradient and induces *pthlha* expression in adjacent perichondrium (3). From these locations (3), *pthlha* forms a shallower gradient with longer range, effectively restricting expansion of the HZ. For simpler visualization of the gradient, the contributions to the gradient from the distal ends of the cartilage (1) were omitted in (B). SA=signaling activity, d=distance.

Pthlh expression domains at early stages of cartilage morphogenesis and differentiation that might initiate ossification patterns.

Finally, some aspects of the *Ihh/Pthlh* negative feedback loop may fit the RD model, yet this possibility remains unaddressed. For instance, in the chimeric mouse experiment previously described, the authors hypothesize that the enlargement of the PZs containing mutant clones was due to induction of *Pthlh* expression near the clones by *Ihh* (Chung et al., 1998). If true, one explanation for this observation could be that, even though *Ihh* from the clones could induce hypertrophic differentiation in some adjacent chondrocytes, the longer range of *Pthlh* diffusion around the clones ensured that they remained isolated from endogenous HZs. This proposed mechanism would fit the RD model in that an additional Turing Pattern was formed in the clone by *Ihh* (Turing, 1990). Therefore, while we hypothesize that *Pthlh* expression domains initially define where *Ihh* is expressed in ossifying cartilages, and that subsequent *Ihh* expression acts on adjacent cartilage to modify the shape of the *Pthlh* gradient, preventing the forming primary HZ from expanding rapidly and preventing the formation of secondary HZs near the primary HZ (Figure 1.6).

Could endochondral ossification patterns originate from signaling events preceding cartilage morphogenesis?

Many of the embryonic molecular events that give rise to the distinct cartilage elements of the craniofacial skeleton are known. Yet whether these earlier patterning events influence how the signaling components required for endochondral ossification are expressed is unknown. In all vertebrates, craniofacial cartilages largely derive from neural crest cells (NCC), which originate from the dorsal neural tube (Le Douarin, 1980;

Noden, 1988; Schilling and Kimmel, 1994). Specifically, craniofacial cartilages form from segments of post-migratory cranial NCC that colonize the pharyngeal arches (PA). In zebrafish, PA1 makes the jaw, PA2 makes jaw supporting cartilages, and PA3-7 make the branchial arches (Mork and Crump, 2015; Schilling and Kimmel, 1994). The identity of these segments is patterned anterior-posteriorly by Hox genes (Minoux and Rijli, 2010). PA1 expresses no Hox genes, while PA2 requires the function of Hox2 genes. Mutations or knockdown of Hox2 genes lead to homeotic transformation of PA2 to a PA1 identity (Gendron-Maguire et al., 1993; Hunter and Prince, 2002; Miller et al., 2004; Rijli et al., 1993).

Within each pharyngeal segment, cartilages are patterned dorsal-ventrally (D-V) post NCC migration (Clouthier et al., 2010). This patterning results in the formation of ventral, intermediate, and dorsal domains that eventually result in the formation of ventral and dorsal skeletal elements in each arch. BMP4 (*bmp4*) induces Heart And Neural Crest Derivatives Expressed 2 (*hand2*), which defines the ventral domain (Alexander et al., 2011; Liu et al., 2005b; Liu et al., 2004; Zuniga et al., 2011). Although Endothelin-1 (*edn1*) contributes to patterning of the ventral domain (Clouthier et al., 1998; Kempf et al., 1998; Miller et al., 2000), it later plays a more prominent role in the formation of the intermediate domain (Zuniga et al., 2011), which it accomplishes by promoting the nested expression of Distal-less Homeobox 5 (*Dlx5*) and *Dlx6* (Sato et al., 2008; Zuniga et al., 2011). Finally, Jagged 1B (*jag1b*) is required for the specification of the dorsal domain, which is defined by the expression of this ligand and the downstream Notch signaling transcriptional effector Hes Related Family bHLH Transcription Factor with YRPW Motif 1 (*hey1*) (Zuniga et al., 2010). Disruptions in any

of these signals leads to partial or complete homeotic transformations of individual D-V elements of the jaw. For instance, overexpression of a dominant-negative form of BMP receptor 1A (*bmpr1a*) to block BMP signaling during arch patterning transforms ventral cartilages to a dorsal identity (Alexander et al., 2011). Furthermore, mutations in *edn1* and Myocyte Enhancer Factor 2CA (*mef2ca*), a transcription factor downstream of *edn1* in the intermediate domain, lead to homeotic transformations of the dermal bones associated with these cartilages: the branchiostegal ray 3, which forms in the intermediate domain, acquires a more dorsal opercular identity (Kimmel et al., 2003).

Despite this detailed understanding of the early patterning events in the PAs, currently there is no evidence to suggest that D-V patterning influences the positions of endochondral bones within cartilages. Therefore, two aims of my thesis work were to (1) find evidence for the existence of expression domains of morphogens such as Pthlh that may pattern HZs in the zebrafish jaw and (2) investigate the mechanisms that initiate the process of endochondral ossification. Here, I show that expression domains of *pthlha* in the mesenchyme surrounding the cartilage are necessary and sufficient to pattern HZs in the zebrafish jaw cartilage by using a combination of analysis of *pthlha* loss-of-function mutants, *in situ* hybridization for *pthlha*, and mosaic ectopic misexpression of *pthlha* in the cartilage. These findings suggest that Pthlh signaling helps establish the Pthlh/Ihh negative feedback loop that regulates GP homeostasis and bone elongation (Chapter II). In addition, using paralysis of zebrafish embryos, I show that mechanical force has at least two distinct functions in developing cartilages: it promotes chondrocyte proliferation in chondrocytes excluded from the hypertrophic zone, and it is required for HZs to develop (Chapter III). In Chapter IV, I identify a new

perichondrial marker, which I use to show that tendon-cartilage attachments and endochondral ossification form in mutually exclusive zones. Finally, in Chapter V, I describe attempts to use laser ablation to study correlations between chondrocyte morphogenesis and polarity and endochondral ossification zones. This work furthers our understanding of endochondral ossification initiation and patterning in embryonic cartilages and helps establish a foundation for further studies to explore the relationship between endochondral ossification patterns and D-V patterning by identifying a population of cells that produce the inhibitory signal that patterns endochondral bones.

CHAPTER II

Patterning of the hypertrophic zone in embryonic zebrafish cartilages requires

pthlha

Introduction

Most bones in our bodies are derived from cartilage via endochondral ossification, a process of cartilage replacement that requires the formation of hypertrophic zones (HZ). In these zones, chondrocytes undergo hypertrophy, which is the last stage of chondrocyte differentiation and the initial step of the ossification program. The locations of these HZs within cartilages determines the position of the growth plates (GP), cartilage structures within bones that drive bone elongation via proliferation and hypertrophic differentiation. The main signals and mechanisms maintaining GPs in bones are known. However, the mechanisms that initially pattern HZs within naive cartilages are not well understood.

Interactions between different cell types within the cartilage involve multiple signaling pathways that maintain mature GPs. Two secreted signals, Indian Hedgehog (Ihh) and Parathyroid Hormone-Like Hormone (Pthlh) form a negative feedback loop that is considered the master regulator of GPs, controlling both their size and shape (Vortkamp et al., 1996). The long bones of higher vertebrates have a primary ossification center, or primary spongiosa, that appears midway along the long axis of the cartilage anlagen, followed by secondary ossification centers that appear at both ends. The chondrocytes in between these centers form GPs, which are subdivided into three basic zones: the HZ adjacent to the primary ossification center, the resting zone

(RZ) adjacent to the secondary ossification center, and the proliferating zone (PZ) in between. The HZ at the leading edge of ossification consists of hypertrophic chondrocytes (HC), which exit the cell cycle, swell with vacuoles, secrete large amounts of extracellular matrix (ECM) proteins such as Collagen X (*Col10a1*), express Indian Hedgehog (*Ihh*), and initiate apoptosis (Kronenberg, 2003). *Ihh* from the HZ induces osteoblasts in the perichondrium, a thin layer of cells surrounding cartilages, which use the ECM left by dying HCs as a template to make bone (St-Jacques et al., 1999). *Ihh* from the HZ also induces *Pthlh* in the RZ, which maintains a reserve chondrocyte population that subsequently proliferates and hypertrophies as the bone grows (Vortkamp et al., 1996). In turn, *Pthlh* delays hypertrophic differentiation in the PZ by inhibiting *Ihh* expression indirectly via its repression of Runt-Related Transcription Factor 2 (*Runx2*), allowing proliferating chondrocytes (PC) to expand the PZ (Chung et al., 1998; Li et al., 2004; Schipani et al., 1997; Weir et al., 1996; Yoshida et al., 2004). As PCs move further away from the RZ and become exposed to *Ihh* from the HZ, PCs become HCs (Vortkamp et al., 1996). Hence, this *Ihh/Pthlh* signaling loop controls the rate at which GPs produce HCs, thereby controlling bone growth rates.

Once GPs are established, *Pthlh* continues to maintain GP architecture due to its long-range and indirect repression of *Ihh*. However, whether *Pthlh* performs this same function in embryonic cartilages and nascent HZs as they form is unclear. Previous studies disrupting *Pthlh* signaling have been inconclusive. First, *Pthlh* knockout leads to premature ossification and decreased cartilage proliferation due to PC depletion, while cartilage-targeted expression of constitutively active *Pthlh* receptor, *Pth1r*, decreases both ossification and proliferation due, at least in part, to reduced *Ihh* expression.

However, these manipulations do not change the locations of initial ossification (Schipani et al., 1997). Second, in mouse chimeric GPs containing a mixture of wild-type (WT) and *Pth1r*^{-/-} mutant cells, mutant cells hypertrophy prematurely, and if located within the PZ, these mutant cells increase PZ size due to local *Pthlh* upregulation. Large enough *Pth1r*^{-/-} mutant cell islands within the PZ form ectopic ossification centers, but these do not alter the basic primary and secondary ossification center patterns of the developing bone, likely due to the relatively large size of mouse cartilages and a preference of cartilages to respond to the presence of small ectopic HZs via proliferation (Chung et al., 1998). Furthermore, cartilage-targeted expression of ectopic *Pthlh* leads to severe ossification delay and morphological defects in primary and secondary ossification centers, which form in a reversed temporal order than their normal sequence of appearance, but basic HZ patterning is largely unaffected (Weir et al., 1996). These studies show that cartilage proliferation and ossification actively adapt to changes in *Pthlh* signaling. However, previous manipulations were either performed too late in cartilage development or were diluted by the size of fetal mouse cartilages to test roles of *Pthlh* in the initial positioning of HZs.

Craniofacial cartilages in the embryonic and larval zebrafish provide a relatively simple system for testing these early roles for *Pthlh*. Most of these cartilages start out with only a few linear rows of chondrocytes with orders of magnitude fewer cells than their mammalian counterparts. The ceratohyal (ch) cartilage in particular, which supports the jaw, is a rod-like cartilage with a primary ossification center in the middle forming between 72-96 hours post-fertilization (hpf), and secondary ossification centers near the ends forming between 6-21 days post-fertilization (dpf), much like cartilages

that prefigure mammalian long bones (Brinkley et al., 2016). However, unlike their mammalian counterparts, zebrafish jaw cartilages do not proliferate until after 96 hpf (Kimmel et al., 1998), meaning that the primary HZ forms before proliferation can play a role in the process. Primary HZ formation in ch has been described using *in situ* hybridization for *ihhb*, *col10a1a*, *runx2b*, and *ptch1* (Eames et al., 2011). However, new transgenic lines that label HCs simplify detection of primary HZs (Mitchell et al., 2013). Zebrafish have two *Pthlh* homologs, *pthlha* and *pthlhb*. While *pthlhb* has a very restricted expression pattern in the zebrafish jaw, *pthlha* is more similar to mammalian *Pthlh* in expression pattern, homology, and loss of function phenotype (Yan et al., 2012). The combination of these factors is ideal to test *pthlha* signaling manipulations on ch primary HZ patterning while avoiding proliferation-dependent effects that complicate interpretation.

Here, using *entpd5a:kaede* transgenic zebrafish as a marker for HZs, we show that *pthlha* expression in the ch cartilage is inversely correlated to that of the forming primary HZ, and that *pthlha* prevents premature primary HZ expansion along the ch. Furthermore, we show that mosaic ectopic *pthlha* expression in subsets of cells within the ch disrupt primary HZ formation depending of their proximity to one another and can produce ectopic HZs well before the normal establishment of secondary ossification sites. This suggests that these ectopic HZs represent true changes in primary HZ patterning.

Materials and Methods

Ethics statement

All animals were handled in strict accordance with good animal practice as defined by the relevant national and/or local animal welfare bodies, and all animal work was approved by the University of California, Irvine Institutional Animal Care and Use Committee.

Animals and transgenics

All zebrafish used were of the AB strain. Zebrafish were raised and staged as previously described (Kimmel et al., 1995; Schilling and Kimmel, 1997). For anesthesia, a tricaine stock solution was prepared as previously described (Westerfield, 2000), and a working solution was prepared by using 5% of the stock solution in embryo medium (EM). The *sox10:lyn-tdTomato* transgenic line was previously generated in our lab (Schilling et al., 2010). Transgenic lines *entpd5a:kaede*, *entpd5a:PK-Red*, and *col10a1a:YFP* were kindly provided by Dr. Stefan Schulte-Merker (Lleras Forero et al., 2018; Mitchell et al., 2013).

Mosaic *pthlha* expression was done using the Gateway Tol2 system (Kawakami and Shima, 1999; Kwan et al., 2007) in combination with Gibson cloning (Gibson et al., 2009). Briefly, primer pairs caaaaaagcaggctggacATGAGGATGTTGTGTTGCAG and ccgatccGCAGCTGTACGGCTGCAG were used to amplify the open reading frame of *pthlha* from the pGEMT-*pthlha* (see *in situ* hybridization section below) by PCR. Primer pairs acagctgcGGATCCGGAGCCACGAAC and gtgctataggctgcaTCAGGAGAGCACACTTGC were used to amplify *T2A-eGFP*-

CAAX from Tol2 Kit plasmid p3E-2A-EGFP-CAAXpA by PCR. Finally, primer pairs tgagagagGGATCCGGAGCCACGAAC and gtgctatagggctgcaCTTGACAGCTCGTCCATGC were used to amplify *T2A-nlsmCherry* from Tol2 Kit plasmid p3E-2A-*nlsmCherry*pA by PCR. To generate pME-*pthlha-T2A-eGFP-CAAX* middle entry vector, NcoI/PstI-digested Tol2 Kit pME-*eGFP* vector was combined with *pthlha* and *T2A-eGFP-CAAX* amplicon in a Gibson reaction prepared as previously described (Gibson et al., 2009). Similarly, pME-*pthlha-T2A-nlsmCherry* middle entry vector was generated using *pthlha* and *T2A-nlsmCherry* amplicons by Gibson cloning. We used a p5E-*col2a1a* plasmid (Dale and Topczewski, 2011) as a promoter. These plasmids were transformed into DH5 α competent cells (in-house generated). pDestTol2pA2-*col2a1a:pthlha-T2A-eGFP-CAAX* and pDestTol2pA2-*col2a1a:pthlha-T2A-nlsmCherry* were assembled according to the Tol2 Kit protocol and transformed into DH5 α competent cells. Transposase mRNA was synthesized from the pCS2FA-transposase plasmid (Kwan et al., 2007) digested with NotI using Invitrogen mMMESSAGE mMACHINE™ T7 ULTRA Transcription Kit (Catalog # AM1345). 500 μ l of cocktail mixes containing 40 ng/ μ l of plasmid and 60 ng/ μ l of transposase mRNA were injected into 1-cell stage embryos.

Alizarin red staining

Alizarin Red S (EM Science, Catalog # AX0485-3) staining was carried out as previously described (Walker and Kimmel, 2007), but with some modifications. Briefly, Alizarin Red was dissolved to 0.5% in H₂O as a stock solution. Staining solution was prepared by adding 10 μ l of this stock solution to 1 ml of EM without methylene blue. Live embryos were kept in staining solution at 28.5°C for 1 hour. After removing the

staining solution and rinsing embryos three times, embryos were left in embryo medium for 30 minutes. After this, embryos were ready for live imaging.

Cyclopamine A treatments

A stock solution of Cyclopamine A (CyA) from LC Labs (Catalog # C-8700) was prepared by resuspending CyA in 100% ethanol to a final concentration of 10 mM. This solution was aliquoted and stored at -20°C. Zebrafish embryos were staged to 72 hpf and treated with a working CyA solution prepared by diluting the stock solution to a final CyA concentration of 50 µM and a final ethanol concentration of 0.5% in zebrafish EM with no methylene blue. A solution of 0.5% ethanol in EM was used as control.

Treatments were carried out in a 28.5°C incubator. Embryos were removed from CyA at 96 hours post-fertilization (hpf), washed with EM 5 times, and placed in EM until they were 120 hpf. At this point, embryos were ready for live imaging.

CRISPR/Cas9 mutagenesis

CRISPR/Cas9 mutagenesis was performed to generate F0 mutants, which were used for our analysis. CRISPR/Cas9 mutagenesis for *pthlha* was carried out following a recently published protocol (Wu et al., 2018). Spacers used to make *pthlha* primers for guide RNA synthesis were the same as in the protocol:

GGGCATCGACGGGCCGCGCCG, AGGATTTTAAGCGGCGCATG,

TCCGGGAGGCGCAGCAGCCC, and TGGTGCCGCGGCGGGTTTG. After

assembling pooled Guide RNA templates by PCR as instructed in the protocol, guide RNAs were synthesized using the MEGAshortscript T7 Transcription Kit from Invitrogen (Catalog # AM1354). Alt-R S.p. Cas9 nuclease 3NLS protein was obtained from

Integrated DNA Technologies (Catalog # 1074182). An injection mix was prepared by diluting the Alt-R S.p. Cas9 nuclease 3NLS protein to 5 μ M and pooled *pthlha* guide RNAs to approximately 800 ng/ μ l in H₂O. This mix was incubated at 37°C for 5 minutes, then proceeded to inject about 500 pl of this mix into 1-cell stage embryos.

Imaging

Embryos for live imaging were embedded in 1% low melting point agarose (APEX, Catalog # 9012-36-6) diluted in EM containing 5% of tricaine stock solution. Embryos labeled by *in situ* hybridization were mounted on slides, then imaged on a Zeiss Axioplan 2 microscope equipped with a MicroPublisher 5.0 RTV camera using Volocity software (Improvision). All live imaging, except for Alizarin red stained embryos, was done using a Leica Sp8 confocal microscope equipped with a HC PL APO CS2 40x/1.10 W objective. Imaging of live Alizarin red stained embryos was done using a Nikon ECLIPSE Ti confocal microscope equipped with a Plan Apo VC 20X/0.75 DIC N2 objective. ImageJ/Fiji was used for image processing. R-suite and plugins dplyr, ggplot2, ggsignif, and plyr plugins were used for quantification, analysis and statistical tests (t-test and Wilcox test).

***In situ* hybridization**

To make a *pthlha* probe, primers CAGGACGTAATGCTGAGCCG and GTGGACGTGAGCATTAGGC were used to amplify *pthlha* cDNA prepared from 72 hpf embryo mRNA. The PCR product was cloned into Promega's pGEM-T Easy Vector (Catalog # A1360) to make a pGEMT-*pthlha* plasmid and transformed it into DH5 α cells (in-house generated). The plasmid was digested with NcoI and probe synthesized using

Roche DIG RNA Labeling Mix (Catalog # 11277073910) and SP6 RNA Polymerase (Catalog # 10810274001) as directed. Whole-mount *in situ* hybridization was carried out as previously described (Thisse et al., 1993), with the following modifications.

Synthesized probe was diluted in hybridization buffer to 100 pg/μl. Anti-Digoxigenin-AP, Fab fragments antibody (Roche, Catalog # 11093274910) dilution was 1/1000.

Results

The primary HZ in some embryonic cartilages forms soon after differentiation

The HZ in higher vertebrates is marked by expression of *lhh* and *Col10a1*, and their zebrafish orthologs show similar expression patterns (Eames et al., 2011; Girkontaite et al., 1996; Vortkamp et al., 1996). The zebrafish *col10a1a:YFP* transgene marks HZs and associated osteoblasts starting at 120 hpf (Mitchell et al., 2013). Surprisingly, we found that the *entpd5a:kaede* transgene, which had previously been reported to mark osteoblasts associated with cartilage and the notochord during development and wound repair (Geurtzen et al., 2014; Lleras Forero et al., 2018; Lopez-Baez et al., 2018), appeared to be expressed in the center of the ceratohyal (ch) cartilage at 72 hpf, in a region similar to *col10a1a:YFP* expression but two days earlier.

To determine the identities of these cells, we first generated *sox10:lyn-tdTomato;entpd5a:kaede* double transgenic embryos, in which chondrocyte plasma membranes were labeled in red, and looked for co-expression with *entpd5a:kaede* (green) in the ch cartilage from 72-96 hpf. At 72 hpf, we detected a few kaede-positive chondrocytes in the pre-HZ (Figure 2.1A, B). By 96 hpf, the number of labeled chondrocytes had increased within the forming HZ (Figure 2.1C, D). The position of

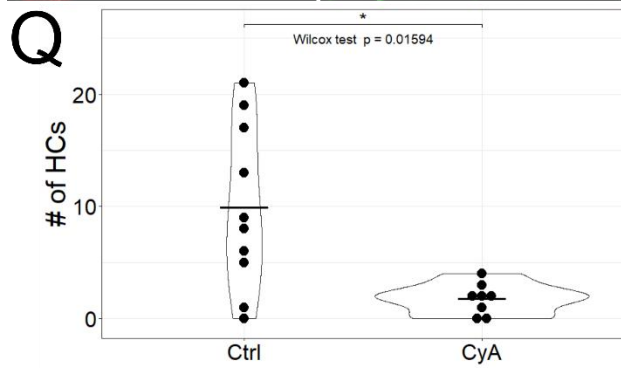
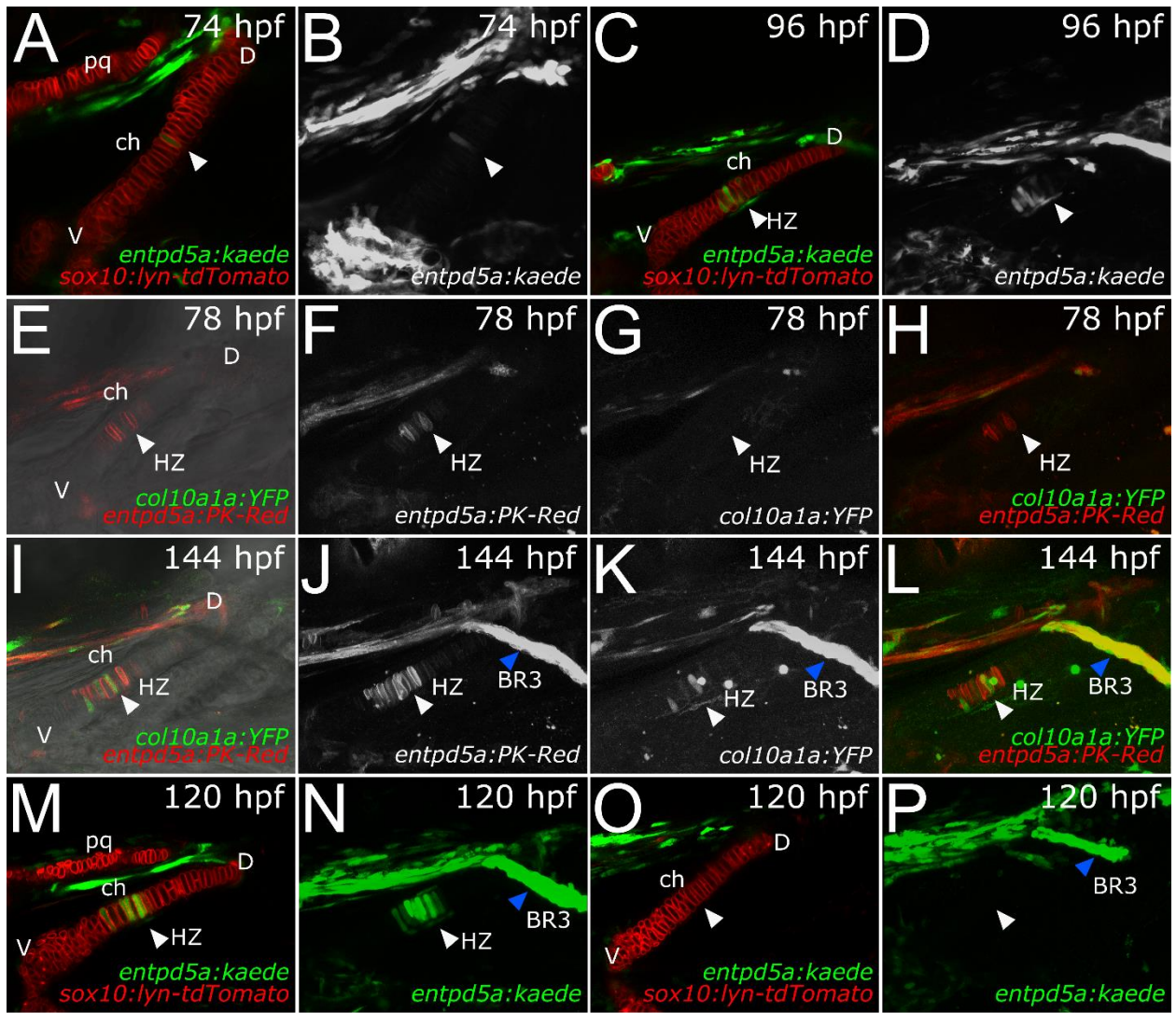


Figure 2.1: Ceratohyal chondrocytes express hypertrophic zone markers soon after embryonic differentiation. (A, B) Live imaging of *sox10:lyn-tdtomato;entpd5a:kaede* double transgenic embryos at 72 hpf, ventral views. (C, D) Live imaging of *sox10:lyn-tdtomato;entpd5a:kaede* double transgenic embryos at 96 hpf, ventral views, anterior to the left. (A, C) Optical slice. (B, D) 3D-projections showing the *entpd5a:kaede* channel. (E-H) Live imaging of *col10a1a:YFP;entpd5a:PK-Red* double transgenic embryos at 78 hpf, ventral views. (I-L) Live imaging of *col10a1a:YFP;entpd5a:PK-Red* double transgenic embryos at 144 hpf, ventral views. (E, I) An optical slice showing the DIC channel. (F, J) Z-projections showing the *entpd5a:PK-Red* channel. (G, K) Z-projections showing the *col10a1a:YFP* channel. (H, L) Z-projections of *col10a1a:YFP;entpd5a:PK-Red* double transgenic embryos. (M-Q) Cyclopamine A treatments of *sox10:lyn-tdtomato;entpd5a:kaede* double transgenic embryos at 120 hpf. (M, N) Vehicle-treated embryos. (O, P) Cyclopamine A-treated embryos. (M, O) Optical slice. (N, P) Z-projections showing the *entpd5a:kaede* channel. (Q) Quantification of *entpd5a:kaede*-positive chondrocytes. White arrowheads indicate the position of the HZ. Blue arrowheads indicate the position of the branchiostegal ray 3. pq= palatoquadrate, ch=ceratohyal, D=dorsal, V=ventral, HZ=hypertrophic zone, BR3=branchiostegal ray 3.

these *entpd5a:kaede*-labeled chondrocytes was consistent with that of well characterized HZ markers (Eames et al., 2011; Mitchell et al., 2013). To confirm that *entpd5a:kaede*-labeled chondrocytes were part of the forming HZ, we generated *entpd5a:PK-Red;col10a1a:YFP* double transgenic embryos and looked for co-expressing cells within the ch cartilage. At 78 hpf, *entpd5a:PK-Red* was already expressed in a few chondrocytes within the forming primary HZ, but *no col10a1a:YFP* expression was detected (Figure 2.1E-H). At 144 hpf, the number of *entpd5a:PK-Red* expressing cells within the primary HZ had increased, and a few *col10a1a:YFP* expressing cells were present within the same zone (Figure 2.1I-L). Moreover, some *col10a1a:YFP*-labeled chondrocytes co-expressed *entpd5a:PK-Red* (Figure 2.1I, L), suggesting that both transgenic lines mark the same HZ. Together, these results suggest that *entpd5a:kaede* precedes *col10a1a:YFP* expression in developing HZs.

If *entpd5a:kaede* marks HZs, it should respond to hedgehog signaling perturbations. HZ formation is delayed in mutants that disrupt *Ihh* signaling (Long et al., 2001; St-Jacques et al., 1999). Therefore, we used the Smoothened (Smo) antagonist cyclopamine A (CyA) to treat *sox10:lyn-tdTomato;entpd5a:kaede* double transgenic embryos from 72-96 hpf and examined the number of *entpd5a:kaede*-labeled chondrocytes at 120 hpf. While mock-treated embryos had an average of 9.9 *entpd5a:kaede*-labeled chondrocytes (n=10), CyA-treated embryos had significantly fewer kaede-positive cells (1.8/embryo; n=8; p = 0.016) indicating that *entpd5a:kaede* expression requires Hh signaling (Figure 2.1M-Q). Together, these results support the hypothesis that *entpd5a:kaede* is the earliest known HZ marker, and that HZs are specified soon after embryonic cartilage differentiation.

Distal expression of *pthlha* is required to pattern the HZ in ch

In the *Ihh/Pthlh* feedback loop that maintains GP homeostasis, *Pthlh* expressed in the RZ represses expansion of the HZ (Chung et al., 1998; Schipani et al., 1997). Its zebrafish ortholog, *pthlha*, is expressed in developing craniofacial cartilages prior to the onset of ossification (Yan et al., 2012). However, the locations of *pthlha* expression with respect to forming HZs have not been carefully examined. If *pthlha* plays a role in patterning HZs in embryonic cartilages, we expect an inverse correlation between sites of *pthlha* expression and HZ patterning. Therefore, we performed whole mount *in situ* hybridization for *pthlha* in zebrafish and found that, both at 66 and 72 hpf, *pthlha* expression in ch was restricted to the ventral and dorsal ends of the cartilage (Figure 2.1), while the mid-region of ch, which corresponds to the location of *entpd5a:kaede* expression and primary HZ formation, showed no *pthlha* expression. These results suggest that *pthlha* is already excluded from the region that forms the primary HZ at early embryonic stages, consistent with a role in spatial and temporal regulation of its formation.

Null *Pthlh* mouse mutants have increased and premature ossification, a lack of chondrocyte proliferation leading to smaller cartilages, and post-natal lethality likely due to respiratory failure as a consequence of ribcage defects (Karaplis et al., 1994). Similarly, morpholino (MO) knock-down of zebrafish *pthlha* led to increased endochondral ossification (Yan et al., 2012), suggesting functional conservation between zebrafish *pthlha* and mouse *Pthlh*. However, this is unlikely to represent a complete *pthlha* knock-down since MOs lose their effectiveness as development

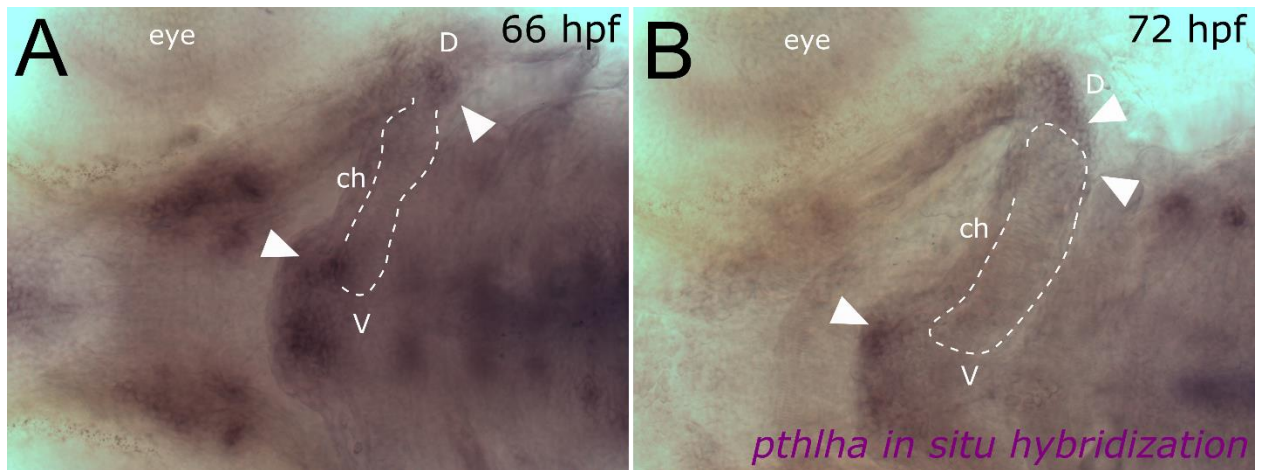


Figure 2.2: *pthlha* is expressed at the distal ends of ch. (A, B) *In situ* hybridization for *pthlha* mRNA at 66 hpf (A) and 72 hpf (B), ventral views, anterior to the left. White arrowheads indicate *pthlha* expression zones. ch=ceratohyal, D=dorsal, V=ventral.

progresses. In order to test if *pthlha* patterns HZs, we took advantage of a recent method for efficient CRISPR-Cas9 F0 mutagenesis (Wu et al., 2018), generated *pthlha* F0 mutants in the *sox10:lyn-tdTomato;entpd5a:kaede* double transgenic background and examined changes in numbers and locations of *entpd5a:kaede-labeled* chondrocytes at 120 hpf. While non-CRISPR-Cas9 injected controls had 15.6 *entpd5a:kaede-labeled* chondrocytes on average (n=8), *pthlha* F0 mutants had significantly more *entpd5a:kaede-labeled* chondrocytes on average (28.5/embryo; n=15; t-test $p=0.0005$) compared with non-injected controls (Figure 2.3A, B, D, E, G). The zone of *entpd5a:kaede-labeled* chondrocytes expanded dorsally along the ch in *pthlha* F0 mutants, as evident from the presence of *entpd5a:kaede-labeled* chondrocytes and perichondrial osteoblasts much closer to branchiostegal ray 3, which extends away from the dorsal edge of the ch, than in non-injected controls (Figure 2.3B, E). Therefore, *pthlha* is required to dorsally restrict PHC in the ch cartilage.

The ch cartilage in juvenile zebrafish, like mammalian long bones, has primary ossification zones in the mid-region along its long axis and secondary ossification zones at the ends. The ventral secondary zone is first visible in Alizarin Red stained embryos at 144 hpf (Figure 2.4D), while the dorsal zone becomes visible by Alizarin Red staining at approximately one month of age (not shown). Interestingly, all *pthlha* CRISPR F0 mutants showed *entpd5a:kaede-labeled* chondrocytes at the ventral end of the ch at 120 hpf, compared to only 1 out of 8 non-injected controls (Figure 2.3A, B, D, E), suggestive of a premature ventral secondary HZ. No *entpd5a:kaede-labeled* chondrocytes were ever observed at the dorsal end of the ch in either controls or F0 mutants at this stage. Furthermore, all *pthlha* CRISPR F0 mutants had an

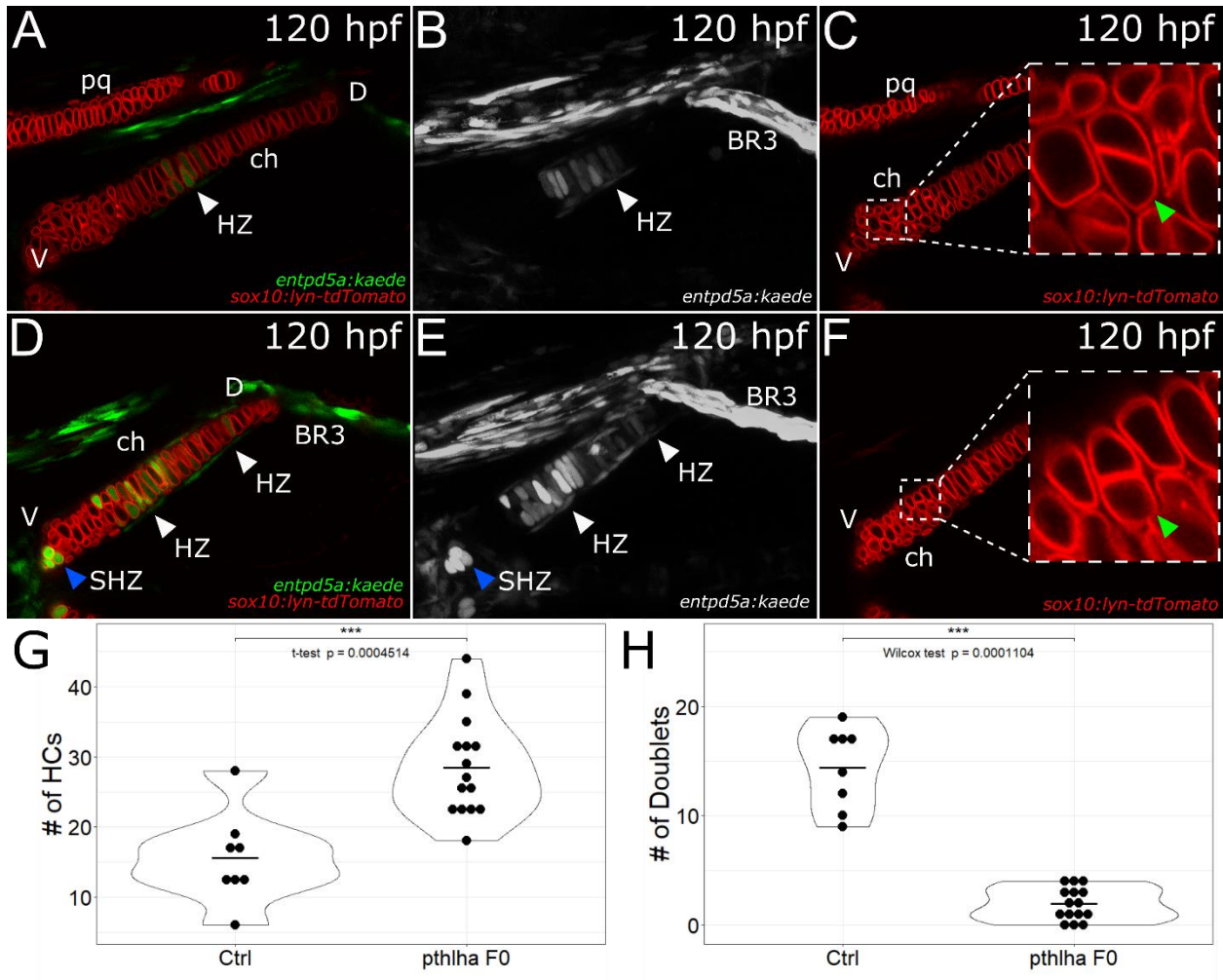


Figure 2.3: *pthlha* restricts dorsal expansion of the ch primary HZ. (A-C) Live imaging of wild-type *sox10:lyn-tdTomato;entpd5a:kaede* double transgenic embryos, ventral views. (D-E) Live imaging of *pthlha* CRISPR F0 *sox10:lyn-tdTomato;entpd5a:kaede* double transgenic embryos, ventral views. (A, D) Optical slices. (B, E) 3D-projections showing the *entpd5a:kaede* channel. (C, F) Optical slices showing the *sox10:lyn-tdTomato* channel. Chondrocyte doublets are shown in insets. (G) Quantification of *entpd5a:kaede*-positive chondrocytes in the ceratohyal. (H) Quantification of chondrocyte doublets in the ceratohyal. White arrowheads indicate the position of the hypertrophic zone. Blue arrowheads indicate the position of the secondary hypertrophic zone. Green arrowheads indicate the position of chondrocyte doublets. pq=palatoquadrate, ch=ceratohyal, HZ=hypertrophic zone, SHZ=secondary hypertrophic zone, D=dorsal, V=ventral, BR3=branchiostegal ray 3.

entpd5a:kaede-free zone between the center and the ventral end of the cartilage (Figure 2.2A, B, D, E). These results suggest that loss of Pthlh signaling leads to early onset and expansion of both primary and secondary HZs.

In addition to the obvious increase cell number and size of the *entpd5a:kaede*-labeled domain, *pthlha* F0 mutants also appeared to have shorter cartilages. Since *Pthlh* mutant mice also have smaller cartilages due to decreased proliferation (Karaplis et al., 1994), we examined proliferation rates in *pthlha* F0 mutants. PCs secrete large amounts of ECM that encapsulates and separates them from each other. However, chondrocytes that have just undergone cytokinesis do not have ECM in between their cellular membranes and appear as symmetrical “doublets”. We took advantage of this to quantify the number of doublet chondrocytes in the same dataset and found that while non-injected controls had 14.8 doublets on average (n=8), *pthlha* F0 mutants had significantly less (1.9/embryo; n=15; p= 0.0001) suggesting that proliferation rates at 120 hpf are reduced in *pthlha* F0 mutants (Figure 2.3 C, F, H). Furthermore, most doublet chondrocytes were detected on the ventral portion of the ch cartilage. Together, these results suggest that *pthlha* plays roles in patterning HZs and maintaining PCs.

Mosaic misexpression of *pthlha* in cartilage leads to bone collar disruption.

Targeted expression of the Jansen Syndrome (constitutively active) human *PTHLH* receptor (*PTH1R*) to differentiating chondrocytes in mice under the control of a rat *Col2a1* promoter delays primary HZ formation, yet ossification patterns appear normal (Schipani et al., 1997). In contrast, targeted expression of human *PTHLH* in mouse cartilages using a mouse *Col2a1* promoter severely delays primary HZ formation, allowing secondary HZs to form first. The primary HZ eventually forms in the

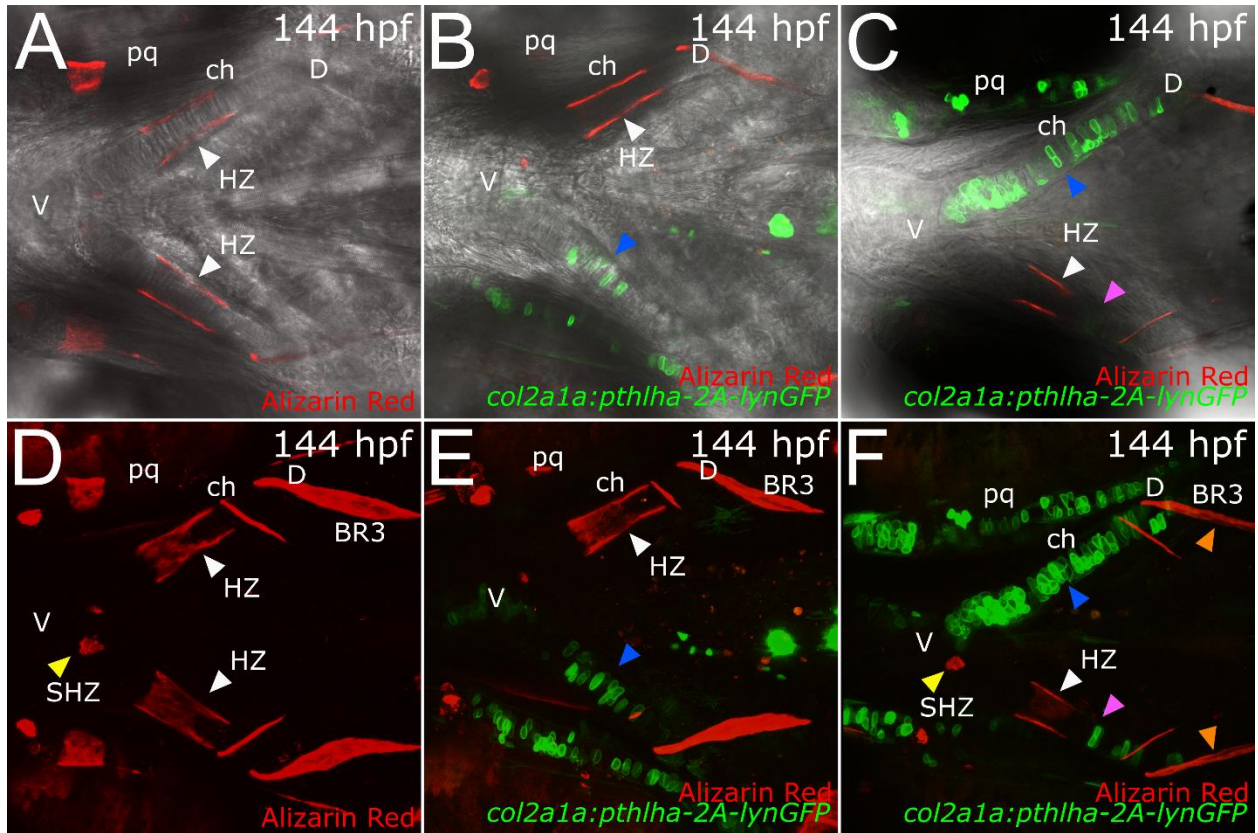


Figure 2.4: Mosaic *pthlha* expression disrupts bone collar as a function of proximity and number of expressing cells. (A, D) Live imaging of wild-type embryos treated with Alizarin Red, ventral views. (B, C, E, F) Live imaging of mosaic *col2a1a:pthlha-2A-lynGFP* transgenic embryos treated with Alizarin Red, ventral views. (A-C) Optical slices showing the DIC channel. (D-F) 3D-projections. White arrowheads indicate the position of the HZ. Blue arrowheads indicate the position of *col2a1a:pthlha-2A-lynGFP* expressing cells. Yellow arrowheads indicate the position of the SHZ. Magenta arrowheads show the position of a *col2a1a:pthlha-2A-lynGFP*-positive cell disrupting bone collar formation. Orange arrowheads indicate the position of the branchiostegal ray 3, which is undisrupted by *pthlha*. pq=palatoquadrate, ch=ceratohyal, HZ=hypertrophic zone, SHZ=secondary hypertrophic zone, D=dorsal, V=ventral, BR3=branchiostegal ray 3.

center of the cartilage element, but only the outermost part of this HZ ossifies (Weir et al., 1996). We hypothesized that the discrepancy between these two experiments is because, unlike *PTH1R*, which should be available in all chondrocytes irrespective of their position within the cartilage, *PTH1H* forms a gradient that accumulates more in the center of the cartilage element, inhibiting ossification. Since both experiments perturbed *PTH1H* or *PTH1R* globally throughout cartilage, we might expect that primary HZ patterning will change if *pth1h* is expressed in localized, ectopic zones within the cartilage.

To test this hypothesis, we made a fusion construct to polycistronically co-express *pth1h* and *lyn-GFP* under the control of a zebrafish *col2a1a* promoter using a backbone that uses a Tol2 transposase-dependent system to integrate into the genome, and injected DNA encoding this construct into 1-cell stage embryos. This resulted in mosaic transgenic F0 zebrafish, which were assessed for effects of localized *pth1h* expression, marked by *lyn-GFP* expression, on ossification (i.e. formation of a bone collar) around the primary HZ. Bone collars formed normally in non-injected 144 hpf embryos, as assessed by live Alizarin Red staining (Figure 2.4A, B). However, mosaic transgenic ch cartilages with ectopic *pth1h* expression in the mid-region of the cartilage had no bone collars (Figure 2.4B, C, E, F), while they formed normally in ch cartilages lacking ectopic *pth1h* expression, including the contralateral ch in many cases, serving as an internal control. In addition, ectopic *pth1h* expression did not disrupt formation of dermal bones, such as the branchiostegal rays associated with ch cartilages (Figure 2.4C, F), which do not develop from a cartilage intermediate and are largely *Ihh* and by inference *Pthlh*, independent (Felber et al., 2011). Interestingly, reductions in bone

collar formation were more severe when the ectopic *pthlha*-expressing cells were greater in number and closer to the middle of the cartilage (Figure 2.4C, F). We never observed ectopic bone collars form in any mosaic transgenics. Together, these results suggest that, if located sufficiently close, cells expressing ectopic *pthlha* can potentially inhibit bone collars forming around primary HZs, though this does not alter the location of these bone collars at 144 hpf.

Mosaic misexpression of *pthlha* in cartilage disrupts primary HZ patterning.

Ectopic mosaic expression of *pthlha* in cartilage led to bone collar loss or reduction but not bone collar patterning changes. However, our analyses of effects at 144 hpf were potentially too early to detect these effects given that previous studies targeting ectopic human *PTH LH* to mouse cartilages led to initial delay in HZ formation, HZ patterning disruptions at later stages, and late bone collar formation at these ectopic HZs (Weir et al., 1996). Therefore, it is possible that ectopic *pthlha* expression simultaneously disrupts HZ patterning and delays bone collar formation, particularly given osteoblast susceptibility to *Ihh* signaling perturbations (Felber et al., 2011). To test this idea, we made a similar DNA construct in which we replaced *lyn-GFP* with nuclear localized mCherry, then tested the effects of mosaic ectopic *pthlha* on *entpd5a:kaede* reporter expression patterns. Since the *entpd5a:kaede* reporter expression is not limited to HZs, brightfield optics were used to draw outlines of ch cartilages, and HCs were localized within the outlines (Figure 2.4A-D). In 120 hpf mosaic transgenic F0 zebrafish, within the same fish, while HZs formed normally in ch cartilages that did not express ectopic *pthlha* (Figure 2.4E, F), HZs had decreased numbers or complete absence of HCs in ch cartilages that expressed ectopic *pthlha* where we expected the HZ to form

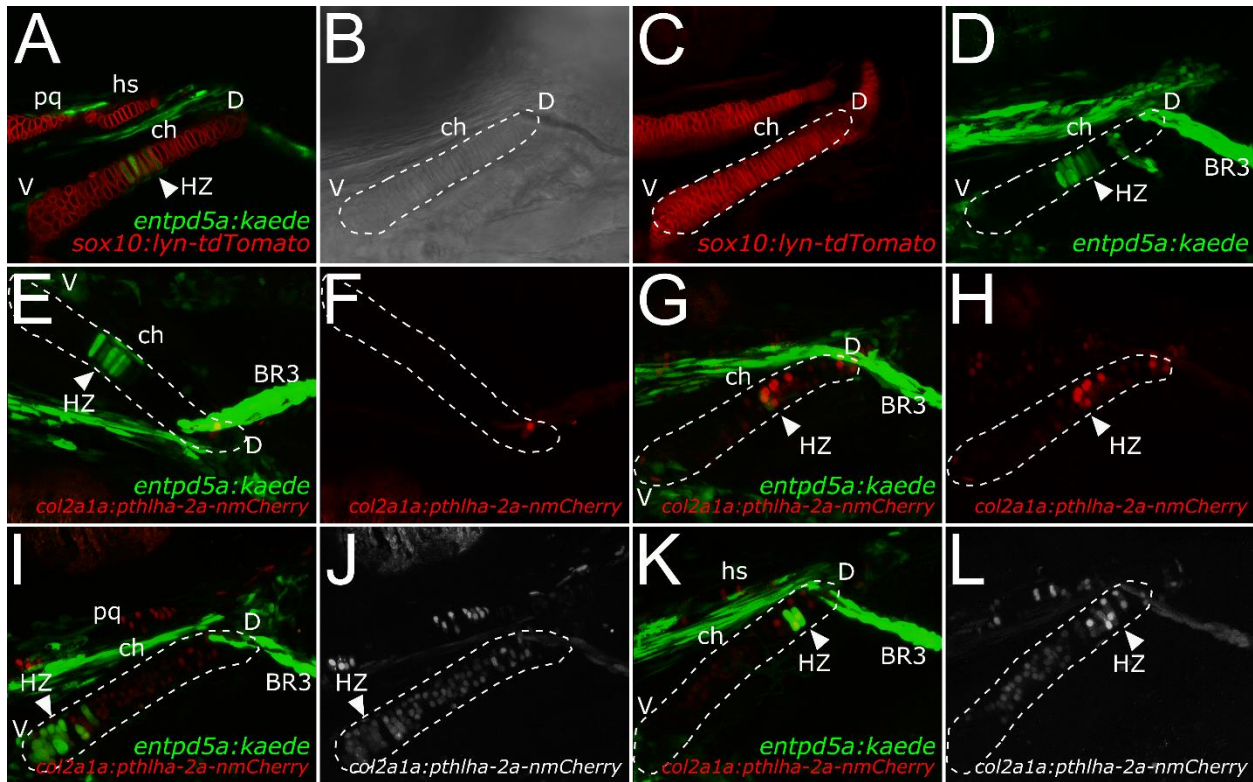


Figure 2.5: Mosaic *pthlha* expression disrupts HZ patterning. (A-D) Live imaging of a wild-type *sox10:lyn-tdTomato;entpd5a:kaede* double transgenic embryo, ventral views, anterior to the left. (A) An optical slice. (B) DIC channel, used to draw an outline of the ceratohyal. (C) 3D-projection showing the *sox10:lyn-tdTomato* channel, outline drawn in (B). (D) 3D-projections showing the *entpd5a:kaede* channel, outline drawn in (B). (E-H) Live imaging of an *entpd5a:kaede* transgenic embryo made mosaic transgenic for *col2a1a:pthlha-2A-nmCherry*, ventral views. (E, F) Control side with no *col2a1a:pthlha-2A-nmCherry* expression; *entpd5a:kaede* in the HZ is undisrupted. (E) An optical slice. (F) 3D-projection only showing the *col2a1a:pthlha-2A-nmCherry* channel. (G, H) Transgenic side with *col2a1a:pthlha-2A-nmCherry* expression, *entpd5a:kaede* in the HZ is disrupted. (G) An optical slice. (H) 3D-projection only showing the *col2a1a:pthlha-2A-nmCherry* channel. (I, J) Live imaging of an *entpd5a:kaede* transgenic embryo made mosaic transgenic for *col2a1a:pthlha-2A-nmCherry*, ventral views; *col2a1a:pthlha-2A-nmCherry* expression moves the HZ to the ventral part of the ceratohyal. (I) An optical slice. (J) 3D-projection showing the *col2a1a:pthlha-2A-nmCherry* channel. (K, L) Live imaging of an *entpd5a:kaede* embryo made mosaic transgenic for *col2a1a:pthlha-2A-nmCherry*, ventral views; *col2a1a:pthlha-2A-nmCherry* expression moves the HZ to the dorsal part of the ceratohyal. (K) An optical slice. (L) 3D-projection showing the *col2a1a:pthlha-2A-nmCherry* channel. White arrows indicate the position of the HZ. pq=palatoquadrate, ch=ceratohyal, hs=hyosymplectic, HZ=hypertrophic zone, D=dorsal, V=ventral, BR3=branchiostegal ray 3.

(Figure 2.4G, H). These results suggest that disruption of bone collar in our mosaic transgenic zebrafish was likely due to abrogation of HZ formation.

Interestingly, in some cases when ectopic *pthlha* expression was in much of the ch cartilage, ectopic HCs appeared either on the ventral (Figure 2.4I, J) or dorsal edge of the ch cartilage (Figure 2.4K, L). In all these cases, at least a few of these ectopic HCs expressed ectopic *pthlha*. Furthermore, chondrocytes expressing ectopic human *PTH1R*, as well as constitutively active *PTH1R*, become hypertrophic, albeit with some delay (Schipani et al., 1997; Weir et al., 1996). However, none of the ectopic HZs had any adjacent osteoblasts, which is consistent with our analysis of bone collars in our *col2a1a:pthlha-2A-lyn-GFP* mosaic transgenic embryos. Altogether, these results suggest that *pthlha* not only restricts the primary HZ to the mid-cartilage region but also determines HZ position along the length of the cartilage. These results also suggest that HZ positioning and chondrocyte hypertrophic differentiation potential are not pre-determined in cartilages but rather plastic and relative to Pthlh signaling.

Discussion

In this study, we show, for the first time, that *pthlha* contributes to determining the initial location of the primary HZ during early patterning of cartilage elements. We find that HZs in embryonic zebrafish cartilages form much earlier than previously suspected, that they require Hh signaling, and that the early onset of distinct zones of *pthlha* expression prefigures these HZs. Perturbation of *pthlha* alters both the timing and spatial distribution of HZs. Thus, the same Pthlh/Ihh feedback loop that maintains GPs later in endochondral bones appears to establish their spatial patterns in the embryo. These results are consistent with previous studies showing that Pthlh signaling maintains a

pool of PCs by controlling the rate of hypertrophic differentiation in HZs (Chung et al., 1998; Schipani et al., 1997; Vortkamp et al., 1996; Weir et al., 1996). However, our analysis of mosaic cartilages ectopically expressing *pthlha* also revealed that Pthlh signaling is both necessary and sufficient to pattern the locations of early HZs along the length of the cartilage, which differs from similar studies in mice where the locations of HZs were essentially unchanged after similar manipulations of Pthlh signaling (Chung et al., 1998; Schipani et al., 1997; Weir et al., 1996).

Expression of *entpd5a:kaede* reveals an early primary HZ in embryonic cartilages

Several lines of evidence support the hypothesis that *entpd5a:kaede* transgenic zebrafish mark early HZs, at least in the ch cartilage. First, some *entpd5a:kaede*-labeled chondrocytes co-expressed *col10a1a:YFP* at 144 hpf. The prehypertrophic zone (PHZ) is a transitional zone between the PZ and the HZ that is defined by prehypertrophic chondrocytes (PHC) that express *Col10a1* and high levels of *Sox9*, contrasting with the HZ which completely lacks *Sox9* expression since *Sox9* functions in PHC to block further hypertrophic differentiation (Akiyama et al., 2004; Bi et al., 2001; Hattori et al., 2010; Zhao et al., 1997). Since *entpd5a:kaede*-labeled chondrocytes lack classic HC morphology, the presence of chondrocytes co-expressing *entpd5a:kaede* and *col10a1a:YFP* suggests that at least some *entpd5a:kaede*-labeled chondrocytes are PHCs. Second, the expression of *entpd5a:kaede* in chondrocytes was sensitive to *Ihh* signaling perturbations. *Ihh* signaling is required for hypertrophy and ossification to take place and for PCs to embark in hypertrophic differentiation (Chung et al., 2001; Mak et al., 2008; St-Jacques et al., 1999). In addition, *Ihh* signaling is required between 72-96 hpf in zebrafish ch cartilage for bone collars to form, suggesting an early requirement for

Ihh in the perichondrium adjacent to developing HZs (Felber et al., 2011). If expression of *entpd5a:kaede* in chondrocytes is sensitive to Ihh signaling disruptions, it would suggest that *entpd5a:kaede*-labeled chondrocytes are a type of PHC.

Finally, *entpd5a:kaede* was detected in the center of the ch cartilage at 72 hpf, a timepoint when HZ zone markers such as *ihha*, *ihhb*, *runx2b*, and *col10a1a* are absent in the middle of the ch cartilage (Eames et al., 2011). Indeed, *col10a1a:YFP* expression was preceded by *entpd5a:kaede* and *entpd5a:PK-Red* expression in chondrocytes in our study. Since *Col10a1* is the earliest known marker for PHCs (Girkontaite et al., 1996), and considering the sensitivity of *entpd5a:kaede* to Ihh signaling disruptions and its co-expression with *col10a1a:YFP* in HZ chondrocytes, these results suggest that *entpd5a:kaede* is then the earliest known marker for chondrocytes in the hypertrophic lineage. For instance, Transcription Factor 7 (*sp7*; also known as *Osterix*) is required for osteoblast differentiation (Nakashima et al., 2002). Despite this, osteoblasts surrounding the notochord are *sp7* negative, but the *entpd5a:kaede* transgene specifically marks these osteoblasts, suggesting that the pattern of notochord and subsequent vertebral segmentation is encoded in notochord sheath cells (Huitema et al., 2012; Lleras Forero et al., 2018; Wopat et al., 2018; Yu et al., 2017). Therefore, early *entpd5a:kaede*-labeled chondrocytes may represent the initial stages of hypertrophy and patterning of HZs. Previous work has shown that a subset of chondrocytes within the ch cartilage HZ express *sp7* and contribute to matrix mineralization starting at 120 hpf (Hammond and Schulte-Merker, 2009). Furthermore, a subset of osteoblasts can be traced to *col2a1a*-expressing chondrocytes in juvenile zebrafish cartilage GPs, suggesting that some

PHCs differentiate into osteoblasts (Giovannone et al., 2019). It would be interesting to test if *entpd5a:kaede* can mark this set of chondrocytes as well.

Pthlh signaling controls spatial-temporal patterns of embryonic chondrocyte hypertrophic differentiation

We show that *pthlha* expresses at the dorsal and ventral edges of the ch between 66 and 72 hpf, timing and pattern which correlate with that of the early primary HZ in the ch cartilage. Using *pthlha* F0 CRISPR mutants, we demonstrate that *pthlha* is required to prevent dorsal expansion of the primary HZ and to delay the formation of the ventral secondary HZ. In addition, using mosaic zebrafish embryos ectopically expressing *pthlha* in cartilages, we show that *pthlha* disrupts HZ and bone collar formation as a function of number and proximity of *pthlha*-expressing cells to HZs. Finally, we show a few cases in which expression of *pthlha* in ch cartilages can change the location where the primary HZ emerges, especially in cases where the primary HZ forms on the dorsal side of the cartilage since the secondary HZ only forms on the dorsal side of the cartilage at 4 weeks of age. Together, these results suggest that Pthlha protein forms gradients that are necessary and sufficient to control the timing and pattern of HZ expansion and localization. While manipulations in Pthlh signaling disrupt the rate of HZ expansion and the timing of HZ emergence in mice, the same manipulations failed to change the locations along the cartilage where HZs initially formed (Chung et al., 1998; Schipani et al., 1997; Weir et al., 1996). We attribute this difference to a combination of factors. First, mouse long bone cartilages contain orders of magnitude more cells than zebrafish cartilages. Therefore, unlike in zebrafish embryonic cartilages, mosaic manipulations in a few cells likely fail to have global effects on murine cartilages.

Second, murine cartilages can respond to Pthlh signaling manipulations by proliferation. For instance, PZs were enlarged in mosaic mice that contained a few cells mutant for the *Pthlh* receptor *Pth1r* within these PZ compared to WT while the locations of endogenous HZs remained unchanged, which is attributed to the ability of *Pthlh* to maintain surrounding WT cells in a proliferative state (Chung et al., 1998). In contrast, while we did not examine proliferation prior to 120 hpf, zebrafish craniofacial cartilages are known not to proliferate until after 96 hpf (Kimmel et al., 1998).

However, we also showed that the primary HZ failed to expand ventrally in *pthlha* mutants. Furthermore, the bulk of chondrocyte proliferation that we detected in the ceratohyal was found on the ventral side of the cartilage. It is generally understood that PCs must stop proliferating in order to become PHCs. However, this could not account for failure of the primary HZ to expand ventrally since our *pthlha* mutants had a marked decrease in proliferation at 120 hpf. Therefore, an unknown mechanism appears to prevent ventral expansion of the primary HZ. One possibility is the action of additional components of the Pthlh signaling pathway. The *pthlhb* gene is a zebrafish orthologue that is less conserved than *pthlha* with mammalian *Pthlh*. Expression of *pthlhb* appears to be restricted to dorsal craniofacial cartilages and bones and not in ch, but long-range interactions cannot be disregarded (Yan et al., 2012). In addition, zebrafish have two Pthlh receptors, *pthr1a* and *pthr1b*, the activation sensitivity of which varies depending on the ligand they bind (Rubin and Juppner, 1999). Moreover, Parathyroid Hormone 1 (*Pth1*) acts like *Pthlh* in cartilages and can be carried in the bloodstream in rodents (Jee et al., 2018; Yukata et al., 2018). Finally, *pth4* is an ancestral Pth found in zebrafish but lost in eutherian mammals that is expressed in the central nervous system, activates

Pthr1 receptors, and acts to repress mineralization in the skeleton at long range (Suarez-Bregua et al., 2017). Therefore, it is possible that at least some of these factors may play a role in repressing ventral expansion of the primary HZ in *pthlha* mutants. Since all these genes are present in the zebrafish genome, mutating each of these genes and testing their effects in *pthlha* mutants should help elucidate their individual contributions to endochondral ossification patterning.

Conserved requirements for Pthlh signaling in vertebrates

Loss-of-function mutations in murine *Pthlh* lead to increased and premature hypertrophic differentiation, smaller cartilages due to failure to maintain PCs, and lethality associated with abnormal skeletal morphology (Karaplis et al., 1994). Pthlh signaling represses hypertrophic differentiation by repressing *Runx2* transcription, which leads to decreased *Ihh* expression (Li et al., 2004; Yoshida et al., 2004). MO knockdown of *pthlha* in zebrafish leads to increased endochondral bone mineralization, consistent with what is known about *Pthlh* in mice and chicks (Yan et al., 2012). Using CRISPR F0 mutants, we show that *pthlha* is required to restrict PC entry into the prehypertrophic state, thereby limiting osteoblast differentiation and bone ECM mineralization in HZ adjacent perichondrium. Our results show that *Pthlh*'s role in regulating hypertrophic differentiation is conserved in zebrafish *pthlha*.

In addition, *Pthlh* mutants have smaller cartilages (Karaplis et al., 1994). Increased hypertrophic differentiation in HZs leads to upregulation of *Runx2* in adjacent perichondrium, which leads to upregulation of *Fgf18* in the perichondrium to inhibit proliferation in the PZ, thereby limiting the number of PCs that transition into the HZ (Hinoi et al., 2006; Liu et al., 2002; Ohbayashi et al., 2002). Although we did not test this

model directly, we show that *pthlh* mutants have decreased proliferation rates at 120 hpf. This effect is likely not due to depletion of the PC pool since we detected most proliferating chondrocytes (doublets) in the ventral ch region that was free of *entpd5a:kaede*-labeled chondrocytes. Therefore, our results suggest that the role for *Pthlh* in maintaining the pool of PCs is conserved in zebrafish *pthlha*.

Pthlh helps establish the Ihh/Pthlh negative feedback loop in embryonic cartilages

We show that *pthlha* expression in the ch cartilage is found mostly at the distal ends and outside of the cartilage. In addition, we show that *pthlha* expression is required to restrict the expansion of the ch primary HZ. In addition, using mosaic *pthlha* misexpression in zebrafish craniofacial cartilages, we show that Pthlha protein inhibits chondrocyte hypertrophic differentiation and bone formation as a function of the amount and proximity of the *pthlha* source, observation which suggest that Pthlha protein can form gradients. Together, our results suggest that Pthlha protein is initially expressed from these distal domains and restricts the initial HZ to the mid region of the ch cartilage. It was previously thought that the Ihh/Pthlh negative feedback loop was not active until 3 weeks post hatching in chick GPs since *Pth1r* expression was absent from PCs and PHCs before this stage (Vortkamp et al., 1996). However, our results suggest that Pthlh signaling is active close to 72 hpf in the ch cartilage since the primary HZ arises and is patterned from this stage onwards. This is earlier in cartilage development than in the studies in the chick. In addition, *pthlha* appears to be expressed through most of the ch cartilage at a 144 hpf (Yan et al., 2012). We suggest a model in which *pthlha* expression at the distal tips of the ch cartilage restricts development of the

primary HZ to the mid region of the cartilage by restricting the domains of *Ihh* expression. As the primary HZ develops, *Ihh* from the primary HZ promotes expression of *pThlha* in nearby perichondrium. In turn, this induced *pThlha* expression ensures that the primary HZ can only expand slowly and that additional HZs do not form near the primary HZ as the cartilage grows via proliferation. Our model does not contradict the model for the *Ihh/Pthlh* negative feedback loop in growth plates since our analysis was done in cartilages preceding the formation of growth zones/plates. However, the formation of ectopic HZs by *Pth1r*^{-/-} cells that do not mix with endogenous HZ and that enlarge the PZs of mosaic *Pth1r*^{-/-} mutant mice, due to induction of *Pthlh* near *Pth1r*^{-/-} cells, supports our model (Chung et al., 1998). Finally, unlike the establishment of left-right asymmetry, where Nodal, the activator signal, accumulates on the left side of the embryo first and induces expression of Lefty, the inhibitory signal, on the left side of the embryo (Tabin, 2006), our model suggests that *pThlha*, the inhibitory signal, is expressed first and patterns the expression of *Ihh*, the activator signal. Once the activator signal expression domains are established, however, both models are very similar in that the longer range of the inhibitory signal ensures that the activator signal expression remains restricted. Hence, our proposed model for early HZ patterning resembles Reaction-Diffusion models once *Ihh* expression domains are established (Turing, 1990).

CHAPTER III

Initiation of hypertrophic differentiation in embryonic zebrafish cartilages requires mechanical force

Introduction

Most of our bones form via endochondral ossification, a process that replaces cartilages with bone at stereotypical locations. These are called hypertrophic zones (HZ) because they are made of hypertrophic chondrocytes (HC), chondrocytes in their final differentiation stage that secrete signals that initiate the ossification process. While most cartilage is eventually replaced by bone, most endochondral bone growth is driven by Growth Plates (GP), locations within bones that are retained as cartilage in order to drive bone elongation via a combination of proliferation and hypertrophic differentiation. While the mechanisms that maintain GPs are known, those that initiate GP formation and HZ development in embryonic cartilages are poorly understood.

GPs drive bone elongation through continuous chondrocyte proliferation, differentiation, and transition through its three distinct zones: The resting zone (RZ), the proliferating zone (PZ), and the HZ. The RZ contains resting chondrocytes (RC) that are slow dividing and provide a reserve pool for the GP. RCs slowly transition into the PZ and increase their proliferating rate, becoming proliferating chondrocytes (PC). As proliferation increases PCs distance from the RZ, they transition into the HZ to become HCs and initiate the ossification process (Kronenberg, 2003). The prehypertrophic zone (PHZ) is a transition zone between the PZ and the HZ made of pre-hypertrophic chondrocytes (PHC) that express SRY-box Transcription Factor 9 (Sox9), which delays

their hypertrophic differentiation, but also express Indian Hedgehog (*Ihh*) (Akiyama et al., 2004; Bi et al., 2001; Hattori et al., 2010; Zhao et al., 1997). *Ihh* promotes proliferation in the PZ, hypertrophic differentiation in the HZ, and osteoblast differentiation in the perichondrium adjacent to the HZ (Mak et al., 2008; St-Jacques et al., 1999). However, these effects are modulated by two secreted signals. *Pthlh* is expressed and secreted from the distal part of the RZ and forms a gradient that determines PZ size through repression of *Ihh* expression (Chung et al., 1998). In turn, *Ihh* promotes *Pthlh* expression in the RZ through an unknown long-range mechanism, forming a negative feedback loop that controls hypertrophic differentiation rates (Vortkamp et al., 1996). In addition, *Ihh* from the HZ induces expression of *Fgf18* in the PZ adjacent perichondrium, which represses proliferation in the PZ, thereby forming a negative feedback loop with *Ihh* that controls the rates at which PCs exit the *Pthlh* gradient (Hinoi et al., 2006; Ohbayashi et al., 2002). However, it is thought that *Ihh* is not expressed at sufficient levels in locations that will become HZs in embryonic cartilages (Eames et al., 2011), so it is unlikely that any of these mechanisms are present prior to the formation of HZs in embryonic cartilages. Therefore, an additional early signal may be required to start hypertrophic differentiation.

Mechanical force has emerged as an important aspect of development and homeostasis of a variety of tissues (Hamada, 2015). For instance, tendon morphogenesis depends on activation of TGF β signaling in tenocytes, which is thought to be initiated via mechanical force-induced release of TGF β ligands from the extracellular matrix (ECM) (Subramanian et al., 2018). In bone, appropriate levels of mechanical stimulation are required for osteocyte survival (Aguirre et al., 2006; Noble et

al., 2003; Plotkin et al., 2005). Mechanical force is also known to be required for normal GP homeostasis. Mechanical stimulation by muscle contraction is required for chondrocyte proliferation in the PZ of chick GPs (Germiller and Goldstein, 1997). Furthermore, oscillatory tensile forces applied to the cranial base GP of rabbits increase the size of the PZ, suggesting increased chondrocyte proliferation (Wang and Mao, 2002). Interestingly, compressive force has been shown to accelerate hypertrophic cartilage differentiation in the midpalatal suture of rats, but it is unclear if this effect is linked to an increase in chondrocyte proliferation (Saitoh et al., 2000). In addition, the length of the retroarticular process, a dentary bone that forms in association to the Meckel's cartilage, varies between closely-related species of cichlid larvae depending on their differential muscle-dependent mechanical stimulation of the jaw, as measured by gaping rate, an opening and closing of the mouth that helps pump water of the gills. Fish that gape more frequently have longer retroarticular processes and higher levels of Patched 1 (*ptch1*) expression (Hu and Albertson, 2017), though whether cartilage is involved in this effect is unclear. Finally, both Piezo Type Mechanosensitive Ion Channel Component 1 (*Piezo1*) and Transient Receptor Potential Vanilloid 4 (*Trpv4*) mechanosensory channels have been shown to be expressed and active in chondrocytes in vitro (Muramatsu et al., 2007; O'Connor et al., 2014; Servin-Vences et al., 2017). However, only *Trpv4* has been shown to affect SRY-box Transcription Factor 9 (*Sox9*) and Collagen Type II Alpha 1 Chain (*Col2a1*) expression in vitro, genes which play roles in chondrocyte differentiation but not directly on hypertrophic chondrocyte differentiation (Muramatsu et al., 2007; O'Connor et al., 2014). Therefore, no study has

ever demonstrated direct effects of mechanical force on hypertrophic chondrocyte differentiation independent of effects on the RZ and PZ such as increased proliferation.

In this study, we show, for the first time, that mechanical force is required for chondrocyte hypertrophic differentiation independently of chondrocyte proliferation. Taking advantage of the fact that HZ development in the zebrafish ceratohyal (ch) cartilage precedes chondrocyte proliferation by 24 hours (See Chapter II), we show that the ch cartilage HZ does not develop in paralyzed zebrafish embryos. We also show that this effect is not due to developmental delay and is cartilage-specific since dermal bones, which develop independently of cartilages, form normally during paralysis. Finally, we show that the bulk of chondrocyte proliferation is found outside the forming HZ, and that this proliferation is severely reduced in paralyzed embryos. Together, these results suggest that mechanical force promotes bone growth via chondrocyte proliferation and hypertrophic differentiation in GPs.

Materials and Methods

Ethics statement

All animals were handled in strict accordance with good animal practice as defined by the relevant national and/or local animal welfare bodies, and all animal work was approved by the University of California, Irvine Institutional Animal Care and Use Committee.

Animals and transgenics

All zebrafish used were of the AB strain. Zebrafish were raised and staged as previously described (Kimmel et al., 1995; Schilling and Kimmel, 1997). For anesthesia, a tricaine

stock solution was prepared as previously described (Westerfield, 2000), and a working solution was prepared by using 5% of the stock solution in embryo medium (EM). The *sox10:lyn-tdTomato* transgenic line was previously generated in our lab (Schilling et al., 2010). The transgenic line *entpd5a:kaede* was kindly provided by Dr. Stefan Schulte-Merker (Lleras Forero et al., 2018).

Alizarin red staining

Live Alizarin Red S (EM Science, Catalog # AX0485-3) staining was carried out as previously described (Walker and Kimmel, 2007), but with some modifications. Briefly, Alizarin red was dissolved to 0.5% in H₂O as a stock solution. Staining solution was prepared by adding 10 μ l of this stock to 1 ml of EM without methylene blue. Live embryos were kept in staining solution at 28.5°C for 1 hour. After removing the staining solution, embryos were washed three times with embryo medium then placed in EM for 30 minutes. After this, embryos were ready for live imaging.

α -Bungarotoxin injections

α -Bungarotoxin (α -BTX) was acquired from TOCRIS (Catalog # 2133). Embryo paralysis was achieved by injecting 5 nl of α -BTX at 500 μ M into the bloodstream near the heart outflow just posterior to the otic vesicle of 68 hours post-fertilization (hpf) embryos.

Bromodeoxyuridin (BrdU) labeling and staining

BrdU (SIGMA, Catalog # B9285-250MG) labeling and staining was carried out as previously described (Kimmel et al., 1998), with the following modifications. Primary mouse monoclonal anti-BrdU (Clone BU 33) antibody (SIGMA, Catalog # B2531) was

used at 1/100 dilution. Secondary Alexa-647 Donkey anti-mouse IgG (H+L) antibody (Jackson ImmunoResearch Laboratories, Catalog # 715-607-003) was used at 1/200.

Imaging

Embryos for live imaging were embedded in 1% low melting point agarose (APEX, Catalog # 9012-36-6) diluted in EM containing 5% of tricaine stock solution. Alizarin red staining was imaged either using a Nikon ECLIPSE Ti microscope equipped with a Plan Apo VC 20X/0.75 DIC N2 and a Plan Apo VC 60X/1.20 WI DIC N2 objectives, or using a Leica Sp8 confocal microscope equipped with a HC PL APO CS2 40x/1.10 W objective. ImageJ/Fiji was used for image processing. R-suite and plugins dplyr, ggplot2, ggsignif, and plyr plugins were used for quantification, analysis and statistical tests (t-test and Wilcox test).

Results

Paralysis during the onset of jaw movements prevents HZ formation in the ch

In Chapter II, we showed that the *entpd5a:kaede* transgene marks chondrocytes in the developing ch cartilage HZ starting at 72 hpf. We also showed that this expression precedes *col10a1a:YFP* expression, which marks PHCs (Mitchell et al., 2013), and that both *entpd5a:PK-Red* and *col10a1a:YFP* transgenes co-localize in the ch cartilage HZ at 144 hpf. Finally, we showed that expression of *entpd5a:kaede* in the ch cartilage HZ requires *Ihh* signaling between 72 and 96 hpf. Together, these results suggest that *entpd5a:kaede* is the earliest known marker for HZs, and that HZs are specified shortly after embryonic cartilage differentiation.

Figure 3.1: Paralysis between 68-96 hpf prevents HZ formation. (A, B) Live imaging of a wild-type *sox10:lyn-tdTomato;entpd5a:kaede* double transgenic embryo at 96 hpf, ventral views. (A) An optical slice. (B) 3D-projection showing the *entpd5a:kaede* channel. (C, D) Live imaging of a paralyzed *sox10:lyn-tdTomato;entpd5a:kaede* double transgenic embryo at 96 hpf, ventral views; the HZ does not develop. (C) An optical slice. (D) 3D-projection showing the *entpd5a:kaede* channel. (E) Quantification of number of *entpd5a:kaede*-positive chondrocytes in the ch. White arrowheads indicate the position of the HZ. pq=palatoquadrate, ch=ceratohyal, hs=hyosymplectic, HZ=hypertrophic zone, D=dorsal, V=ventral.

Two studies have implicated mechanical force in bone growth (Hu and Albertson, 2017; Wang and Mao, 2002). However, mechanical force also promotes cartilage proliferation in PZ, so given the organization of GPs, this would be expected to result in increased hypertrophic differentiation as PCs move away from the RZ at faster rates. Therefore, whether mechanical force has a proliferation-independent effect on chondrocyte hypertrophic differentiation remains unaddressed. Given that zebrafish craniofacial cartilages do not proliferate until after 96 hpf (Kimmel et al., 1998), that craniofacial muscles begin contracting and applying force to cartilage between 66-72 hpf (Subramanian et al., 2018), and our observation that HZ development in the ch cartilage begins around 72 hpf, we hypothesized that mechanical initiates hypertrophic differentiation.

To test this hypothesis, we paralyzed 68 hpf *sox10:lyn-tdTomato;entpd5a:kaede* double transgenic embryos by injecting them with alpha bungarotoxin (α -BTX), an acetyl-choline receptor antagonist into the bloodstream, and examined the number of co-expressing cells in the primary HZ of the ch cartilage at 96 hpf. While non-injected embryos had 12.70 co-expressing cells in the primary HZ on average (n=20), α -BTX-injected embryos had significantly fewer co-expressing cells on average (0.45/embryo, n=20; p= 1.286e-07), suggesting that HZ development in embryonic cartilages requires mechanical force (Figure 3.1). In addition, ch cartilages in paralyzed embryos appeared shorter than those of non-injected embryos. This effect is not due to reduced proliferation since chondrocytes do not proliferate between 68 and 96 hpf (Kimmel et al., 1998). Together, these results suggest that mechanical force is required for the onset of HZ formation in embryonic cartilages.

Loss of hypertrophic differentiation during paralysis is not due to developmental delay.

Our results from paralyzed embryos suggested that mechanical force is required for HZ development. However, one concern is that this effect may be due to developmental delay and not a specific effect on chondrocytes. The branchiostegal ray 3 (BR3) is a dermal bone that forms independently of cartilage via direct ossification of mesenchymal progenitors. In addition, the BR3 and the ch cartilage are derived from adjacent neural crest-derived progenitors. Therefore, the BR3 serves as a control for cartilage-specific versus global maturation effects. Therefore, we monitored the development of BR3 in *sox10:lyn-tdTomato;entpd5a:kaede* double transgenic embryos during paralysis (Figure 3.2A-C). At 72 hpf, the BR3 was absent, and an occasional *entpd5a:kaede*-positive BR3 progenitor was detected (Figure 3.2A). By 96 hpf, Alizarin Red live staining of *sox10:lyn-tdTomato;entpd5a:kaede* double transgenic embryos revealed that the BR3 was already present and had formed mineralized bone matrix in between the osteoblasts marked by *entpd5a:kaede* (Figure 3.2D-E). A developing HZ in the ch cartilage was also present at 96 hpf (Figure 3.2F). By 144 hpf, Alizarin Red live staining showed that the BR3 continued to grow (Figure 3.2B, C). In double transgenic siblings that were injected with α -BTX at 68 hpf and subsequently stained live with Alizarin Red, the BR3 was also present and had formed mineralized bone matrix just as in non-injected embryos despite the absence of a developing HZ marked by *entpd5a:kaede*-labeled chondrocytes (Figure 3.2G-I). These results suggest that paralysis by α -BTX injection does not cause developmental delay and has a specific effect on cartilage development.

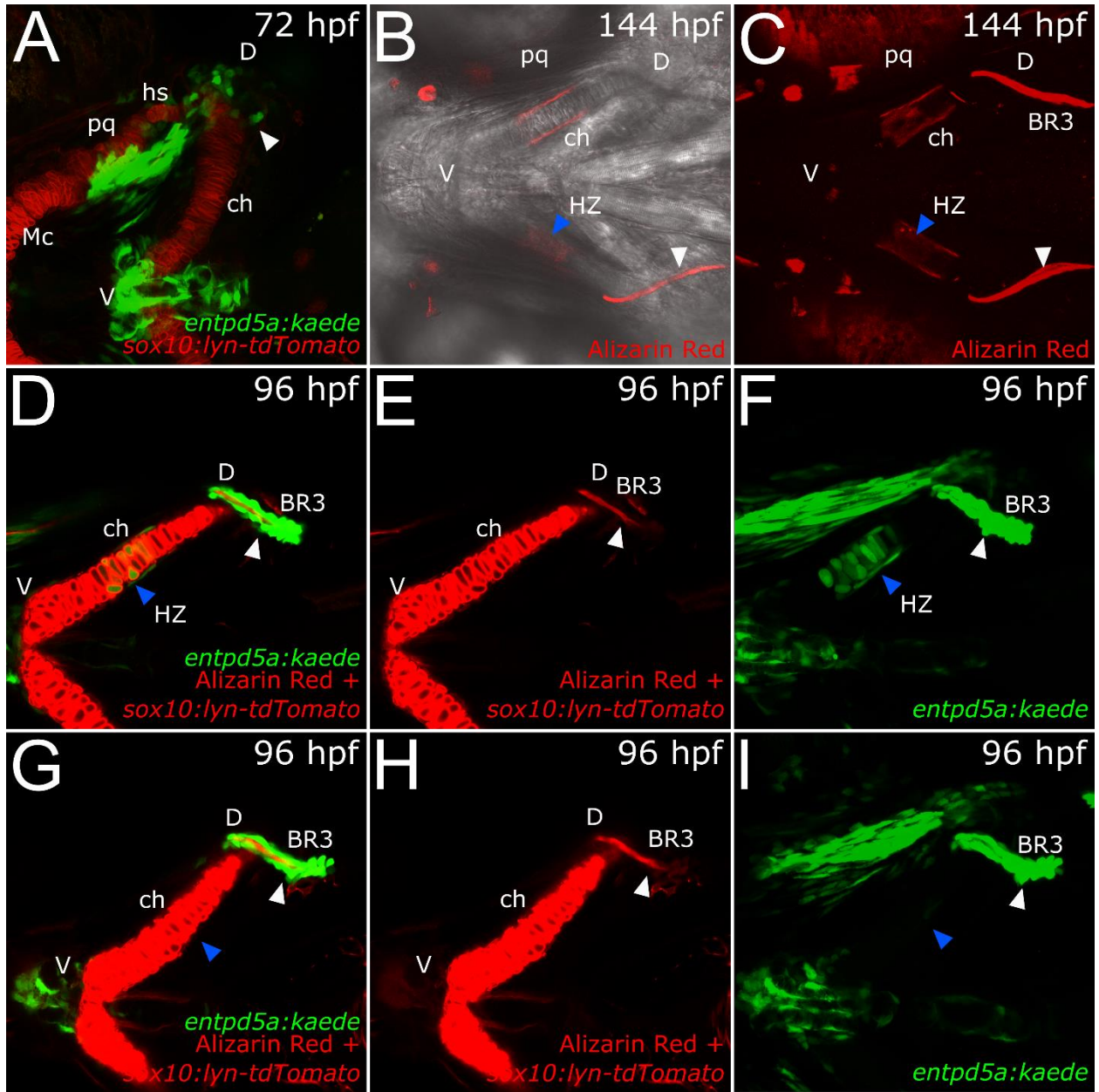


Figure 3.2: HZ loss during paralysis is not due to developmental delay. (A-C) Development of the branchiostegal ray 3 (BR3). (A) A 3D-projection from live imaging of a wild-type *sox10:lyn-tdTomato;entpd5a:kaede* double transgenic embryo at 72 hpf, ventral views; BR3 has not yet formed. (B, C) Live imaging of wild-type embryos stained with Alizarin Red, ventral views. (B) An optical slice showing the DIC channel. (C) 3D-projection. (D-F) Live imaging of a wild-type *sox10:lyn-tdTomato;entpd5a:kaede* double transgenic embryo stained with Alizarin Red at 96 hpf, ventral views. (G-I) Live imaging of a paralyzed *sox10:lyn-tdTomato;entpd5a:kaede* double transgenic embryo stained with Alizarin Red at 96 hpf, ventral views. (D, G) An optical slice. (E, H) An optical slice excluding the *entpd5a:kaede* channel. (F, I) 3D-projection showing the *entpd5a:kaede* channel. White arrowheads indicate the position of the BR3, which develops normally and stains with Alizarin Red regardless of paralysis. Blue arrowheads indicate the position of the HZ, which is absent in paralyzed embryos. pq=palatoquadrate, ch=ceratohyal, hs=hyosymplectic, Mc=Meckels, HZ=hypertrophic zone, D=dorsal, V=ventral, BR3=branchiostegal ray 3.

Paralysis from 72 to 120 hpf leads to loss of chondrocyte proliferation.

Our results suggested that paralysis between 68-96 hpf caused a specific impairment of HZ development. However, previous studies in other species suggest that mechanical force promotes proliferation in GPs (Hu and Albertson, 2017; Wang and Mao, 2002). To test this possibility, despite the fact that chondrocytes in zebrafish craniofacial cartilages do not proliferate until after 96 hpf (Kimmel et al., 1998), we monitored proliferation in paralyzed embryos with BrdU (Figure 3.3). First, we injected *sox10:lyn-tdTomato* transgenic embryos at 68 hpf with an increased dose of α -BTX, which kept injected embryos paralyzed for almost 48 hours. Next, we treated injected and non-injected embryos with BrdU from 96-120 hpf, fixed them at 120 hpf, and performed anti-BrdU antibody staining. By counting the number of BrdU-positive chondrocytes in the ch cartilage using *sox10:lyn-tdTomato* signal as a reference, we found that most BrdU-labeled chondrocytes in non-injected embryos were restricted to the ventral third of the ch cartilage, with a few in the dorsal tip and occasionally one or two near the middle where the HZ develops (Figure 3.3A, B). However, while non-injected embryos had 31.2 BrdU-labeled chondrocytes in the ch cartilage on average (n=5), α -BTX injected embryos had a dramatic reduction in BrdU-labeled chondrocytes (0.8/embryo; n=5; Wilcox test, p=0.011), suggesting that chondrocyte proliferation was virtually eliminated in the absence of mechanical force (Figure 3.3). This effect was also observed in other cartilages, but not in the surrounding cell types including muscle or the central nervous system. We detected BrdU-labeled chondrocytes in the symplectic (sy), hyoid (hy), and palatoquadrate (pq) cartilages of non-injected embryos. In contrast, α -BTX injected embryos had no BrdU-labeled chondrocytes in any of these cartilages. These

Figure 3.3: Paralysis between 72-120 hpf leads to loss of chondrocyte proliferation. (A, B) Optical slices from BrdU Alexa-647 staining of a wild-type *sox10:lyn-tdTomato* embryo, ventral views. (C, D) Optical slices from BrdU Alexa-647 staining of a paralyzed *sox10:lyn-tdTomato* embryo, ventral views; BrdU staining is absent from cartilages, but not from other tissues. (A, C) Both *sox10:lyn-tdTomato* and BrdU Alexa-647 channels showing. (B, D) Only the BrdU Alexa-647 channel showing. (E) Quantification of BrdU-positive cells in the ceratohyal. pq=palatoquadrate, ch=ceratohyal, hs=hyosymplectic, cb=ceratobranchial, D=dorsal, V=ventral.

results suggest cartilage specific requirements for mechanical force in chondrocyte proliferation.

Discussion

In this study, we show, for the first time, that mechanical force is required for chondrocyte hypertrophic differentiation independent of any effects on proliferation. Previous studies showed that mechanical force promotes chondrocyte proliferation (Germiller and Goldstein, 1997; Wang and Mao, 2002). However, our studies suggest that mechanical force also promotes hypertrophic chondrocyte differentiation independently of proliferation. Since zebrafish jaw cartilages do not proliferate until after 96 hpf (Kimmel et al., 1998), and given that we previously showed that the ch cartilage HZ forms around 72 hpf (See Chapter II), our observation that paralysis from 68 to 96 hpf prevented ch cartilage HZ development but not dermal bone development supports this hypothesis. In addition, we found that most chondrocyte proliferation after 96 hpf occurred in the ventral third of the ch cartilage and outside of the developing HZ, and that paralysis severely reduced this proliferation. In addition, our observation that cartilages in paralyzed embryos were shorter than controls at 96 hpf could be explained by defects in convergent extension (Shwartz et al., 2012), indicating mechanical force requirements throughout the cartilage. These observations support the hypothesis that mechanical force is required in chondrocytes for both proliferation or hypertrophic differentiation, but that whether chondrocytes undergo one or the other is likely determined by their location and/or signaling context within the cartilage. In addition, these results suggest that reported effects of mechanical force on hypertrophic differentiation and bone growth rates may be at least in part due to a direct effect on the

chondrocyte differentiation program and not just chondrocyte proliferation (Hu and Albertson, 2017; Saitoh et al., 2000).

Could Trpv4 and Piezo1 mediate mechanotransduction in chondrocytes?

Our results suggest that muscle contraction is required for both proliferation and hypertrophic differentiation of chondrocytes. Since this force is relayed to cartilages through tendons that attach only in some parts of the cartilage, it is reasonable to think that one of the effects these forces have on cartilages is the stretching of chondrocytes. In this context, Piezo Type Mechanosensitive Ion Channel Component 1 (*Piezo1*) and *Piezo2*, mechanosensitive ion channels that are activated by stretching forces on cell membranes, are expressed in chondrocytes (Lee et al., 2014; Servin-Vences et al., 2017; Wu et al., 2017). Although functions for Piezo receptors in cartilage are still poorly understood, *Piezo1* activity has been linked to activation of apoptosis in chondrocytes (Lawrence et al., 2017). Since *Piezo1* is required for the epithelial cell division response to stretching forces (Gudipaty et al., 2017), it is possible that *Piezo1* plays a similar role in chondrocyte proliferation given our results. However, there is insufficient data to speculate on *Piezo1* potential roles on chondrocyte hypertrophic differentiation.

In addition, Transient Receptor Potential Vanilloid 4 (*Trpv4*), a $\text{Ca}^{+2}/\text{Na}^{+}$ channel that is activated by a variety of stimuli involving mechanical force and hypotonic stress, is expressed in chondrocytes (Muramatsu et al., 2007; Nilius et al., 2004; O'Connor et al., 2014; Servin-Vences et al., 2017). *Trpv4* activity has been shown to be required for *Sox9* expression in differentiating chondrocytes *in vitro* (Muramatsu et al., 2007). Furthermore, *Trpv4* activity promotes the production of Type II Collagen and other extracellular matrix (ECM) proteins characteristic of differentiating chondrocytes

(O'Connor et al., 2014). Therefore, one possibility is that *Trpv4* role in regulating *Sox9* expression and chondrocyte-specific ECM protein secretion is required to maintain PCs such that lack of mechanical force leads to downregulation of these factors, thereby decreasing chondrocyte proliferation. Similarly, the decrease in hypertrophic differentiation caused by paralysis could be an effect of *Sox9* downregulation, as failure to maintain PCs could prevent them from initiating hypertrophic differentiation.

However, identifying the type of mechanical stimulus exerted on chondrocytes by muscle contraction will be important in determining the pertinent mechanoreceptor. For instance, the mechano-electrical response to stretching forces in chondrocytes is mainly mediated by *Piezo1* and not *Trpv4* (Servin-Vences et al., 2017). If muscle contraction mainly exerts stretching forces on chondrocytes of the zebrafish jaw cartilages, *Trpv4* would be unlikely to mediate chondrocyte proliferation and hypertrophic differentiation. However, *Trpv4* may still play a role in sensing mechanical loading, which is the same type of mechanical stimulus that osteocytes require to survive (Aguirre et al., 2006; Noble et al., 2003; Plotkin et al., 2005).

Is chondrocyte response to mechanical force cell-autonomous?

Our results suggest that mechanical force promotes HZ development in embryonic cartilages. However, the mechanism that controls chondrocyte hypertrophic differentiation remains unclear. One possibility is that chondrocyte mechanotransduction cell-autonomously modulates their ability to become hypertrophic. Since *Ihh* from the HZ is required for osteoblasts to form in adjacent perichondrium (Felber et al., 2011; St-Jacques et al., 1999), the absence of perichondrial osteoblasts in the ch cartilage of paralyzed embryos suggests that chondrocyte *Ihh* expression could be downregulated

in paralyzed embryos. Since chondrocytes sense mechanical force via *Trpv4* and *Piezo1* receptors *in vitro* (Servin-Vences et al., 2017), mechanotransduction may be required for *Ihh* expression in developing HZs. Alternatively, *Ihh* signaling and mechanotransduction are required in parallel for chondrocyte hypertrophic differentiation. However, there is not enough data to determine the likelihood of any of these possibilities.

Alternatively, mechanical force may be required to repress *Pthlh* expression, hence regulating chondrocyte hypertrophic differentiation non cell-autonomously. The lack of HZ development and adjacent osteoblasts in paralyzed embryos could also support this hypothesis. However, this hypothesis is incongruent with the model for *Pthlh* regulation in GPs. In GPs, *Ihh* promotes expression of *Pthlh* in the RZ at a distance while *Pthlh* represses *Ihh* expression in PCs, thus forming a negative feedback loop (Vortkamp et al., 1996). Although we have no data on the effect of *Ihh* on *Pthlh* expression in zebrafish ch cartilages between 68 and 96 hpf, *Pthlh* upregulation upon HZ development failure, which would lead to *Ihh* downregulation, would constitute a significant departure from the negative feedback loop model. Given that zebrafish *pthlha* is already expressed in the jaw cartilage primordia from 48 hpf (Yan et al., 2012), which is far earlier than the onset of zebrafish jaw muscle contraction (Subramanian et al., 2018), upregulation of *Pthlh* in paralyzed embryos is unlikely. Furthermore, since our results suggest that mechanical force has effects on chondrocyte hypertrophy and proliferation in all the ch cartilage, it is unclear how mechanical force may selectively repress *pthlha* expression in some parts of the cartilage so that *pthlha* is expressed at the distal ends of the cartilage at 72 hpf.

CHAPTER IV

Characterization of embryonic perichondrium

Introduction

One underappreciated cell population in cartilage is the perichondrium. During cartilage morphogenesis, peripheral mesenchymal cells form the perichondrium by flattening and wrapping around chondrocytes in the cartilage periphery. This process begins with upregulation of *Sox9* in cells at the center of undifferentiated mesenchyme leading to chondrocyte differentiation and initiation of convergent extension (CE) such that chondrocytes intercalate resembling coin stacks, which shape and elongate cartilages (Bi et al., 1999; Kimmel et al., 1998; Yan et al., 2005). Much of what is known about the perichondrium comes from the study of growth plates (GP) in endochondral bones in which GPs control bone growth through a combination of proliferation and cartilage replacement that involves signaling to and from surrounding perichondrium. However, little is known about spatial or temporal regulation of these signals or the functions of the perichondrium during early cartilage development.

For instance, the perichondrium is thought to be involved in a negative feedback loop that regulates GP function. GPs elongate bones through chondrocyte proliferation such that chondrocytes transition from the resting zone (RZ) to the proliferative zone (PZ), and then to the hypertrophic zone (HZ). Within the RZ, distally located resting chondrocytes (RC) and perichondrium secrete Parathyroid Hormone-Like Hormone (Pthlh) to form a gradient that maintains the RZ and extends into the PZ (Vortkamp et al., 1996). RCs that transition into the PZ form stacked columnar arrays of proliferative

chondrocytes (PC), elongating this zone along the long axis of the bone. PCs transitioning into the HZ become hypertrophic chondrocytes, the last stage of chondrocyte differentiation, and secrete Indian Hedgehog (*Ihh*) to promote hypertrophic differentiation in adjacent chondrocytes and induce osteoblastogenesis in adjacent perichondrium. These osteoblasts in the surrounding extracellular matrix (ECM) subsequently make bone after HCs have undergone apoptosis (Kronenberg, 2003). These zones are maintained by a negative feedback loop involving *Ihh* and *Pthlh*. First, *Pthlh* represses Runt-Related Transcription Factor 2 (*Runx2*) expression in the PZ, which is required for *Ihh* expression (Chung et al., 1998; Li et al., 2004; Weir et al., 1996; Yoshida et al., 2004). Then, *Ihh* from the HZ promotes *Pthlh* expression in the RZ through a long-range mechanism that is not well understood (Vortkamp et al., 1996). One model suggests that *Ihh* acts on adjacent perichondrium to generate an intermediary signal that relays to the RZ to promote expression of *Pthlh* (Alvarez et al., 2002; Dentice et al., 2005). Testing this model requires perichondrium-specific genetic manipulations accomplished via specific promoters. However, no perichondrium-specific regulatory elements that could drive such expression have been identified.

Another interesting question regarding the perichondrium is how it develops. Previous work has shown that chick perichondrium is composed of an inner cambial layer and an outer fibroblastic layer. The inner layer is thought to differentiate into chondrocytes that integrate in the PZ and contribute to bone elongation (Bairati et al., 1996; Pathi et al., 1999), but there is no direct evidence for this since no perichondrium cell tracing tools are available. Also, the inner layer likely plays more of a role in GP regulation through regulatory factor secretion. For example, *Runx2* expression in the

perichondrium upregulates *Fgf18* in these cells, which represses excessive proliferation in the PZ, thereby controlling the number of cells that transition into the HZ (Hinoi et al., 2006; Liu et al., 2002; Ohbayashi et al., 2002). In contrast, the outer layer likely plays more of a structural role by providing attachment sites for ligaments and tendons (Scott-Savage and Hall, 1980). Whether the perichondrium forms as a bilayer or from a single non-specialized layer during initial cartilage development remains unaddressed because tracing perichondrium cells is currently not possible.

The zebrafish craniofacial cartilages provide an advantage in testing candidate perichondrium-specific promoters and enhancers over GPs in mammals. First, embryonic zebrafish craniofacial cartilages are morphologically relatively simple. Each of these cartilages in the pharyngeal arches (PA) consists of several orders of magnitude fewer cells than their homologues in mammals such that whole cartilages can be captured in a single confocal frame with single cell resolution (Kimmel et al., 1998). Second, whole mount *in situ* hybridization in zebrafish embryos allows for visualization of expression in the whole cartilage in 3 dimensions. In contrast, testing for gene expression in GP perichondrial cells in mammals can only be done by either histological sectioning followed by *in situ* hybridization (ISH) or dissection of the perichondrium followed by quantitative Polymerase Chain Reaction. Third, a genomic binding profile of modified histones indicating potential sites for transcription factor binding is available for zebrafish (Aday et al., 2011). These data combined with genomic conservation data across different fish and other vertebrate species can help identify candidate regulatory regions. Finally, generating transgenic lines for live imaging in zebrafish is straightforward using a transposon-based system and efficient enough to

use injected embryos to test the expression patterns driven by candidate regulatory sequences. Therefore, identifying candidate genes that express in the perichondrium, isolating candidate regulatory sequences for these genes, and testing their expression patterns can be performed rapidly.

Here I describe regulatory regions that drive expression of two genes in the perichondrium in zebrafish. First, I identified candidate perichondrium marker genes from the literature (Bandyopadhyay et al., 2008; Reed and Mortlock, 2010; Thisse, 2004). Next, I performed whole mount ISH for these genes and found that Growth/differentiation Factor-5 (*gdf5*) and Cellular Retinoic Acid Binding Protein 2b (*crabp2b*) were expressed in zebrafish craniofacial cartilage perichondrium. While I failed to find regulatory regions near the *gdf5* locus that could drive expression in the perichondrium using the transient expression system, I found two regulatory regions in the *crabp2b* locus that could drive expression in the perichondrium as well as in chondrocytes. Using these regulatory regions to drive fluorescent protein expression in living embryos I observed that the zebrafish perichondrium initially develops as a single, 1-cell thick layer. Finally, I found that expression driven by *crabp2b* regulatory regions colocalized with that of a tendon transgenic marker in craniofacial cartilages, suggesting that parts of this single layer also serve as tendon attachment sites.

Materials and methods

Ethics statement

All animals were handled in strict accordance with good animal practice as defined by the relevant national and/or local animal welfare bodies, and all animal work was

approved by the University of California, Irvine Institutional Animal Care and Use Committee.

Animals and transgenics

All zebrafish used were of the AB strain. Zebrafish were raised and staged as previously described (Kimmel et al., 1995; Schilling and Kimmel, 1997). For anesthesia, a tricaine stock solution was prepared as previously described (Westerfield, 2000), and a working solution was prepared by using 5% of the stock solution in embryo medium (EM). The *sox10:lyn-tdTomato* transgenic line was previously generated in our lab (Schilling et al., 2010). The *scxa:mCherry* transgenic line was kindly provided by Dr. Jenna Galloway (McGurk et al., 2017).

Bacterial chromosome (BAC) recombineering was carried out by Dr. Daniel Dranow. Bacterial strains for recombineering were obtained from the National Cancer Institute (NCI)—Frederick Biological Resources Branch. BAC CH73-166-O16 containing the *gdf5* coding sequence including upstream sequence was obtained from the Children's Hospital Oakland Research Institute BACPAC Resources Center. BAC recombineering was performed as described (Dranow et al., 2016; Suster et al., 2011).

Primers were (BAC sequence homology underlined) *gdf5_eGFP_fwd*:

GGTAGAGCTGTCCATTTCTCCATCACCGAAGCTCAGAGGAAGATCAGAGGgccaccat
gGTGAGCAAGGGCGAGGAGCTGTTC and *gdf5_frt_KAN_frt_rev*:

CGATACTGTCCCCTAACGGTGGGGCATGCTGTCACTGTTGGAGATTAAccgcgtgt
aggctggagctgcttc for amplification of the eGFP cassette. For PCR amplification of the

eGFP cassette to verify recombination and for sequencing, *gdf5_fwd*:

GGAGCTGGATCACTATGGTTCTGAA, *gdf5_rev*:

CTGAGACTGGGGCTATCTATCACAC. Primers *gdf5_fwd* and *pA_seqR*:
GAATAGGAACTTCCTGCAGGAATTC were used as sequencing primers with the PCR
product as template. For PCR genotyping injected male founders by sperm squeeze,
gdf5_fwd and *eGFP_rev*: AGATGAACTTCAGGGTCAGCTTGC were used.

The *-4.9sox10:eGFP-Ntr* and *-5.0gdf5:eGFP-Ntr* constructs were generated by
assembling multiple pieces into a *pDestTol2pA2* vector (Kwan et al., 2007) using
Gibson cloning and reaction mix as previously described (Gibson et al., 2009). The
sox10:eGFP-Ntr plasmid was made using primers
gtctgaaacacaggccagatgggccGGATCCCCTTATCAGAGTCAAC (*sox10F*),
cgcccttgctcaccatcgggtccactcGTTCTGCGGCCACAGGTG (*sox10R*),
gagtggaccgatgGTGAGCAAGGGCGAGGAG (*eGFPP1*),
ccataccagaaccaccCTTGTACAGCTCGTCCATGC (*eGFPR*),
cgagctgtacaagggtggttctggtATGGATATTATTAGTGTGGCC (*NtrF*), and
atgtctggatcatcatcgatggtacTCACACCTCTGTCAGTGTG (*NtrR1*) to amplify *-4.9sox10*
from genomic DNA, *eGFP* from Tol2 kit plasmid *pME-eGFP*, and *Ntr* from *pCS2-epNtr*
plasmid (Addgene, Catalog # 62213). The *gdf5:eGFP-Ntr* plasmid was made using
primers *gtctgaaacacaggccagatgggccGAGTCCTGAGCTTACCTG* (*gdf5F*),
cgcccttgctcacCATCCTCTGATCTTCCTCTG (*gdf5R*),
agatcagaggatgGTGAGCAAGGGCGAGGAG (*eGFPP2*), *eGFPR*, *NtrF*, and *NtrR1* to
amplify *-5.0gdf5* from BAC CH73-166O16, *eGFP* from Tol2 kit plasmid *pME-eGFP*, and
Ntr from *pCS2-epNtr* plasmid. Sets of amplicons were Gibson cloned into a *Apal/KpnI*
digested *pDestTol2pA2* vector. Plasmids were transformed into DH5 α competent cells
(in-house generated).

The *-1.1crabp2b:eGFP-Ntr*, *+1.2crabp2b-gata2a:eGFP-Ntr*, and *crabp2bL:eGFP-Ntr* plasmids were made using the Gateway Tol2 system (Kawakami and Shima, 1999; Kwan et al., 2007) and Gibson cloning. A middle entry vector pME-*eGFP-Ntr* plasmid was generated using primers tacaaaaaagcaggctggacGTGAGCAAGGGCGAGGAG (eGFPP3), eGFPR, NtrF, and aagctgggtgtagggctgcaTCACACCTCTGTCAAGTGTG (NtrR2) to amplify *eGFP* from Tol2 kit plasmid pME-*eGFP*, and *Ntr* from pCS2-*epNtr* plasmid, and cloning these fragments into a NcoI/PstI-digested pME-*eGFP* plasmid. The 5' entry plasmid p5E-*1.1crabp2b* was made using primers gtatagaaaagttgaaggGCATTCATAAAGGCGTTG (*crabp2bF1*) and ctatagtgtcacctaaatcaGTTTCTGCGTGTCTTTCTTTCACTC (*crabp2bR1*) to amplify *-1.1crabp2b* from genomic DNA and Gibson cloning it into a HindIII/StuI-digested p5E-*CMV-SP6* plasmid (Kwan et al., 2007). The 5' entry plasmid p5E-*1.2crabp2b* was made using primers gggccggcccttcggaAGCTCCGAAAACCTTCGAG (*crabp2bF2*) and ttctattaatgaatcggCGTCCATCCACCGTAGTC (*crabp2bR2*) to amplify *+1.2crabp2b* from genomic DNA and Gibson cloning it into an AscI-digested p5E-Fse-Asc-*gata2a* plasmid (Kwan et al., 2007). Finally, the 5' entry plasmid p5E-*crabp2bL* was made using primers ttgtatagaaaagttgaaggCTTGCTGATGTGCTTTTAGGGG (*crabp2bF3*), ttcggagcttGTCTTGTAGGCTATAGTGACCTGG (*crabp2bR3*), cctacaagacAAGCTCCGAAAACCTTCGAGGA (*crabp2bF4*), ttatgaatgcCGTCCATCCACCGTAGTCTC (*crabp2bR4*), tggatggacgGCATTCATAAAGGCGTTGTTCTGAC (*crabp2bF5*), and *crabp2bR1* to amplify *-4.2crabp2b*, *+1.2crabp2b*, and *-1.1crabp2b* fragments, respectively, and Gibson cloning them into a HindIII/StuI-digested p5E-*CMV-SP6* plasmid. The plasmids

pDestTol2pA2-1.1*crabp2b:eGFP-Ntr*, pDestTol2pA2-1.2*crabp2b-gata2a:eGFP-Ntr*, and pDestTol2pA2-*crabp2bL:eGFP-Ntr* were assembled according to the Tol2 Kit protocol and transformed into DH5 α competent cells. Transposase mRNA was synthesized from the pCS2FA-transposase plasmid (Kwan et al., 2007) digested with NotI using Invitrogen mMESSAGING mMACHINE™ T7 ULTRA Transcription Kit (Catalog # AM1345). 500 μ l of cocktail mixes containing 40 ng/ μ l of plasmid and 60 ng/ μ l of transposase mRNA were injected into 1-cell stage embryos.

Imaging

Embryos for live imaging were embedded in 1% low melting point agarose (APEX, Catalog # 9012-36-6) diluted in embryo medium containing 5% of tricaine stock solution. Embryos labeled by *in situ* hybridization were mounted on slides, then imaged on a Zeiss Axioplan 2 microscope equipped with a MicroPublisher 5.0 RTV camera using Volocity software (Improvision). All live imaging, except for Alizarin red stained embryos, was done using a Leica Sp8 confocal microscope equipped with a HC PL APO CS2 40x/1.10 W objective. Imaging of live Alizarin red stained embryos was done using a Nikon ECLIPSE Ti microscope equipped with a Plan Apo VC 20X/0.75 DIC N2 objective. ImageJ/Fiji was used for image processing.

***In situ* hybridization**

Probes were made from the following primers: AGTTCAGTGACGATGCCAGG (col14a1aF), ACTGGCCCATGATGTACTGC (col14a1aR), TAAACTGACCTGGGACACGC (col14a1bF), GTACTGTGTGTTCTGGGCTCA (col14a1bR), CTGCGCAACTTTCTCCCTGA (lgals2aF),

GACAATGGTTAGCATGTACCGC (lgals2aR), AGCTCCACCAACAACACTCAGC (lgals2bF), AGTGGATTTATTGACACTGCAGT (lgals2bR), GGAGCAAACGATGAGTGACG (dkk3aF), GAGTAAAGTGTGTCGGTGAGC (dkk3aR), CAGTGGGCAGTTCAGTTCAC (dkk3bF), TGTCTCTCATCCACACACACT (dkk3bR), GGAGGTGCTGGGAAACATGA (thbs2F), GGCATCGTTCTCAGGACACA (thbs2R), TAAAGGCTGACGGAAACCCT (gdf5F), CTGGATGATGGCGTGATTGG (gdf5R), AGTGAAAGAAAGACGCGCAG (crabp2bF), TGCCTAAACTCACCATTAGTTCA (crabp2bR). We assembled the corresponding PCR products into Promega's pGEM-T Easy Vector (Catalog # A1360) and transformed them into DH5 α cells (in-house generated). We digested the vector with SpeI or NcoI, depending on the plasmid, and synthesized the probe using Roche DIG RNA Labeling Mix (Catalog # 11277073910), SP6 RNA Polymerase (Catalog # 10810274001), and T7 RNA Polymerase (Catalog # 10881767001) as required and directed by the protocol. Whole-mount *in situ* hybridization was carried out as previously described (Thisse et al., 1993), with the following modifications. Anti-Digoxigenin-AP, Fab fragments antibody (Roche, Catalog # 11093274910) dilution was 1/1000.

Metronidazole treatments

Metronidazole (Mtz) treatments were done as previously described (Curado et al., 2008). Mtz was obtained from SIGMA (Catalog # M3761-25G). Mtz solution was always prepared fresh from powder. Mtz was dissolved in EM without methylene blue containing 0.2% dimethyl sulfoxide (DMSO). Mtz final concentrations ranged between 2.5 and 10 mM. EM with 0.2% DMSO solution was used as a negative control.

Results

Both *gdf5* and *crabp2b* express in embryonic perichondrium

Genes previously described as expressed in the perichondrium in chick include Cellular Retinoic Acid Binding Protein-1 (*Crabp1*), Collagen Type XIV Alpha 1 Chain (*Col14a1*), ABI Family Member 3 Binding Protein (*Abi3bp*), Dickkopf WNT Signaling Pathway Inhibitor 3 (*Dkk3*), Thrombospondin 2 (*Thbs2*), Galectin 1 (*Lgals1*), and MAF bZIP Transcription Factor B (*Mafb*) (Bandyopadhyay et al., 2008). To determine if these genes have similar perichondrial expression in zebrafish, we performed ISH in embryos between 48-96 hours post-fertilization (hpf). Previous studies suggested that *crabp1a*, *crabp1b*, and *mafb* are not expressed in zebrafish craniofacial cartilages (Liu et al., 2005a; Rauch et al., 2003; Toro et al., 2009), evidence for *col14a1a*, *lgals2a*, and *lgals2b* was equivocal (Thijssen et al., 2006; Thisse, 2001), and no expression data were available for *abp3bpa*, *abi3bpb*, *dkk3a*, *dkk3b*, or *thbs2a*. However, the *crabp1b* paralog *crabp2b* appeared to be expressed in zebrafish craniofacial cartilages (Sharma et al., 2005; Thisse, 2004). In addition, *Gdf5* is well known to express in the interdigital mesenchyme of murine and avian phalanges (Brunet et al., 1998; Merino et al., 1999; Storm and Kingsley, 1996), and zebrafish *gdf5* is expressed in craniofacial cartilage perichondrium (Reed and Mortlock, 2010). We selected *col14a1a*, *lgals2a*, *lgals2b*, *dkk3a*, *dkk3b*, *thbs2a*, *crabp2b*, and *gdf5* for our ISH screening. We never tested for *abp3bpa* or *abi3bpb* expression.

ISH for these potential perichondrial marker genes revealed that, while *col14a1b* expression was non-specific, *col14a1a* was expressed in the pharyngeal endoderm,

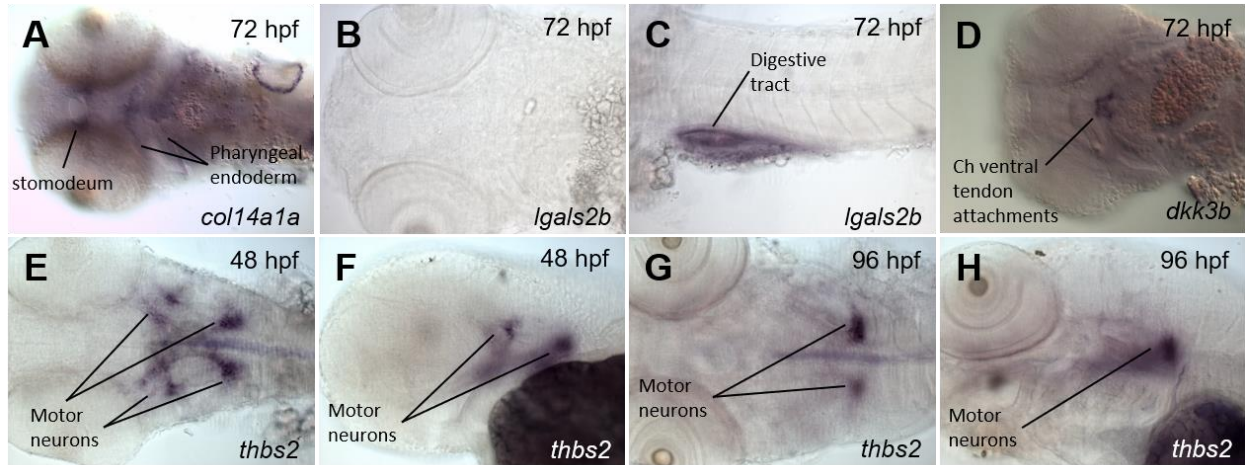


Figure 4.1: Neither *col14a1a*, *lgals2b*, *dkk3b*, or *thbs2* are expressed in the perichondrium. (A) *In situ* hybridization for *col14a1a* at 72 hpf, ventral view. (B) *In situ* hybridization for *lgals2b* at 72 hpf, ventral view, head. (C) *In situ* hybridization for *lgals2b* at 72 hpf, lateral view, tail. (D) *In situ* hybridization for *dkk3b* at 72 hpf, ventral view. (E-H) *In situ* hybridizations for *thbs2* at 48 (E, F) and 72 hpf (G, H). (E, G) Ventral views. (F, H) Lateral views. ch=ceratohyal.

stomodeum, and in the pectoral fin apical ectodermal ridge (AER) at 60 hpf (Figure 4.1A). In addition, while *lgals2a* was expressed ubiquitously (not shown), *lgals2b* appeared to be expressed only in the intestinal tract at 72 hpf (Figure 4.1B, C). Also, *dkk3a* expression was entirely absent in the jaw (not shown), and *dkk3b* was expressed in the ceratohyal cartilage ventral tendon attachments at 72 hpf (Figure 4.1D). Finally, *thbs2a* expression was detected in a subset of central nervous system (CNS) neurons between 48-96 hpf (Figure 4.1E-H). Thus, none of these genes presented themselves as perichondrial markers between 48-96 hpf.

Next, we found that *gdf5* was transiently expressed in the perichondrium. Expression of *gdf5* was first detected in the undifferentiated mesenchyme of the pq at 54 hpf (Figure 4.2A). At 60 hpf, *gdf5* was expressed in the pq and ch perichondrium, and in the jaw synovial joint. Expression of *gdf5* was also detected in the Mc and dorsal part of the hs cartilages, but whether this expression included the perichondrium could not be determined (Figure 4.2B, C). This *gdf5* expression pattern was maintained at 66 hpf, and increased in the ventral ch cartilage (Figure 4.2D, E). Finally, *gdf5* expression became restricted to the jaw synovial joint and the ventral part of the ch cartilage at 72 hpf (Figure 4.2F).

Finally, we tested for *crabp2b* expression between 48-72 hpf and found a dynamic expression pattern. At 48 hpf, *crabp2b* expression was detected in Meckels (Mc), ceratohyal (ch), hyosymplectic (hs), ceratobranchials (cb), and pectoral fin cartilage primordia (Figure 4.2G). At 54 hpf, *crabp2b* expression was detected in Mc, ch, hs, cb, and pectoral fin cartilages. Most *crabp2b* expression in Mc and ch cartilages was detected in the perichondrium (Figure 4.2H). At 66 hpf, *crabp2b* expression was

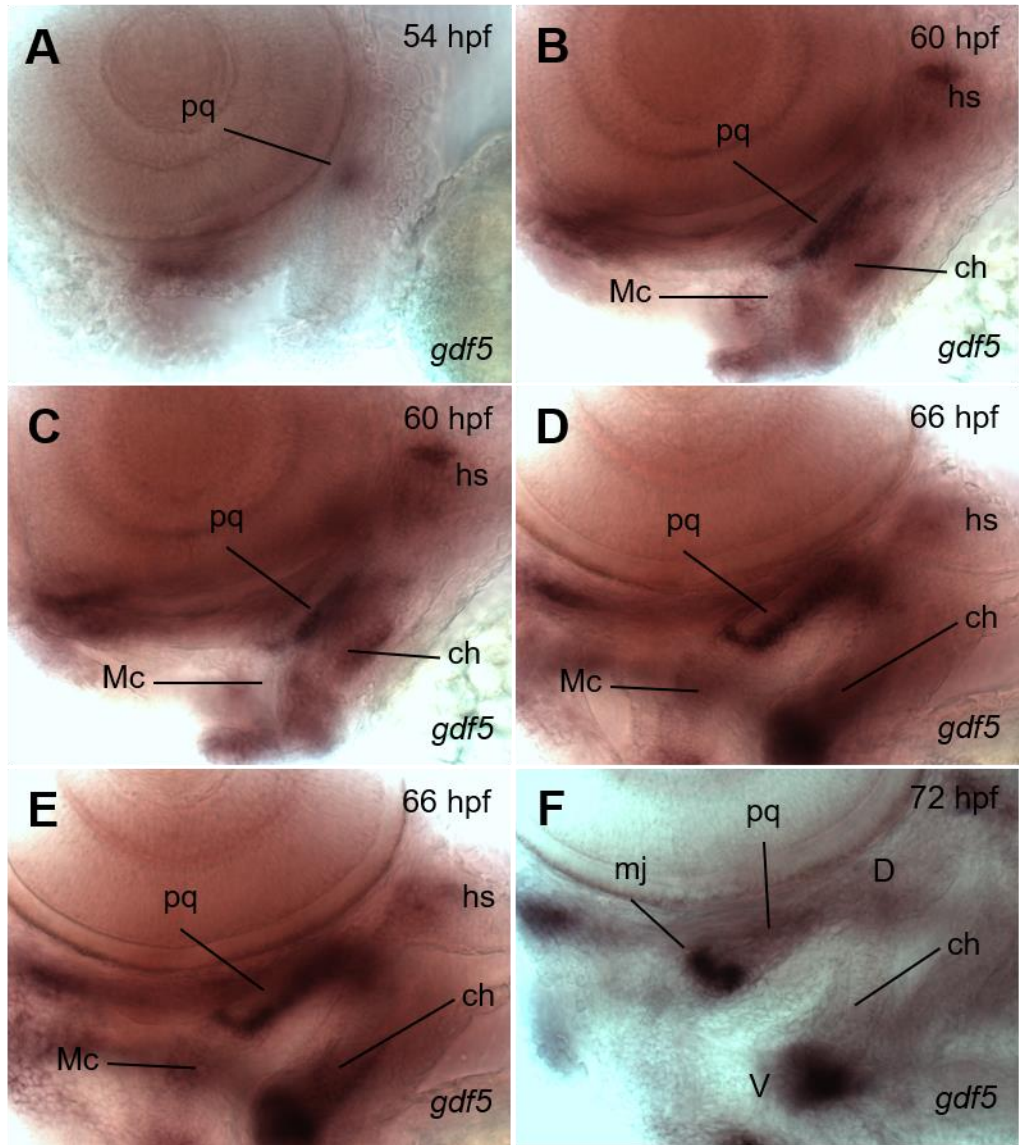


Figure 4.2: *gdf5* is expressed in the perichondrium. (A-F) *In situ* hybridizations for *gdf5* at 54 (A), 60 (B, C), 66 (D, E), and 72 hpf (F), lateral views. pq=palatoquadrate, ch=ceratohyal, Mc=Meckels, hs=hyosymplectic, mj=mandibular joint, D=dorsal, V=ventral.

detected in ch and hs perichondrium, as well as in cb and pectoral fin cartilages (Figure 4.2I, J). By 72 hpf, *crabp2b* was expressed in ch, hs, cb, and pectoral fin cartilages. In ch cartilage, *crabp2b* expression was only detected in the perichondrium (Figure 4.2K, L). Together, these results suggest that *gdf5* and *crabp2b* are perichondrial markers and good candidates to isolate perichondrium-specific regulatory regions.

Analysis of regulatory regions upstream of *gdf5* failed to identify perichondrial elements

A recent study found that mouse *Gdf5* expression was controlled by two sets of regulatory regions. One set contains R1 and R2. R1 is 5 kilobases (kb) upstream of the *Gdf5* promoter and its sequence is not conserved in chick. R2 is adjacent to the promoter and is somewhat conserved in zebrafish. Another set of three regulatory regions is within the introns of *Uqcc1*, a gene downstream of *Gdf5*. The sequences of this set are conserved in chick but not in zebrafish (Chen et al., 2016). In order to find zebrafish *gdf5* regulatory regions that would drive perichondrium-specific expression in zebrafish, we sought to obtain bacterial chromosomes (BAC) that contain genomic regions syntenic to those in the mouse where *gdf5* regulatory regions are found. First, we used BAC recombineering to generate transgenic lines containing these regulatory elements. Dr. Daniel Dranow in our lab did this part due to his extensive experience in BAC recombineering. Second, I used these BACs as templates to isolate smaller regulatory regions and test their expression pattern in zebrafish embryos injected at the 1-cell stage. Therefore, I obtained CH73-166O16 (Accession number CU463256.4), a BAC which encompasses the whole *gdf5* locus and the upstream regulatory regions (Figure 4.4A). However, no suitable BACs encompassing *uqcc1* were available.

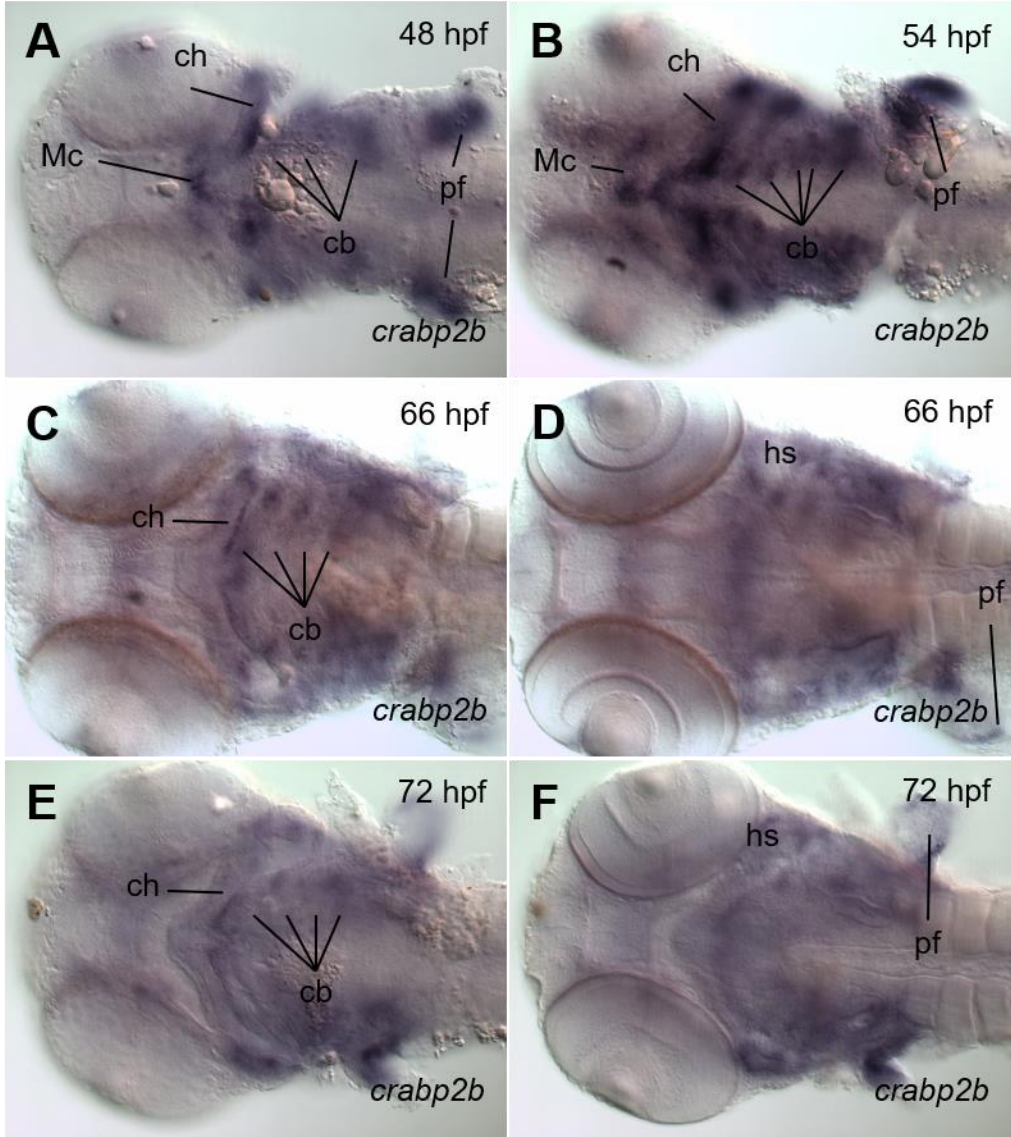


Figure 4.3: *crabp2b* is expressed in the perichondrium. (A-F) *In situ* hybridizations for *crabp2b* at 48 (A), 54 (B), 66 (C, D), and 72 hpf (E, F), ventral views. ch=ceratohyal, Mc=Meckel's, hs=hyosymplectic, cb=ceratobranchial, pf=pectoral fin.

Moreover, we were unable to design primers to isolate candidate regions within *uqcc1* from genomic DNA.

We focused our efforts on regulatory regions upstream of *gdf5*. Therefore, I isolated a 5 kb DNA fragment upstream of *gdf5* coding sequence, which contained the promoter region (*-5.0gdf5*) and cloned it directly upstream of an eGFP-Nitroreductase (Ntr) fusion protein. Ntr is a bacterial protein and a target of the antibiotic Metronidazole, which crosslinks genomic DNA when in its active form, activating apoptosis. Expression of Ntr under the appropriate promoter and timed addition of Mtz provides a method for spatial-temporal control of cell ablation in live animals. Furthermore, fusing Ntr with a fluorescent protein facilitates detection of ablated cells (Curado et al., 2008). As a positive control regulatory sequence, I used a 4.9 kb fragment upstream of *sox10* (*-4.9sox10*) that is well characterized and expresses in differentiating chondrocytes (Le Pabic et al., 2014; Wada et al., 2005). I injected these constructs into 1-cell stage zebrafish embryos and looked for expression in jaw cartilages between 48-120 hpf. No expression was detected for the *-5.0gdf5:eGFP-Ntr* construct at any stage (not shown). In contrast, my *-4.9sox10:eGFP-Ntr* construct expressed mosaically in chondrocytes at 78 hpf, as expected (Figure 4.4B, E). Then we treated these embryos with either 2.5 or 10 mM Mtz at 78 hpf. At 120 hpf, only eGFP-positive cell debris was left in place of the cells that expressed the fusion construct at 78 hpf (Figure 4.4C, F). In contrast, embryos treated with DMSO only had intact cartilages (Figure 4.4D). Because both constructs shared the same fusion protein DNA fragment, and because the only difference between them was the upstream regulatory sequence, these results suggest that the lack of expression from our *-5.0gdf5:eGFP-Ntr* construct was not due to a defective

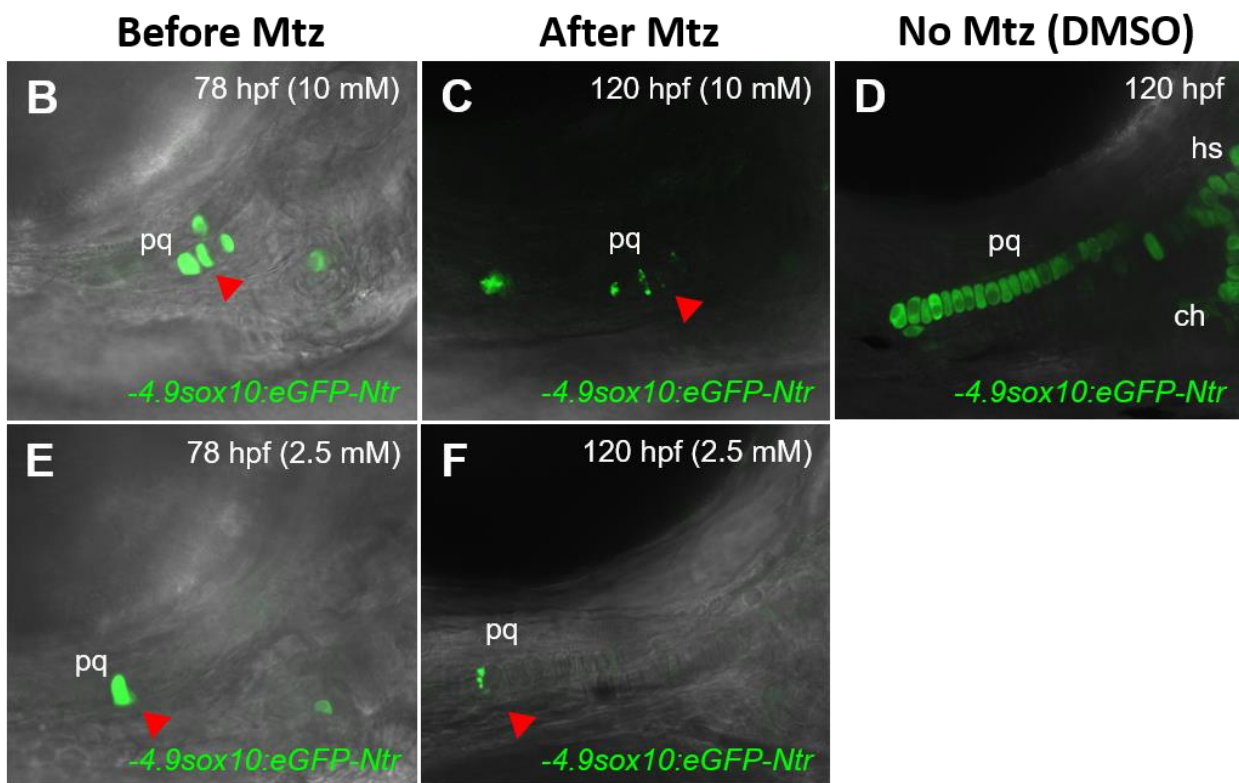
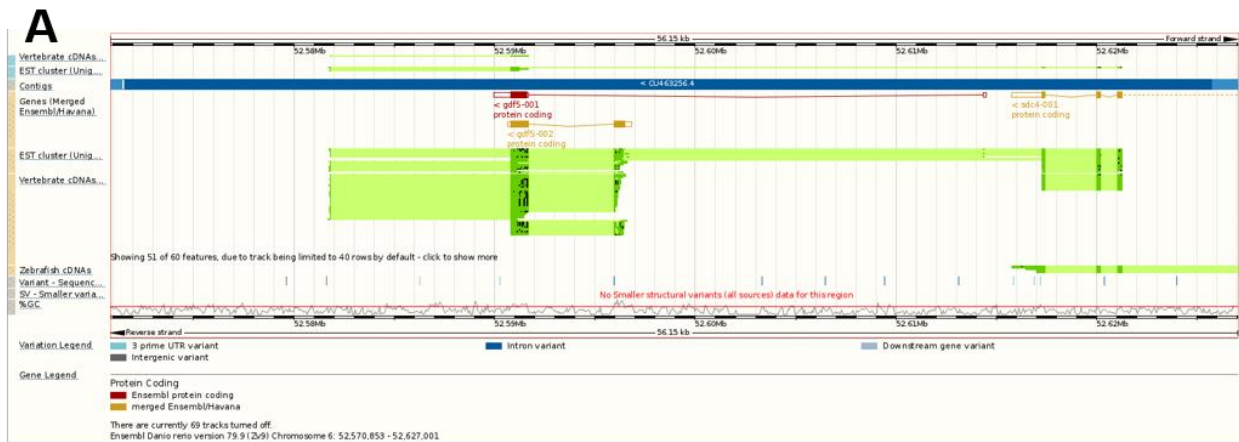


Figure 4.4: *gdf5* upstream sequence yielded no expression. (A) A snapshot of Ensembl genome browser showing the genomic sequence covered by the CH73-166O16 (Accession number CU463256.4, shown in blue). Ensembl denomination for two *gdf5* isoforms are shown in red (*gdf5-001*) and yellow (*gdf5-002*). Vertebrate cDNA and EST cluster alignments are shown in green. (B-F) Metronidazole (Mtz) treatments of *-4.9sox10:eGFP-Ntr* mosaic transgenic embryos, lateral views. (B, E) Before Mtz treatment. (C, F) After Mtz treatment. (D) Embryo treated with vehicle (DMSO). (B, C) 10 mM Mtz treatment. (E, F) 2.5 mM Mtz treatment. Red arrowheads indicate ablated cells before and after Mtz treatment. pq=palatoquadrate, ch=ceratohyal.

fusion protein. In addition, Dr. Daniel Dranow recombined our CH73-166O16 BAC such that the *gdf5* coding sequence was replaced by eGFP. However, this construct failed to express in any tissue (not shown). These results prompted us to stop pursuing *gdf5* as a perichondrial marker.

Two regulatory regions from *crabp2b* drive expression in the perichondrium

The *crabp2b* gene is expressed throughout zebrafish jaw cartilage morphogenesis, but becomes restricted to the perichondrium of the Mc, ch, and hs cartilages (Figure 4.3). We reasoned that this may be due to the presence of different regulatory sequences in the vicinity of *crabp2b* that control expression in different tissues and at different developmental timepoints. Therefore, I sought to isolate candidate genomic regions around *crabp2b*. I identified regions of interest using the University of California Santa Cruz (UCSC) Genome Browser (GB) in combination with a track displaying curated data from a study that used Chromatin Immunoprecipitation combined with Deep DNA Sequencing to identify genomic regions that were bound to Histone 3 that were either mono or trimethylated at lysine 4 (H3K4me1 or H3K4me3, respectively) in 24 hpf zebrafish embryos (Aday et al., 2011; Zhang et al., 2008). H3K4me1 indicates possible enhancers, while H3K4me3 indicates promoter regions. In this manner, I identified three regions of interest: a 1.1 kb region upstream of *crabp2b* coding sequence (*-1.1crabp2b*) that was marked by H3K4me3, a 1.2 kb region that corresponded to *crabp2b* intron 1 (*+1.2crabp2b*) and was marked by H3K4me1, and a 4.2 kb region located 2.4 kb upstream of *crabp2b* coding sequence (*-4.2crabp2b*) that was marked by H3K4me1 and displayed some sequence conservation with *O. latipes*, *G. aculeatus*, and *X. tropicalis* (Figure 4.5A). We noticed some sequence conservation in non-coding regions within

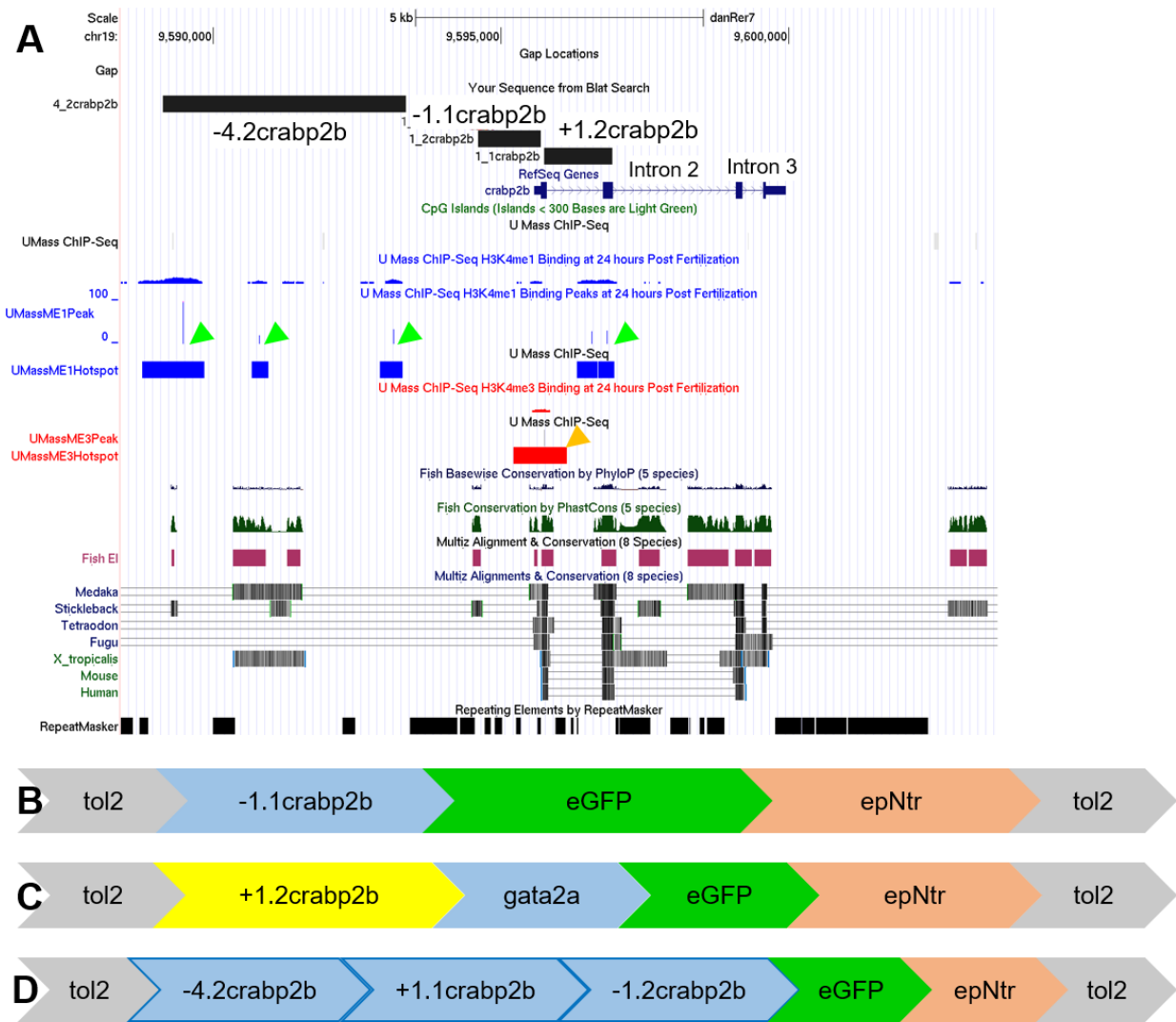


Figure 4.5: Identification of two genomic regions within the *crabp2b* locus that drive perichondrial expression. (A) A snapshot of the University of California Santa Cruz Genome Browser showing the genomic region around the *crabp2b* locus. Isolated genomic regions by PCR are labeled *-4.2crabp2b*, *-1.1crabp2b*, and *+1.2crabp2b*, which correspond to an upstream sequence, the sequence upstream of the *crabp2b* start codon, and intron 1 of the *crabp2b* gene, respectively. H3K4me1 marks are shown in blue and hotspots indicated by green arrowheads. H3K4me1 marks are shown in red and hotspots indicated by orange arrowheads. (B-D) Graphical representation of the constructs made from the isolated genomic regions around the *crabp2b* locus for testing of the expression pattern they drive. (B) The *-1.1crabp2b:eGFP-Ntr* construct. (C) The *+1.2crabp2b-gata2a:eGFP-Ntr* construct. (D) The *-4.2crabp2b-1.2crabp2b-1.1crabp2b:eGFP-Ntr* construct, or *crabp2bL:eGFP-Ntr* construct for short.

introns 2 and 3 and in a small downstream region, but we did not test these as their histone modification profile did not appear promising (Figure 4.5A). We isolated the -1.1*crabp2b*, +1.2*crabp2b*, and -4.2*crabp2b* fragments directly from genomic DNA and made constructs such that our candidate regulatory regions would drive eGFP-Ntr fusion protein expression. We cloned -1.1*crabp2b* directly upstream of eGFP-Ntr since -1.1*crabp2b* contained the native *crabp2b* promoter (Figure 4.5B). In contrast, +1.2*crabp2b* lacks a promoter, so we cloned it upstream of a *gata2a* minimal promoter, and eGFP-Ntr fusion protein downstream of *gata2a* (Figure 4.5C). We failed to clone -4.2*crabp2b* independently into a construct, but we concatenated -4.2*crabp2b*, +1.2*crabp2b*, and -1.1*crabp2b*, in that order, which we termed *crabp2bL*, and used this to drive expression of eGFP-Ntr fusion protein (Figure 4.5D). Next, we injected these constructs into 1-cell stage *sox10:lyn-tdTomato* transgenic embryos, which mark differentiating chondrocyte plasma membranes in red, and looked for eGFP-Ntr expression between 72 and 96 hpf. However, none of these constructs reproduced the *crabp2b* native gene expression pattern. First, our -1.1*crabp2b*:eGFP-Ntr and +1.2*crabp2b*-*gata2a*:eGFP-Ntr constructs both drove expression in several tissues, including perichondrium and chondrocytes (Figure 4.6A-D). Second, expression in the perichondrium appeared to be enhanced in our *crabp2bL*:eGFP-Ntr construct, but remained unrestricted as in the previous two constructs at 72 hpf (Figure 4.6E, F). In all three cases, we detected eGFP signal in the pq cartilage, a further indication that these regulatory regions were insufficient to reproduce the *crabp2b* native expression pattern.

Since *crabp2b* gene expression became restricted to the perichondrium by 72 hpf, I hypothesized that GFP-Ntr positive chondrocytes in our 72 hpf *crabp2bL*:eGFP-

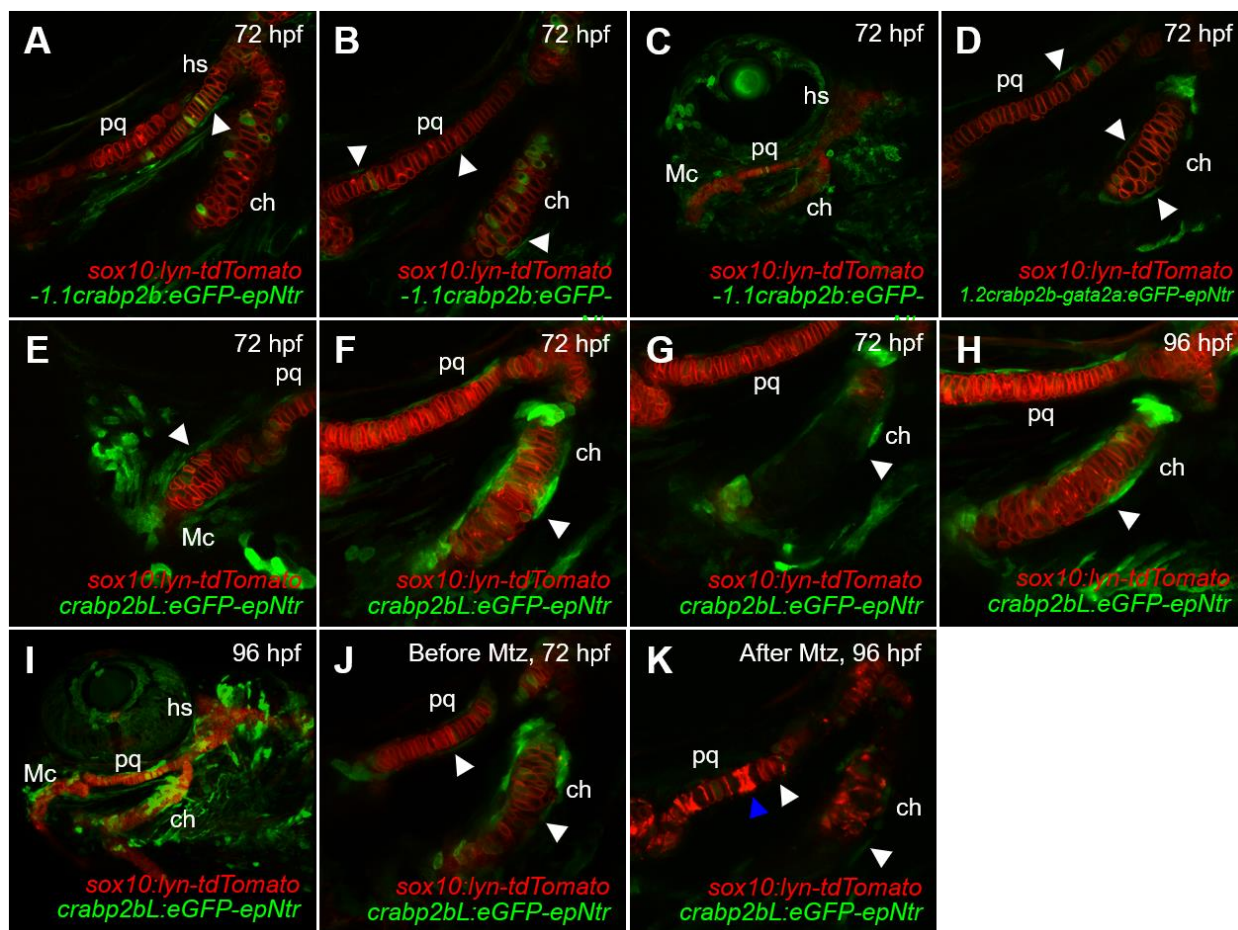


Figure 4.6: Two *crabp2b* regulatory regions drive expression in the perichondrium. (A-C) Live imaging of *sox10:lyn-tdTomato* embryos injected with the -1.1*crabp2b:eGFP-Ntr* construct at the 1-cell stage, imaged at 72 hpf, lateral views. (A, B) Optical slices. (C) 3D projection of the embryo head. (D) Live imaging (optical slice) of *sox10:lyn-tdTomato* embryos injected with the +1.2*crabp2b:eGFP-Ntr* construct at the 1-cell stage, imaged at 72 hpf, lateral views. (E-I) Live imaging of *sox10:lyn-tdTomato* embryos injected with the *crabp2bL:eGFP-Ntr* construct at the 1-cell stage, imaged between 72 and 96 hpf, lateral views. (E) An optical slice at 72 hpf. (F-I) 3D projections. (F) The ceratohyal (ch) cartilage prior to eGFP photobleaching at 72 hpf. (G) The ceratohyal cartilage after eGFP photobleaching at 72 hpf. (H) Fluorescent recovery after photobleaching of the ch at 96 hpf. (I) Fluorescent recovery after photobleaching showing the whole embryo head at 96 hpf. (J, K) Live imaging (optical slices) of *sox10:lyn-tdTomato* embryos injected with the +1.2*crabp2b:eGFP-Ntr* construct at the 1-cell stage and treated with metronidazole (Mtz) for 24 hours, imaged between 72 and 96 hpf, lateral views. (J) The embryo before Mtz treatment. (K) The embryo after 24 hour Mtz treatment. White arrowheads indicate the position of perichondrial cells labeled with the *crabp2b* constructs. Blue arrowheads indicate the position of ablated chondrocytes. pq=palatoquadrate, ch=ceratohyal, hs=hyosymplectic, Mc=Meckels.

Ntr injected embryos indicated residual expression from earlier timepoints. Therefore, we photobleached eGFP in the ch cartilage of one of these embryos at 72 hpf. We stopped our eGFP photobleaching when we noticed complete photobleaching of lyn-tdTomato in ch chondrocytes. This left some eGFP signal in the perichondrium (Figure 4.6F, G). At 96 hpf, lyn-tdTomato signal recovered in chondrocytes while eGFP signal recovered both in perichondrium and chondrocytes (Figure 4.6H, I). Furthermore, treatment of *crabp2bL:eGFP-Ntr* injected embryos with Mtz led to ablation of perichondrium and chondrocytes (Figure 4.6J, K). These results suggest that while the regulatory elements we isolated from *crabp2b* drove perichondrial expression, this was not entirely cell-type restricted, complicating interpretation of ablations or other manipulations using these elements.

Embryonic zebrafish perichondrium forms as a single layer that contributes to tendon attachment site formation

One outstanding question in cartilage biology is how the perichondrium develops into a bilayer. Histological observations in the ossifying ch and cb cartilage suggest that the perichondrium of these cartilage elements consists of a single cell layer (Eames et al., 2011; Laue et al., 2008; Reed and Mortlock, 2010). Our data on *gdf5* and *crabp2b* gene expression, as well as *crabp2bL:eGFP-Ntr* transgenic embryos, gave us an insight into perichondrium morphology during zebrafish embryonic development. First, the perichondrium of the early pq and ch cartilages appeared to consist of only a single cell layer. Expression of *gdf5* in the pq was detected one layer of flattened cells surrounding the cartilage (Figure 4.2B-E). This was also the case with *crabp2b* expression in ch perichondrium (Figure 4.3E). By 72 hpf, *crabp2bL:eGFP-Ntr* expression in pq and ch

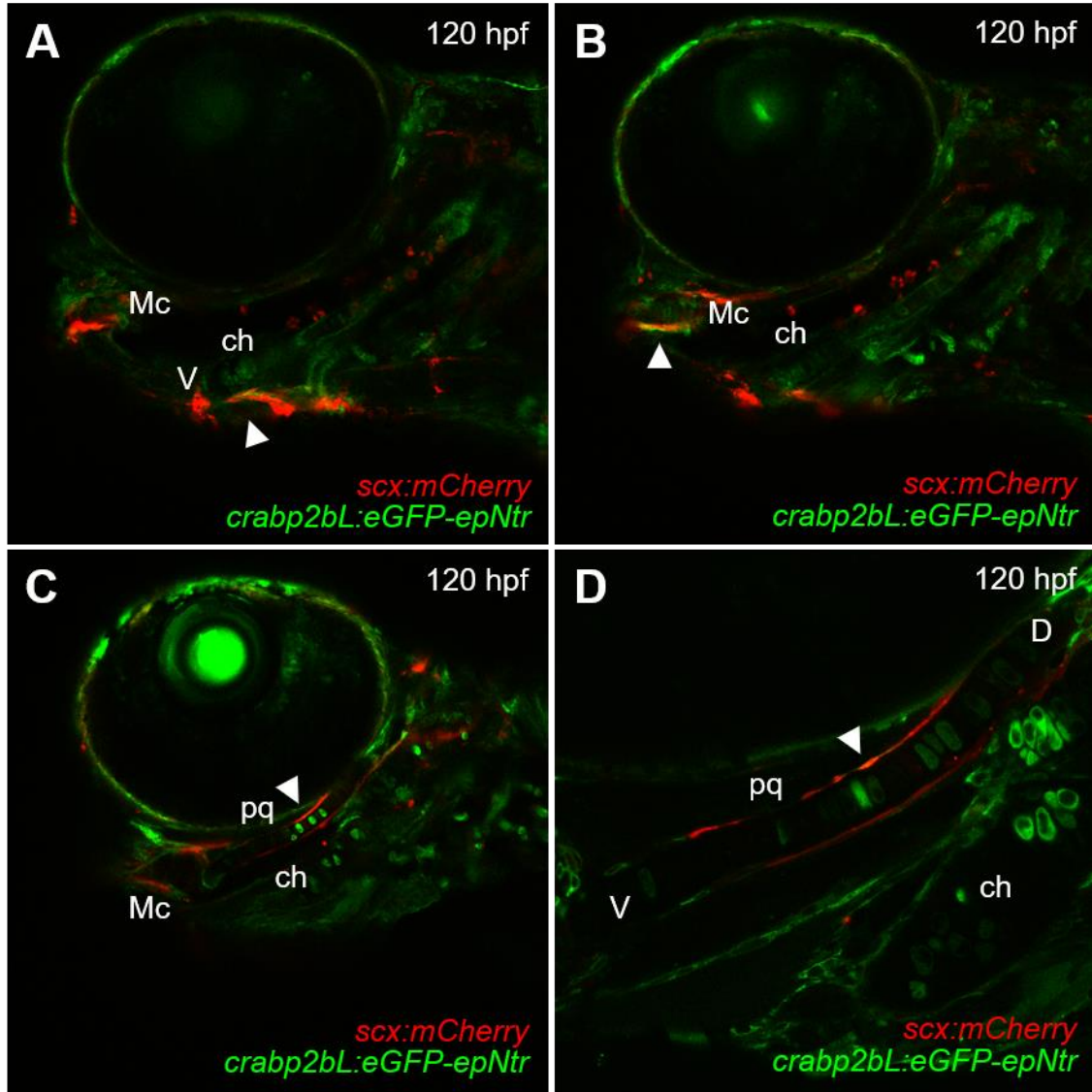


Figure 4.7: Tendon attachment zones colocalize with *crabp2b* regulatory region-driven expression. (A-D) Live imaging (optical slices) of *scxa:mCherry* transgenic embryos injected with the *crabp2bL:eGFP-Ntr* construct at the 1-cell stage, imaged at 120 hpf, lateral views. (A) Colocalization of the transgenic markers at the ventral ceratohyal tendon attachment zone is shown. (B) Colocalization of the transgenic markers at the Meckels tendon attachment zone is shown. (C, D) Colocalization of the transgenic markers at the palatoquadrate tendon attachment zones is shown, with a closer look (D). White arrowheads indicate the positions of colocalization of the two transgenic markers. pq=palatoquadrate, ch=ceratohyal, Mc=Meckels, D=dorsal, V=ventral.

perichondrium showed a single layer of flattened cells (Figure 4.5A-D, F-H). The Mc perichondrium was the exception. Expression of *crabp2b* was detected in a 2-cell thick layer around the Mc cartilage at 54 hpf (Figure 4.3B), and our *crabp2bL:eGFP-Ntr* transgenic embryos reflected this observation (Figure 4.6E). However, we did not observe any morphological differences between inner and outer cells of this layer. These results suggest that the embryonic perichondrium surrounding at least most cartilages in zebrafish forms as a single layer.

Given our results, we wanted to know if tendons attached directly to the single-layered perichondrium. Therefore, we injected our *crabp2bL:eGFP-Ntr* construct into *scxa:mCherry* transgenic embryos, which label tendons in red (McGurk et al., 2017), and looked for colocalization in the perichondrium. We found that *crabp2bL:eGFP-Ntr* co-expressed with *scxa:mCherry* in perichondrium where tendon or ligament attachment sites were present in the Mc, pq, and ch cartilages (Figure 4.7A-D). Together, these results suggest that, despite being a single layer, the early perichondrium is heterogeneous, and cells within it can contribute to tendons or ligaments.

Discussion

To identify genes expressed in the embryonic perichondrium in zebrafish and isolate perichondrial regulatory elements that might be used as drivers, we found two promising candidate genes, *gdf5* and *crabp2b*. *gdf5* was transiently expressed in the jaw perichondrium between 60 and 66 hpf, while *crabp2b* was expressed earlier in jaw cartilage perichondrium, except in pq cartilage, starting around 54 hpf. However, neither a *gdf5* BAC nor upstream sequence drove expression in cartilage. In contrast, two *crabp2b* regulatory regions drove expression in the perichondrium, but also in

chondrocytes and other tissues. We made a *crabp2bL:eGFP-Ntr* construct by concatenating these two regions with a third one, which resulted in enhanced, but still not totally specific, perichondrium expression. The expression patterns of *gdf5*, *crabp2b*, and the *crabp2bL:eGFP-Ntr* transgene in the pq and ch cartilages suggest that zebrafish perichondrium initially forms as a single layer, which is in agreement with histological observations from previous studies in ch and cb cartilages (Eames et al., 2011; Laue et al., 2008; Reed and Mortlock, 2010). Furthermore, co-expression of the *crabp2bL:eGFP-Ntr* transgene with *scxa:mCherry* in the perichondrium suggests that parts of this single-layered perichondrium also functions in cartilage-muscle attachments, observation which is congruent with mammalian long bone entheses arising from in *Sox9* and *Scx* co-expressing perichondrial cells (Blitz et al., 2013).

Early perichondrial markers differ from those in mature perichondrium

We show that *gdf5* is expressed transiently in embryonic perichondrium between 60-66 hpf. Moreover, we show that *gdf5* expression becomes restricted to the mandibular synovial joint and ventral edge of the ch at 72 hpf, and this expression pattern maintains after 72 hpf (Reed and Mortlock, 2010). *Gdf5* in amniotes is initially expressed in the peripheral mesenchyme of precartilaginous condensations to induce chondrocyte differentiation by potentially inducing *Sox9* expression, but it eventually becomes restricted to joint primordia to maintain developing joints (Buxton et al., 2001; Francis-West et al., 1999; Hatakeyama et al., 2004; Merino et al., 1999; Tsumaki et al., 2002). Therefore, zebrafish *gdf5* likely promotes chondrocyte differentiation during cartilage morphogenesis between 60-66 hpf and maintains joint primordia at later stages (Le Pabic et al., 2014; Yan et al., 2005).

Expression of *crabp2b* becomes restricted to the perichondrium between 54-72 hpf. We never tested for *crabp2b* expression beyond 72 hpf, but fluorescence recovery after photobleaching driven by the *crabp2bL:eGFP-Ntr* transgene suggests that -

1. *1crabp2b* and +1.2*crabp2b* regulatory regions can drive expression beyond 72 hpf. Circumstantial evidence for *crabp2b* continued expression beyond 72 hpf is provided by the expression of Cytochrome P450 Family 26 Subfamily B Polypeptide 1 (*cyp26b1*) in the 84 hpf perichondrium, where it delays and patterns ossification zones (Laue et al., 2008). While *crabp2b* is a Retinoic Acid (RA) binding protein that likely transports RA within the cell, *cyp26b1* is an enzyme that degrades RA and helps and likely helps shape RA gradients (Cai et al., 2012; Laue et al., 2008). This co-expression in embryonic cartilage perichondrium hints at the possibility that *crabp2b* plays a role in early cartilages by aiding the patterning of ossification zones.

In contrast, we failed to find evidence for expression of any of the genes known to be expressed in chick GP perichondrium in embryonic zebrafish perichondrium. *Crapb1*, *Abi3bp*, and *Col14a1* are expressed in the outer perichondrial layer, while *Dkk3*, *Mafb*, *Thbs2*, *Lgals1* are expressed in the inner layer (Bandyopadhyay et al., 2008). We never tested for *abi3bpa* or *abi3bpb* expression in embryonic zebrafish cartilages, nor did we for *crabp2b* in juvenile zebrafish GPs. However, our observations support the hypothesis that gene expression in the perichondrium changes as development progresses such that *gdf5* and *crabp2b* are required early in embryonic cartilage development, while genes such as *col14a1a* and *thbs2* likely play roles in mature perichondrium found in GPs.

Perichondrial expression of *gdf5* and *crabp2b* is likely controlled by multiple regulatory regions

A previous report found that murine *Gdf5* expression was controlled by two regions upstream of the *Gdf5* promoter and three other regions located within the introns of *Uqcc1*, a gene downstream of *Gdf5*. These regions were isolated from an upstream BAC that contains the two upstream regions and a downstream BAC that contains all five regions. However, only the regulatory region proximal to the *Gdf5* promoter displays some conservation in zebrafish. The murine upstream regions drive expression in jaw, ribs, vertebrae, and limbs (Chen et al., 2016), yet we failed to detect any expression driven by these elements contained within the CH73-166O16 BAC or the 5 kb region we isolated. This suggests that the upstream regulatory elements are insufficient to drive expression in the zebrafish jaw.

It is possible that zebrafish require the downstream regulatory elements to drive *gdf5* expression in jaw cartilage perichondrium. We were unable to test the downstream regulatory elements in zebrafish, which mainly drive limb expression in mice (Chen et al., 2016). However, there are several lines of evidence that suggest that the downstream regulatory elements are required for regulation of zebrafish *gdf5*. First, syntenic conservation in the genomic region containing *Uqcc1* and *Gdf5* in mice, humans, and zebrafish suggests interdependency between these the *Gdf5* and *Uqcc1* loci. Second, regulatory elements can be functionally conserved across species despite lacking sequence conservation. This is due to shuffling of transcription factor binding sites (TFBS) and changes in TFBS motif sequence in diverging species (Weirauch and Hughes, 2010). For instance, regulatory elements driving rhombomere-specific

Homeobox B2 (*Hoxb2*) expression are found in the *Hoxb2-Hoxb3* intergenic region and contain TFBS that are functionally conserved from zebrafish to humans, but their location and orientation within this intergenic region varies across species (Scemama et al., 2002). In addition, regulatory region sequences for Ret Proto-Oncogene Receptor Tyrosine Kinase (*RET*) are not conserved between humans and zebrafish, yet the human *RET* regulatory elements drive *ret* specific expression in zebrafish (Fisher et al., 2006). Therefore, additional *gdf5* elements likely exist in other locations relative to the gene in zebrafish. Finally, the spatial-temporal expression patterns produced by *Gdf5* downstream elements or BAC in murine phalanges and by zebrafish *gdf5* in jaw cartilage are similar (Chen et al., 2016; Merino et al., 1999). In addition, the downstream BAC that has all five regulatory elements have very similar expression pattern to that of the *Gdf5* construct containing the downstream elements in mice (Chen et al., 2016), suggesting that the downstream elements modulate the activity of the upstream elements in mice, and that zebrafish downstream elements may play a similar role in *gdf5* regulation. Therefore, it could be worthwhile looking for *gdf5* downstream regulatory elements in zebrafish if an appropriate BAC became available.

In addition, we found two regulatory regions in the *crabp2b* locus, *-1.1crabp2b* and *+1.2crabp2b*, that drive expression in the perichondrium as well as in chondrocytes and other tissues. Several lines of evidence suggest that these two regulatory elements are insufficient to reproduce *crabp2b* native expression, let alone drive perichondrium-specific expression. First, we show that *crabp2b* expression is largely restricted to cartilage between 48 and 72 hpf, in agreement with previous reports (Sharma et al., 2005; Thisse, 2004). Furthermore, single and concatenated *crabp2b* regulatory

elements drove expression in the pq perichondrium, contrasting with native *crabp2b* gene expression which is absent in the pq cartilage. These results would suggest that additional regulatory regions are needed to restrict this expression to the perichondrium. Two regions located within *crabp2b* introns and another one located downstream of *crabp2b* coding sequence showed some conservation, but histone modification profiles indicates weak or no transcription factor binding activity at 24 hpf (Aday et al., 2011; Zhang et al., 2008). The unavailability of similar histone modification binding profile data between 48-72 hpf limited our analysis. Obtaining different BACs that contain different sequence sizes around the *crabp2b* locus and that are appropriate for BAC recombineering could help identify distant elements regulating *crabp2b* expression. However, one conclusion that can be drawn from our study is that spatial-temporal regulation of perichondrial expression is likely controlled by multiple enhancers and repressors as cartilages mature. For instance, *crabp2b* was initially expressed in whole cartilage primordia at 48 hpf but progressively became restricted to the perichondrium by 72 hpf, timing that coincides with increasing *sox9a* activity in differentiating chondrocytes (Yan et al., 2005). Since Sox9 can act as a repressor in differentiating chondrocytes, it is possible that either *sox9a* or its downstream transcriptional effectors binds a regulatory region in the *crabp2b* locus to repress it in differentiating chondrocytes (Leung et al., 2011).

Perichondrial contributions to tendon and bone are likely modulated by multiple signaling pathways

We show that some *crabp2bL:eGFP-Ntr*-labeled perichondrial cells co-express *scxa:mCherry*, a marker for tendons, in specific cartilages sites where attachments to

muscles and tendons form (McGurk et al., 2017; Subramanian et al., 2018). Interestingly, we find that *crabp2bL:eGFP-Ntr,scxa:mCherry* co-expressing perichondrial cells are never anywhere near sites of endochondral ossification (Brinkley et al., 2016). For instance, we detected co-expressing cells across most of the length of the pq perichondrium except near the mandibular joint, the initial site of endochondral ossification in the pq cartilage. Similarly, endochondral ossification in the ch cartilage begins in the middle, but we only observed attachment sites in distal locations, suggesting a mechanism that selects tenogenic versus osteogenic differentiation exists in the perichondrium. Recent studies have shed light on this mechanism. The enthesis of murine long bones arises from cells co-expressing *Scx* and *Sox9* (Blitz et al., 2013). On the one hand, perichondrial osteogenic differentiation requires hedgehog (HH) signaling activation in the perichondrium to repress perichondrial *Sox9* expression, thereby repressing chondrogenic fate (Hojo et al., 2013; Leung et al., 2011). On the other hand, Fibroblast Growth Factor 2 (*Fgf2*) is expressed in cells surrounding the condyle in the murine jaw and targets Fibroblast Growth Factor Receptor 2 (*Fgfr2*) in adjacent perichondrium to promote enthesis formation via upregulation of *Scx* (Roberts et al., 2019). In turn, *Scx* activates *Bmp4* expression, which promotes *Sox9* expression at the enthesis primordium (Blitz et al., 2013; Blitz et al., 2009). Therefore, our observation that *crabp2bL:eGFP-Ntr,scxa:mCherry* co-expressing perichondrial cells that form cartilage-tendon attachment sites away from ossification zones is consistent with a model in which high HH signaling patterns ossification zones and represses tenogenic fate while high Fgf signaling is left to promote tenogenic fate away from ossification zones.

One caveat in this model is that the perichondrium forms in zebrafish craniofacial cartilages from cells in the periphery of cartilage primordia that fail to activate a positive feedback loop between *fat3/dchs2* signaling and *sox9a*. Consequently, perichondrial cells lack *sox9a* expression levels found in differentiating chondrocytes (Le Pabic et al., 2014). *Sox9* is required at high levels in RCs and PCs of GPs to promote chondrogenic fate (Bi et al., 1999; Zhao et al., 1997). *Sox9* is also required in other tissues such as the dorsal neural tube to promote neural crest specification but is eventually downregulated in most migrating neural crest (Cheung and Briscoe, 2003). However, *Sox9* expression in other tissues appears to be lower than that in cartilage (Zhao et al., 1997). Therefore, one possibility is that low levels of *sox9a*, when co-expressed with *scxa*, are sufficient to specify enthesis formation in zebrafish cartilages. Alternatively, *scxa/sox9a* co-expressing cells may only exist transiently during the initial stages of cartilage differentiation such that *sox9a* is subsequently be turned off in the perichondrium as cartilages develop. If the *crabp2bL:eGFP-Ntr* transgene is expressed in Mc cartilage primordium at 48 hpf embryos as *crabp2b* is, it would be possible to monitor Mc cartilage primordium development in live *crabp2bL:eGFP-Ntr;scxa:mCherry* double transgenic embryos and determine when *scxa:mCherry*-labeled perichondrium arises. This would provide context for when to look for *sox9a/scxa* co-expressing cells.

CHAPTER V

Correlations between chondrocyte polarity and ossification patterning

Introduction

Cartilages contribute to bone formation by serving as templates for most of our bones during embryonic and fetal development and by promoting bone growth via growth plates (GP) until adulthood. The formation of GPs requires that cartilages begin ossifying in specific locations. The basic pathways involved in shaping cartilages and those driving ossification of cartilages are known. However, whether the mechanisms involved in shaping cartilages influence where ossification zones begin is unknown.

A lot of what is known about endochondral ossification was learned studying the GP in amniote long bones. The GP is a specialized structure where chondrocytes transition from the Resting Zone (RZ) to the Proliferation Zone (PZ), and finally to the Hypertrophic Zone (HZ) where ossification begins. The RZ is where slow-dividing Resting Chondrocytes (RC) that serve as a reserved population for the GP reside. These eventually transition into the PZ and become Proliferating Chondrocytes (PC), which expand the PZ via proliferation. PCs eventually transition into the HZ and become hypertrophic chondrocytes (HC), the final stage of chondrocyte differentiation (Kronenberg, 2003). Two signals, Indian Hedgehog (*Ihh*) and Parathyroid Hormone-Like Hormone (*Pthlh*), form a negative feedback loop that coordinates transition between zones and ossification rates (Vortkamp et al., 1996). *Ihh* from the HZ promotes hypertrophic differentiation in PCs adjacent to the HZ and promotes *Pthlh* expression in the resting zone (St-Jacques et al., 1999; Vortkamp et al., 1996). *Pthlh* is expressed in

the RZ and represses hypertrophic differentiation in the PZ (Chung et al., 2001; Schipani et al., 1997; Weir et al., 1996). However, the mechanism that patterns initial HZs in cartilages is not well understood.

Prior to initiation of HZ development, embryonic cartilages are formed by convergent extension (CE)-like movements controlled by pathways known to coordinate Planar Cell Polarity (PCP) in epithelia (Kronenberg, 2003). PCP is the polarity of epithelial cells along the plane of the tissue, and two pathways known to control this process are required for cartilage morphogenesis and bone elongation. The first one has been more extensively studied in *Drosophila*. It involves heterotypical binding of protocadherins Fat (*Ft*) and Dachsous (*Ds*) (Matakatsu and Blair, 2004). *Ft* is expressed across the tissue uniformly, while *Ds* is expressed in a gradient (Yang et al., 2002). The Golgi resident protein Four-jointed (*Fj*) is expressed in an opposite gradient to *Ds* and adds phosphate groups to the cadherin extracellular domains of *Ds*, which modifies *Ds* ability to bind *Ft* (Simon, 2004; Strutt et al., 2004; Yang et al., 2002; Zeidler et al., 1999). This in turn creates a gradient of PCP activity across tissues that influences the asymmetrical subcellular localization of effectors such as Dachs (*D*) (Mao et al., 2011). Additionally, Atrophin (*Atro*), a transcriptional repressor, interacts with the *Ft* intracellular domain and is required for fruit fly eye polarization, though how it accomplishes this is still unclear (Fanto et al., 2003).

A recent study shows that CE in zebrafish jaw cartilages requires *fat3*, *dchs2*, and *rerea*, which are orthologs of *Drosophila*'s *Ft*, *Ds*, and *Atro*, respectively. However, *fat3* and *dchs2* also form a positive feedback loop with *sox9a*, which is required for chondrocyte differentiation, such that only differentiating chondrocytes in the center of

the cartilage anlagen undergo CE. This results in stacking of chondrocytes like a pile of coins along the length of the cartilage where the orientation of Microtubule Organizing Centers (MTOC), an indicator of cell polarity, is reproducibly biased in specific directions within cartilages. Peripheral cells of the primordium become perichondrium, a thin layer of cells that wrap around chondrocytes, (Le Pabic et al., 2014). Despite these findings, no graded expression for any of these PCP components has been observed in cartilages.

The second pathway controlling PCP is known as the core pathway. In *Drosophila*, it relies on asymmetrical subcellular distribution and recruitment to adherens junctions of 6 proteins. The first three are transmembrane components Frizzled (*Fz*), Van Gogh (*Vang*), and Flamingo (*Fmi*), and the remaining ones are cytosolic components Dishevelled (*Dsh*), Prickle (*Pk*), and Diego (*Dgo*) (Goodrich and Strutt, 2011). Their asymmetrical distribution is transmitted to neighboring cells via interactions between *Fz*, *Fmi*, and *Vang* (Chen et al., 2008; Strutt and Strutt, 2008; Wu and Mlodzik, 2008). While the mechanism that generates core PCP component asymmetrical distribution is not well understood, it is thought that it involved an upstream signaling gradient that, and there is evidence to suggest that this upstream signaling gradient may involve the *Ft/Ds* pathway (Olofsson et al., 2014; Sharma and McNeill, 2013; Sharp and Axelrod, 2016; Yang et al., 2002). In contrast, there is no evidence to suggest that this signaling gradient involves Wnt signaling through *Fz* since polarization proceeds normally in absence of several Wnts (Chen et al., 2008; Lawrence et al., 2002).

In contrast, core PCP signaling in vertebrates requires non-canonical Wnt signaling, or Wnt-PCP. In cartilage, Wnt Family Member 5A (*Wnt5a*) ligand binds to Tyrosine Kinase Orphan Receptor 2 (*Ror2*) (Oishi et al., 2003), activating a downstream signaling cascade that is required for proper Vangl Planar Cell Polarity 2 (*Vangl2*) asymmetrical subcellular localization (Gao et al., 2011; Qian et al., 2007). These observations and the fact that *Wnt5a* expression is highest within the HZ of murine GPs has led to the proposition that *Wnt5a* signaling gradients may be responsible for generating core PCP component asymmetry in cartilages (Andrade et al., 2007). However, no direct evidence for this has been found. Recent studies in zebrafish show that *wnt5b*, a *Wnt5a* paralog, and *gpc4* are required for CE in jaw cartilages during the same developmental stage as *fat3* and *dchs2* (LeClair et al., 2009; Sisson et al., 2015). Beyond this, nothing else is known regarding how Wnt-PCP works in cartilages.

Interestingly, chondrocyte polarity appears to mark the location of future ossification zones. Unpublished observations from our lab show that the 72 hpf ceratohyal (ch), a rod-like cartilage that provides support for the zebrafish jaw and begins ossifying in the middle like mammalian long bones, can be subdivided in two zones along its length. While the ventral half of the ch is defined by a dorsally oriented chondrocyte polarity bias, the dorsal half is defined by a ventrally oriented chondrocyte polarity bias. The polarity transition zone between these two segments corresponds to the future HZ initial location. However, this correlation is unlikely to reflect a causal relationship since the location of HZs in *gpc4* zebrafish mutants is largely unchanged (LeClair et al., 2009). In addition, unpublished observations from our lab show that HZ patterning is also unaffected in *wnt5b* mutants. These observations suggest that

chondrocyte polarity does not determine HZ patterning. However, cartilage HZ and polarity patterning may be determined by shared upstream signals.

To test mechanisms of polarity propagation during cartilage morphogenesis and to address correlations between chondrocyte polarity and HZ patterning, we used 2-photon laser ablation to disrupt chondrocyte polarity and reduce cartilage size. Here we show that ablating differentiating chondrocytes in the ch reduced total cell numbers and appeared to disrupt their polarity at 72 hpf in the ablation zone, though the difference was not significant. In addition, this local ablation did not disrupt chondrocyte polarity in adjacent non-ablated zones of the cartilage. Finally, we were unable to test correlations between chondrocyte polarity and ossification patterning in the ch due to technical reasons.

Materials and methods

Ethics statement

All animals were handled in strict accordance with good animal practice as defined by the relevant national and/or local animal welfare bodies, and all animal work was approved by the University of California, Irvine Institutional Animal Care and Use Committee.

Animals and transgenics

All zebrafish used were of the AB strain. Zebrafish were raised and staged as previously described (Kimmel et al., 1995; Schilling and Kimmel, 1997). For anesthesia, a tricaine stock solution was prepared as previously described (Westerfield, 2000), and a working solution was prepared by using 5% of the stock solution in embryo medium (EM). The

sox10:lyn-tdTomato transgenic line was previously generated in our lab (Schilling et al., 2010). The *entpd5a:kaede* transgenic line was kindly provided by Dr. Stefan Schulte-Merker (Lleras Forero et al., 2018).

Dr. Daniel Dranow generated the *ubi:cent4-GFP* transgenic line using the Gateway Tol2 system (Kawakami and Shima, 1999; Kwan et al., 2007) in combination with Gibson cloning (Gibson et al., 2009). First, primers
gtacaaaaaagcaggctggacGCCACCATGGTGAGCAAGGG (eGFPPF),
gaagccggacgccatTAGGGCTGCAGAATCTAGAGGCTC (eGFPR),
gattctgcagccctaATGGCGTCCGGCTTCAGGAA (*cent4F*), and
gtgctatagggctgcagaatctagTCAGTACAGATTGGTTTTCTTCATAATCC (*cent4R*) were used to amplify *eGFP* and Centrin 4 (*cent4*) from a pME-*eGFP* plasmid (Kwan et al., 2007) and cDNA, respectively, by PCR. These fragments were cloned into a pME-*eGFP* NcoI/XbaI-digested plasmid via Gibson cloning as previously described (Gibson et al., 2009) to generate middle entry vector pME-*cent4-eGFP*. The 5' entry vector carrying a Ubiquitin B (*ubb*) promoter, p5E-*ubb*, has previously been described (Mosimann et al., 2011). These plasmids were transformed into DH5 α competent cells (in-house generated). pDestTol2CG2-*ubb:cent4-GFP* was assembled according to the Tol2 Kit protocol (Kwan et al., 2007) and transformed into DH5 α competent cells. Transposase mRNA was synthesized from the pCS2FA-transposase plasmid (Kwan et al., 2007) digested with NotI using Invitrogen mMESSAGING mMACHINE™ T7 ULTRA Transcription Kit (Catalog # AM1345). 500 μ l of cocktail mixes containing 40 ng/ μ l of plasmid and 60 ng/ μ l of transposase mRNA were injected into 1-cell stage embryos.

Stable *ubb:cent4-GFP* transgenic zebrafish lines were maintained by selecting for embryos with green fluorescent hearts (Kwan et al., 2007).

Imaging

Embryos for live imaging were embedded in 1% low melting point agarose (APEX, Catalog # 9012-36-6) diluted in EM containing 5% of tricaine stock solution. Embryos labeled by *in situ* hybridization were mounted on slides, then imaged on a Zeiss Axioplan 2 microscope equipped with a MicroPublisher 5.0 RTV camera using Volocity software (Improvision). Live embryos between 50-52 hours post-fertilization (hpf) from Figure 1 were imaged on a Zeiss LSM780 confocal microscope using a 63x/1.15 W C-APO objective. Live embryos between 72-120 hpf were imaged using a Nikon ECLIPSE Ti confocal microscope equipped with a PLAN APO VC 60X/1.20 WI objective. ImageJ/Fiji was used for image processing. For cell polarity measurements, each cell was divided into 4 quadrants to determine MTOC position. MTOC positions were plotted as rosette diagrams and Watson's U2 tests for significance were conducted using Vector Rose (PAZ software). Cartilage length plot (Figure 4) was made using Excel, and one-way ANOVA test was conducted independently using an online calculator (Stangroom, 2018).

***In situ* hybridization**

The *col10a1a* probe was previously described (Avaron et al., 2006). The plasmid containing the probe was transformed into DH5 α cells (in-house generated). The plasmid was digested with EcoRI and probe synthesized using Roche DIG RNA Labeling Mix (Catalog # 11277073910) and T3 RNA Polymerase (Catalog #

11031163001) as directed. Whole-mount *in situ* hybridization was carried out as previously described (Thisse et al., 1993), with the following modifications. Anti-Digoxigenin-AP, Fab fragments antibody (Roche, Catalog # 11093274910) dilution was 1/1000.

2-photon laser ablation

2-photon laser ablations for this study were done using in two different units. 2-photon palatoquadrate (pq) laser ablations (Figure 1A-D) and in the ch of *sox10:lyn-tdTomato;ubi:cent4-GFP* double transgenic embryos (Figure 3D, E) were done in a Zeiss LSM780 confocal microscope using a 63x/1.15 W C-APO objective and equipped with a Spectra-Physics MAI TAI 2-photon Laser. The remaining ablations were done in a Zeiss LSM880 confocal microscope using an Olympus LUMPlanFL N 40x/0.80 W Details objective and equipped with a Spectra-Physics MAI TAI HP 1020 2-photon laser. For ablations in the pq, the 2-photon laser was targeted to a rectangle of about 16x16 μm in the desired region of interest. For ablations in the dorsal ceratohyal (ch), the 2-photon laser was targeted to two rectangles of about 16x16 μm drawn next two each other along the length of the cartilage, one at a time. For ablations in the ventral ch, the approach was as in dorsal ch ablations, except that the rectangles were of about 12x12 μm . In all cases, 2-photon laser power was set to 100%, and scanning speed was set to the fastest. Using detectors for the visible spectra, we waited for an air bubble to form in the region being ablated in order to stop laser exposure.

Results

Disruption of chondrocyte intercalation after ablation is restricted to the ablation zone

Zebrafish jaw cartilages begin CE around 50 hpf. By 54 hpf, cartilage stacks are clearly visible in *sox10:lyn-tdTomato* transgenic embryos, which mark chondrocyte plasma membranes in red. Chondrocyte CE slows down after 54 hpf, and chondrocyte CE is done in most jaw cartilages by 72 hpf (Le Pabic et al., 2014). To disrupt cartilage morphogenesis without causing holes in the cartilage, we ablated patches of cells within the cartilage condensations at 52 hpf, when chondrocyte progenitors are still moving and intercalating. We selected ablation zones by observing where cells were actively intercalating in developing cartilages. Intercalating cells are often triangular, a result of their CE movements (Le Pabic et al., 2014). We noticed that intercalating cells in the pq were brighter than surrounding cells and easier to identify. This is due upregulation of the *sox10:lyn-tdTomato* transgene that serves as an indirect readout of *sox9a* activation in differentiating chondrocytes, which leads to *fat3* and *dchs2* upregulation. (Le Pabic et al., 2014). The lateral part of the pq cartilage began intercalating first, and forming chondrocyte stacks were visible by 52 hpf (Figure 5.1A). The remainder of the pq formed by progressive chondrocyte intercalation from the anterior, medial, and posterior edges of the formed stack, resulting in a flat cartilage which in cross section appears as a single cell row (Figure 5.1D). Since polarization relies on non-cell autonomous induction of PCP component asymmetrical distribution via cell-to-cell contact (Ambegaonkar et al., 2012; Bosveld et al., 2012; Brittle et al., 2012; Chen et al., 2008; Strutt and Strutt, 2008; Wu and Mlodzik, 2008), we hypothesized that these movements

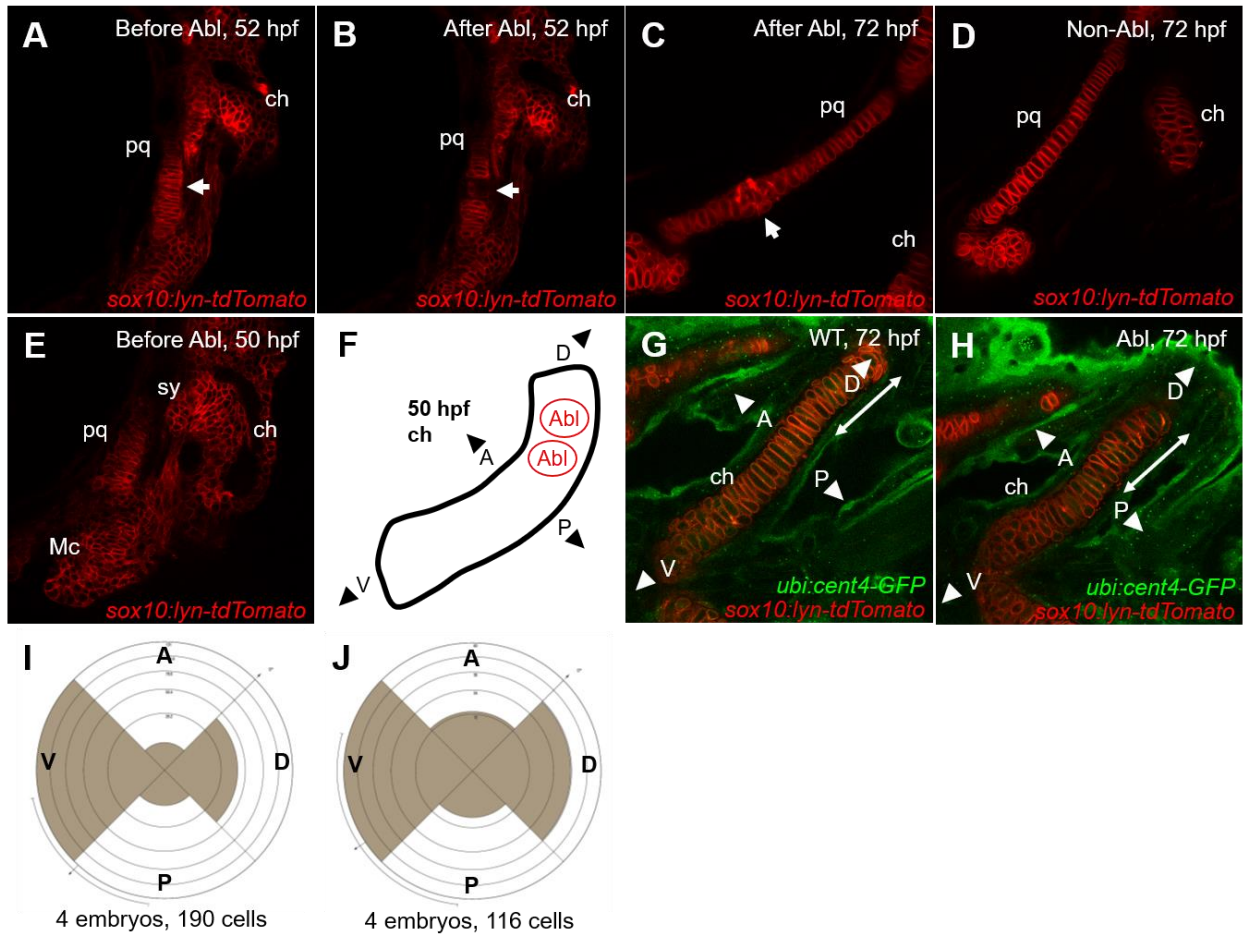


Figure 5.1: Laser ablations locally disrupt cartilage intercalation and polarity. (A-D) Live imaging (optical slices) of *sox10:lyn-tdTomato* embryos laser ablated in the palatoquadrate (pq) at 52 hpf, imaged between 52 and 72 hpf, lateral views. (A) The forming pq is shown before laser ablation at 52 hpf. (B) The forming pq is shown after laser ablation at 52 hpf. (C) The ablated pq is shown after laser ablation at 72 hpf. (D) The pq of a non-ablated embryo is shown at 72 hpf. (E-J) Live imaging (optical slices) and analysis of *sox10:lyn-tdTomato;ubi:cent4-GFP* double transgenic embryos laser ablated in the dorsal ceratohyal (ch) at 50 hpf, imaged between 50 and 72 hpf. (E) The dorsal region of the forming ch is shown prior to laser ablation at 50 hpf, lateral views. Only the *sox10:lyn-tdTomato* channel is shown. (F) A representation of the developing ceratohyal at 50 hpf is shown, including the zones targeted by laser ablation and the anterior-posterior and dorsal-ventral axis used to quantify cell polarity, lateral view. (G, H) The chs of wild-type (G) and ablated (H) embryos are shown, including the anterior-posterior and dorsal-ventral axis used to quantify cell polarity, and the zone where 10-cell chondrocyte rows were counted, ventral views. (I, J) Graphical representation of the number of cells polarized in any direction in 4 embryos that were either wild-type (I) or ablated (J). White arrows indicate the sites of ablation in the pq. White and black arrowheads indicate the directions of the anterior-posterior and dorsal-ventral axis. Bidirectional arrows indicate the region where 10-chondrocyte rows were counted. pq=palatoquadrate, ch=ceratohyal, sy=symplectic, Mc=Meckels, A=anterior, P=posterior, D=dorsal, V=ventral.

could help relay a spatial-temporal gradient of PCP signaling across the pq cartilage. Therefore, we ablated a patch of intercalating cells on the lateral edge of the pq cartilage primordium and looked for intercalation defects (Figure 5.1A, B). We observed *sox10:lyn-tdTomato*-positive cell debris was apparent at the ablation zone at 72 hpf, which marked the ablation zone and suggested that laser cell ablations were successful (Figure 5.1C). While non-ablated pq cartilages stacked normally and formed single cell rows, cells within the ablated zone in ablated pq cartilages failed to form a single cell row at 72 hpf (Figure 5.1C, D). Chondrocyte stacking in adjacent regions of the cartilage was not disrupted (Figure 5.1C). Since medial pq cartilage forms after the more lateral intercalating stacks that we targeted for ablation, this result suggests that laser ablation does not disrupt CE beyond the ablation zone.

Ablations disrupt cartilage polarity bias

We showed that laser ablation led to CE defects in the pq cartilage, leading us to hypothesize that chondrocyte polarity would also be disrupted by 72 hpf. To test this, we used *sox10:lyn-tdTomato;ubi:cent4-GFP* double transgenic embryos in which chondrocyte membranes are labeled red, and microtubule organizing centers (MTOCs) are labeled green. Next, we assigned quadrants, which corresponded to ventral, dorsal, anterior, and posterior orientation of the ch within the embryo to each individual chondrocyte. Next, we assigned a polarity for each chondrocyte based on which quadrant the MTOC was located, and we quantified the number of chondrocytes polarized in either direction. A similar approach was used previously (Le Pabic et al., 2014).

In order to test the effects of laser ablations on chondrocyte polarity, we targeted the dorsal half of the ch primordium at 50 hpf, which we identified by using the intercalating symplectic (sy) cartilage and a group of bright *sox10:lyn-tdTomato* positive cells posterior to the sy as a reference (Figure 5.1E, F). We were unable to determine the number of ablated cells for each experiment due to low *sox10:lyn-tdTomato* signal and photobleaching in the ch anlagen, limiting image quality during the ablation process. We mounted these embryos ventrally in order to see a cross section along the length of the ch and determine chondrocyte polarity. We observed that ablated ch cartilages had decreased total number of chondrocytes when compared to wild-types (WT) in average at 72 hpf, though this decrease in ablated cartilages was variable. We interpreted ablated cartilages with lower total cell count to be successful ablations. Therefore, we selected 4 ablated ch cartilages with the lowest total cell count and 4 WTs for analysis. Average total cell counts were 138.75 in WT (n=4) and 90.75 in ablated embryos (n=4). We first compared polarity bias in the ablated dorsal part of the ch cartilage. Since we were unable to see cell debris from our ablations, we selected a segment of the ch starting from the dorsal edge where 10 intercalated cells in a row could be counted along the length of the ch and quantified the polarity of all cells contained within the length of the selected cell row (Figures 5.1G, H). We counted a total of 116 cells in ablated embryos (n=4) and 190 cells in WT embryos (n=4). Within this section of the cartilage, we noticed several instances where chondrocyte polarity was reversed in adjacent chondrocytes, and the locations of these reversals appeared random from embryo to embryo. Despite this, our cell polarity counts in WTs showed that 131 were ventrally biased, 43 dorsally biased, 10 anteriorly biased, and 6

posteriorly biased, reflecting a ventral polarity bias within this segment and confirming previous observation in our lab showing that the dorsal half of the ch cartilage is ventrally biased (Figure 5.1I). In contrast, cell polarity counts in ablated cartilages showed that 60 were ventrally biased, 35 dorsally biased, 8 anteriorly biased, and 13 posteriorly biased, suggesting that ventral polarity bias was reduced in ablated dorsal ch when compared to WTs (Figure 5.1J). The difference in polarity bias between ablated and WT dorsal ch was not significant. This result suggests that laser ablation disrupts chondrocyte polarization.

Laser ablations do not affect chondrocyte polarity in distant parts of the cartilage

Given the two distinct zones of polarity bias within the ch, our observation that intercalation defects were localized to the ablation zone in pq cartilages led us to hypothesize that the polarity of one zone was independent of the other zone. To test this idea, we used *sox10:lyn-tdTomato,ubi:cent4-GFP* double transgenic embryos and carried out 2-photon laser ablations in the ventral sections of the ch at 50 hpf (Figure 5.2A). Then, we mounted these embryos laterally and quantified polarity bias in the dorsal portion of the ch at 72 hpf. Ablations on the ventral ch decreased *sox10:lyn-tdTomato* expression locally when compared to WT, suggestive of chondrocyte failure to differentiate (Figure 5.2B, C). For this reason, we were unable to determine total cell number in ablated ch cartilages. Like in the previous experiment, we counted 10-cell rows along the length of the ch cartilage starting from the dorsal edge and quantified the polarity of the chondrocytes located within the length of the cartilage covered by the 10-cell row. We counted the polarity of 135 chondrocytes in WTs (n=4) and 150 chondrocytes in ablated embryos (n=4). We attributed this difference in cell counts to

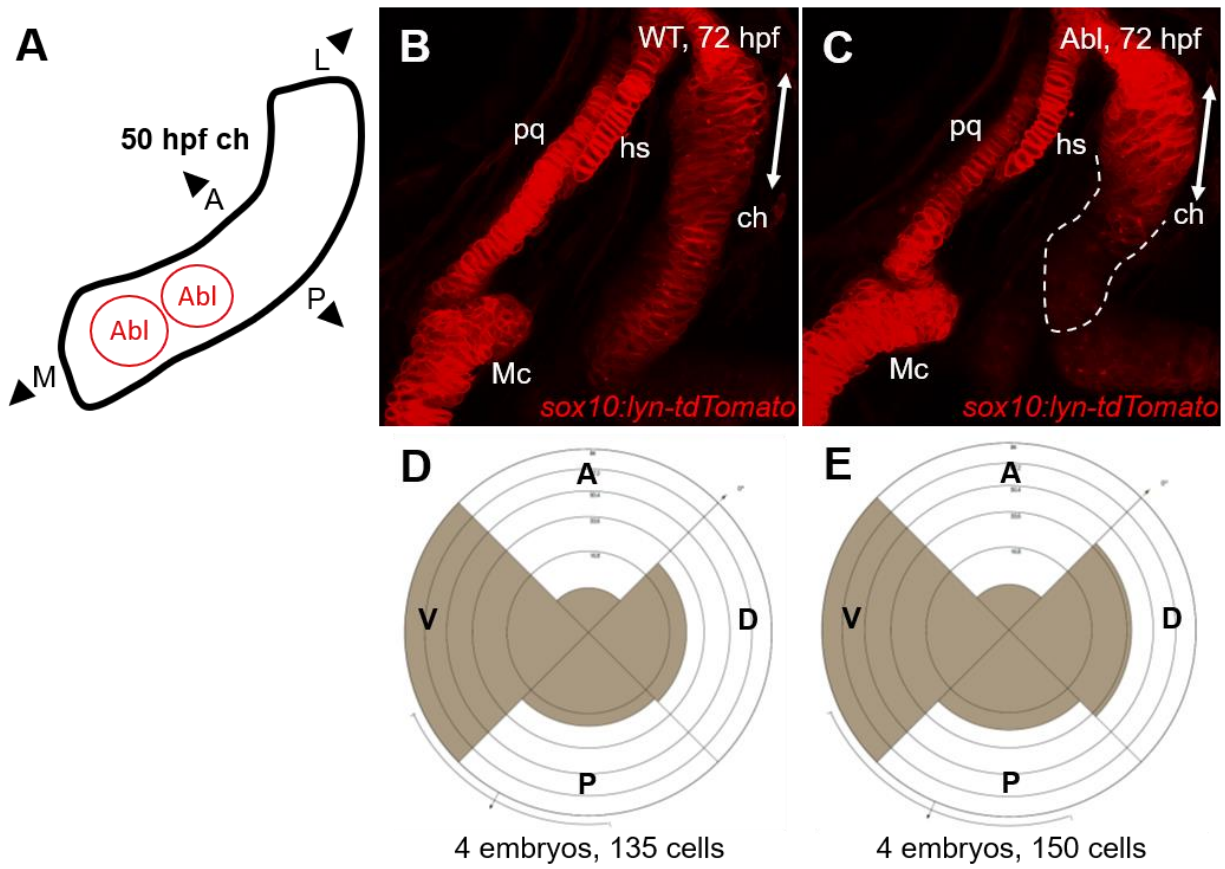


Figure 5.2: Laser ablations in the ventral section of the ch do not affect cell polarity dorsally. (A) A representation of the developing ch at 50 hpf is shown, including the zones targeted by laser ablation and the anterior-posterior and dorsal-ventral axis used to quantify cell polarity, lateral view. (B, C) Live imaging (3D projections) of *sox10:lyn-tdTomato,ubi:cent4-GFP* double transgenic embryos laser ablated in the ventral ch at 50 hpf, imaged at 72 hpf. Only the *sox10:lyn-tdTomato* channel is shown. The ch of wild-type (B) and ablated (C) embryos are shown, including the zone where 10-cell chondrocyte rows were counted, ventral views. (D, E) Graphical representation of the number of cells polarized in any direction in 4 embryos that were either wild-type (D) or ablated (E). Black arrowheads indicate the directions of the anterior-posterior and dorsal-ventral axis. Bidirectional arrows indicate the region where 10-chondrocyte rows were counted. pq=palatoquadrate, ch=ceratohyal, hs=hyosymplectic, Mc=Meckels, A=anterior, P=posterior, D=dorsal, V=ventral.

the fact that the ch appeared transversely into the z-stack due to our lateral mounting, so small variations in mounting angle may have slightly affected the angle in which the ch was imaged, slightly changing the number of cells contained within the length of the 10-cell row. Cell polarity counts in WTs showed that 84 were ventrally biased, 36 dorsally biased, 24 anteriorly biased, and 6 posteriorly biased, showing that the ventral bias is still observed in this segment regardless of the angle in which the ch cartilage is imaged (Figure 5.2D). In comparison, cell polarity counts in ablated cartilages showed that 84 were ventrally biased, 24 dorsally biased, 22 anteriorly biased, and 5 posteriorly biased, a polarity bias distribution that appears virtually unchanged when compared to WTs (Figure 5.2E). This result suggests that, just as in CE, laser ablations can only disrupt chondrocyte polarity locally.

Testing correlation between chondrocyte polarity and ossification patterning

A recent study showed that the PZ of juvenile *gpc4* mutant zebrafish GPs lose their flattened and stacked morphology, yet ossification patterning was undisrupted (LeClair et al., 2009). In addition, CE in zebrafish jaw cartilages requires *wnt5b* and *gpc4* (Sisson et al., 2015), and preliminary data from our lab shows that jaw cartilage polarity is disrupted in *wnt5b* and *gpc4* mutants. Together, these observations suggest that polarity itself does not determine HZ locations within cartilages. Since we confirmed that ablations reduce total cell numbers in 72 hpf cartilages and that polarity is only disrupted locally by ablations, we thought that the position of the ch HZ would relocate to the new mid region of ch cartilage if we could reduce ch cartilage length on one side via laser ablation. This hypothesis was based on the premise that a long-range repressive signal such as Pthlh may be responsible for initial HZ patterning.

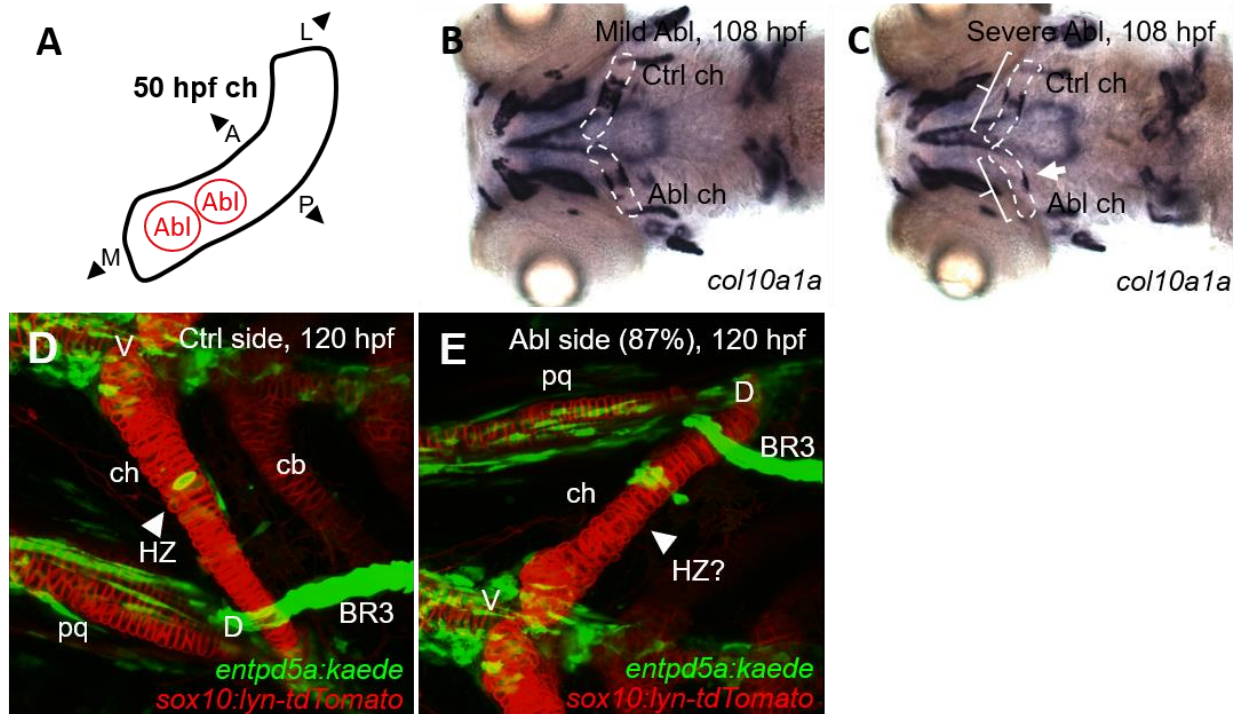


Figure 5.3: The effects of laser ablations in the ventral ch assayed by *in situ* hybridizations and live imaging are incongruent. (A) A representation of the developing ch at 50 hpf is shown, including the zones targeted by laser ablation and the anterior-posterior and dorsal-ventral axis used to quantify cell polarity, lateral view. (B,C) *In situ* hybridizations for *col10a1a* in embryos where the ventral section of the right ch was laser ablated at 50 hpf, ventral views. Embryos were fixed at 108 hpf. (B) Example of an ablation showing a mild effect. No cartilage size or ch *col10a1a* expression differences are noticeable. (C) Example of an ablation showing a more severe effect. The ablated ch cartilage appears slightly smaller and *col10a1a* expression appears reduced. (D, E) Live imaging (3D projections) of a *sox10:lyn-tdTomato:entpd5a:kaede* double transgenic embryo showing the non-ablated left ch (D) and the right ch (E) ablated at 50 hpf, imaged at 120 hpf, ventral views. This embryo showed the biggest reduction in ch length (87% the length of the non-ablated ch), and the hypertrophic zone is absent. Black arrowheads indicate the directions of the anterior-posterior and dorsal-ventral axis. The white arrow indicates the position where *col10a1a* expression is decreased. Dashed lines outline the ch cartilage. White brackets show the length of the right and left ch cartilages in the severe example of an ablation (C). White arrowheads indicate the position of the HZ. pq=palatoquadrate, ch=ceratohyal, cb=ceratobranchial, HZ=hypertrophic zone, D=dorsal, V=ventral, BR3=branchiostegal ray 3, Ctrl=control, Abl=ablated.

To test this idea, we grew the embryos that we ablated in the ventral ch to 108 hpf, performed *in situ* hybridization for *col10a1a*, which marks the ch cartilage HZ (Eames et al., 2011; Girkontaite et al., 1996; Mitchell et al., 2013), and used the ch cartilage in the non-ablated side of the embryo as an internal control to monitor the effects of ablations on HZ development and position within the cartilage. While some ablated cartilages appeared largely undisturbed when compared to the control side (Figure 5.3B), other ablated ch cartilages showed decreased *col10a1a* staining in the ch cartilage HZ when compared to the control side (Figure 5.3B). In addition, some ablated ch cartilages appeared shorter when compared to their control side, and the HZ moved dorsally as if to maintain the distance from the HZ to the ventral edge of the cartilage at the expense of the distance from the HZ to the dorsal edge (Figure 5.3B). However, we did not quantify this since fixing, staining, and mounting these embryos could have introduced artifacts that could affect our measurements. Instead, we used *sox10:lyn-tdTomato;entpd5a:kaede* double transgenic embryos, which mark chondrocyte plasma membranes in red and osteoblasts in green (Geurtzen et al., 2014; Le Pabic et al., 2014). We repeated our 2-photon laser ablation on the ventral side of the ch, imaged live embryos at 120 hpf to allow the *entpd5a:kaede* transgene to sufficiently mark the HZ (Figure 5.3D, E), and measured ch cartilage length. We carried out several sets of ablation experiments but the ch cartilage length reductions we obtained were often negligible. To avoid diluting our results with seemingly unsuccessful ablation attempts, we selected the ablation experiment where we obtained the biggest ch cartilage size reduction. We ablated the right ch cartilage in 9 embryos at 50 hpf and compared them to 6 WT embryos. In WTs, average cartilage length was 237.24 (Std. Dev. 7.62)

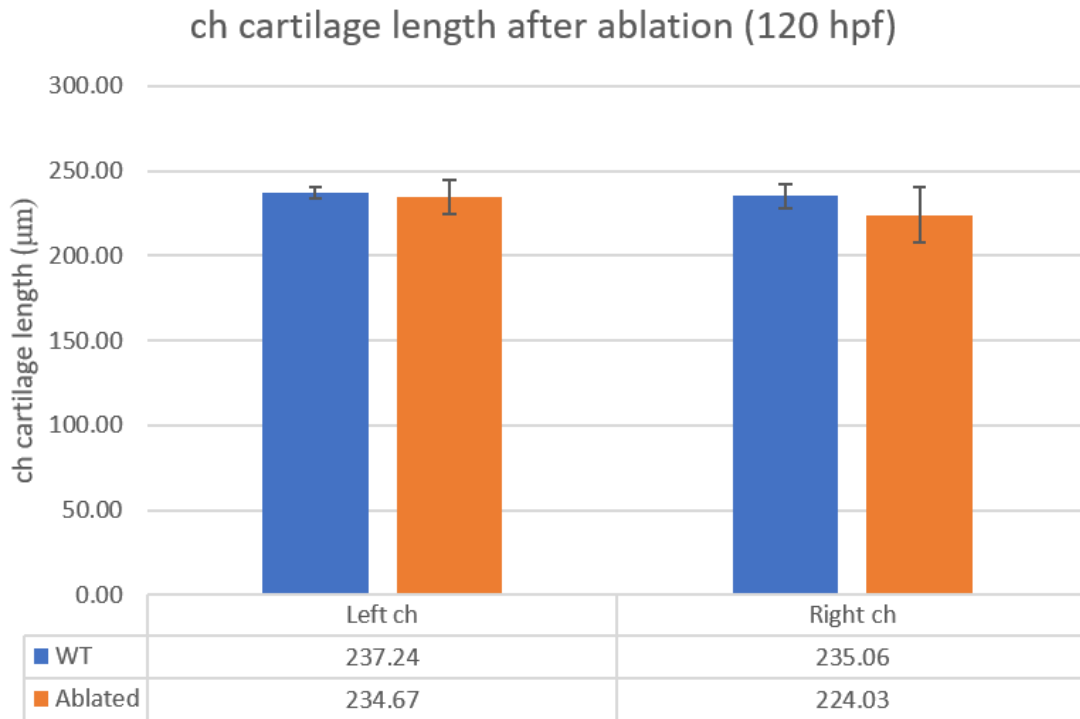


Figure 5.4: The difference in length between ablated and non-ablated ch cartilages in live imaged embryos is negligible. Graphical representation of ch cartilage length corresponding to the experimental set in Figure 5.3D and E. The X axis shows left versus right ch cartilages and wild-type (blue) versus ablated (orange) embryos. Only the right chs were ablated. Error bars represent the standard deviation. ch=ceratohyal, WT=wild-type.

microns (μm) for the left ch and 235.06 (Std. Dev. 6.83) μm for the right ch (Figure 5.4). In contrast, average cartilage length in ablated embryos was 234.67 (Std. Dev. 10.02) μm for the left ch and 224.03 (Std. Dev. 16.25) μm for the right (ablated) ch (Figure 5.4). The right ch was 4.5% of the length of the left ch in ablated embryos, suggesting that ablations caused a small reduction in ch cartilage length. However, one-way ANOVA revealed that this reduction was not significant (F-ratio=2.04; $p=0.135$). The single largest difference in ch cartilage length obtained in this experiment was for an embryo for which we measured the left ch at 218.78 μm and the right ch at 189.73 μm (Figure 5.3D, E). This was a 13.3% reduction in ch cartilage length, yet most ablations failed to reduce ch cartilage length beyond 5%. Such cartilage length reduction was insufficient to test our hypothesis. After realizing this, I stopped working on this project.

Discussion

This work describes the effects of laser ablation on chondrocyte polarity in the ch cartilage. First, we showed that laser ablations in the pq cartilage anlagen at the onset of cartilage morphogenesis can lead to local stacking defects that are contained to the ablation zone at 72 hpf. Next, we found that laser ablations performed at 50 hpf in the ch primordium appear to locally disrupt chondrocyte polarity without affecting chondrocyte polarity in unablated regions of the cartilage at 72 hpf. Finally, initial observations suggested that ch cartilages that were ablated in their ventral region were shorter, but that the position where the HZ formed was unchanged relative to the ventral edge such that the length of the cartilage between the HZ and the dorsal edge of the ch cartilage was reduced. This led us to hypothesize that endochondral bones were likely patterned by a repressive signal originating from the ventral edge of the ch. However,

we were unable to test this hypothesis because we failed to detect similar reductions of ch cartilage length in live embryos.

Long-range chondrocyte polarity propagation cell-to-cell is unlikely

Unpublished data from our lab shows that zones of chondrocyte polarity bias exist within craniofacial cartilages, so one of our aims was to determine how these patterns arise. We first observed that CE in the pq cartilage primordium initiates at the lateral edge of the cartilage and proceeds medially as a wave. This phenomenon has also been observed during fruit fly eye morphogenesis and zebrafish gastrulation CE (Heberlein et al., 1993; Myers et al., 2002). Since asymmetrical distribution of *Ft* and *Ds* and core PCP components depends on non-cell autonomous cell-to-cell interactions (Ambegaonkar et al., 2012; Bosveld et al., 2012; Brittle et al., 2012; Chen et al., 2008; Strutt and Strutt, 2008; Wu and Mlodzik, 2008), we thought that a polarity pattern could arise initially at the lateral edge of the pq cartilage primordium and be relayed to more medial cells as the CE front advances. Our approach was to cause disruptions in stacking and/or polarity by laser ablation. However, perturbations of stacking on the lateral edge of the pq cartilage primordium were restricted to the ablation zone and did not propagate medially. Similarly, perturbations of cell polarity in the ch appeared to be contained to the ablation zone and did not affect the opposite side of the cartilage. Ablations likely disrupt cell-to-cell interactions between cells repopulating the ablation zone resulting in mislocalization of core PCP components, which we infer from MTOC orientation. However, cells beyond the ablation zone retain undisturbed PCP signaling, so they polarize properly. Either the degree of polarity disruption we achieved by ablations is insufficient to propagate polarity defects beyond the ablation zone, or

chondrocyte polarity propagation likely depends on local cues and not long-range cell-to-cell interactions.

A different model proposes that signaling activity between *Ft* and *Ds* regulate a secondary signal that polarizes cells at distance independently of cell contacts. The observations that *Ft* and *Ds* regulate polarity through physical interactions with *Atro*, a transcriptional repressor, and that fruit fly ommatidial polarity inside of *Ft* and *Ds* mutant clones is rescued more than one cell row inside the clone boundary led to the proposition of this model (Fanto et al., 2003; Sharma and McNeill, 2013). However, chondrocytes contact and slide past each other, which complicates any interpretation of mosaic analysis aimed to test this model. Furthermore, detection of subtle long-range effects by mosaic manipulations in the fruit fly eye is aided by the fact that polarity is predictable and uniform starting from the eye equator up to the poles. On the other hand, it seems as if individual chondrocyte polarity can only be defined by the probability of a given chondrocyte to be polarized in a direction, which depends on the zone of the cartilage where a chondrocyte is found. This makes the effects of small mosaic manipulations harder to detect, which is why our polarity disruptions failed to pass the significance threshold. Finally, testing such subtle effects on neighboring cells requires tracking of individual chondrocytes next to the disrupted zone. Such tracking requires time-lapsed live imaging, which we avoided because it could lead to CE defects. Additionally, tracking individual cells could be achieved by photoconverting the ablation zone, but this was beyond our technical capability because we lacked a technique to photoconvert in three dimensions, and because we were already using

GFP to image MTOCs. Therefore, we could not address this model with our technique. Despite this, our results do not contradict this model.

A final model for polarization across tissues involves upstream signaling gradients that either pattern graded expression of PCP components across tissues or modify PCP component asymmetrical subcellular distribution. The opposing graded expression of *Ds* and *Fj* promoted by Wingless (*Wg*) at the poles and notch signaling at the equator of the fruit fly eye, respectively, exemplifies how graded expression of PCP components across tissues leads to their asymmetrical subcellular distribution (Simon, 2004; Yang et al., 2002; Zeidler et al., 1999). Furthermore, although core PCP proteins promote polarization by their asymmetrical subcellular localization, studies into different isoforms of Prickle (*Pk*) suggest that asymmetrical subcellular localization of core PCP components likely results from their interpretation of an upstream signaling gradient, which is thought to be related to *Ft/Ds* activity (Olofsson et al., 2014; Sharp and Axelrod, 2016). Although *in situ* hybridizations do not show graded expression of *dchs2* across jaw cartilages (Le Pabic et al., 2014), it is possible that *dchs2* gradients are weak or temporal and *in situ* hybridizations are not sensitive enough to detect it. Though we could not directly test this model with our technique, our results do not rule it out.

Despite these limitations, we confirmed that average chondrocyte polarity in the dorsal half of the ch cartilage is biased towards the mid region (ventrally). Though we observed contiguous groups of chondrocytes that are polarized in the opposite direction at random positions, the average chondrocyte polarity bias is reproducible. One critical piece of evidence that we are missing is whether individual chondrocyte polarity is maintained between 54-72 hpf. One possibility is that all chondrocytes may be polarized

uniformly at first, but contiguous groups of chondrocytes may revert their polarity as cartilages matures. Though downregulation of critical PCP components in contiguous groups of chondrocytes as cartilages develop may cause randomization of chondrocyte polarity, this would not explain the coordinated polarity reversals that we observe. Alternatively, if polarity reversals appear as chondrocyte polarity is specified and subsequently maintained until 72 hpf, then long-range cell-to-cell polarity propagation across cartilages is unlikely because the polarity reversals found within zones of polarity bias would impede such propagation. Since *fat3*, *dchs2*, and *rerea* are required for chondrocyte polarization (Le Pabic et al., 2014), it is possible that weak *dchs2* and *fjx1* expression gradients may be sufficient to establish polarity bias in cartilage zones but insufficient to generate a uniform polarity field. In this context, an alternative interpretation for the observed polarity bias reduction upon laser ablation in the ch cartilage may be that removal of a subset of cells within the cartilage disrupts gradients of *dchs2* and/or *fjx1* expression in the cartilage, leading to increased polarity randomization at the ablation zone.

Alternatively, a polarizing signal downstream of *fat3* and *dchs2* could also propagate polarity bias in cartilages. The fact that transplantation of a few WT cells into either *fat3*, *dchs2*, or *rerea* deficient embryos can rescue chondrocyte stacking beyond cell-to-cell contacts provides evidence for this possibility in cartilages (Le Pabic et al., 2014). Though the effective range such a signal is unclear, local fluctuation of this signal acting downstream of *fat3* and *dchs2* may be sufficient to produce the polarity reversals we observed within the dorsal ch. One study shows that *Wnt5a* is asymmetrically expressed in developing murine phalanges. Furthermore, *Wnt5a* activates *Ror2*, which

phosphorylates *Vangl2* in a *Wnt5a* dose-dependent manner, allowing for asymmetrical subcellular localization of core PCP components. Finally, overexpressing *Wnt5a* disrupts the asymmetrical subcellular distribution of core PCP proteins. These observations led to a model where *Wnt5a* gradients direct asymmetrical subcellular localization of core PCP proteins in the developing mouse phalanges (Gao et al., 2011). Interestingly, *wnt5a* paralog *wnt5b*, which is required for jaw cartilage morphogenesis, is expressed in chondrocytes (Sisson et al., 2015). However, there is no evidence to suggest that *Wnt5a* acts downstream of *Ft/Ds* signaling. Additionally, functional disruption of several Wnts in *Drosophila* yield no PCP phenotypes (Chen et al., 2008; Lawrence et al., 2002), suggesting that Wnt ligand requirements for PCP may be vertebrate-specific.

Laser ablations possibly make cartilages thinner, not shorter

We thought that shortening the ch cartilage on one side by ablation would reveal that HZ initial locations are determined by long-range repressive signals such as Pthlh such that the location of the HZ would adapt to different cartilage lengths, unlike polarity which does not adapt in ablated cartilages. *In situ* hybridizations for *col10a1a* suggested this, but we failed to repeat it in live imaged embryos. One explanation is found in our ablations of dorsal ch cartilages. Despite measuring the same 10-cell row length of cartilage, we counted 190 cells in 4 WT embryos but only 116 cells in ablated embryos, suggesting that ablated cartilages were likely thinner on the ablated side, and that cartilages likely maintain their length over thickness when ablated. Because fixation and the subsequent treatments from the *in situ* hybridization process tend to shrink the

embryos, these results could be explained as an artifact caused by laser-induced changes to the ECM properties, causing wounded cartilages to shrink differently.

Additionally, the incongruence between the *in situ* hybridization and live imaging results could be attributed, at least in part, to differences in power output from the 2-photon laser units we used to ablate cartilages. In fact, the 2-photon laser unit we used to ablate *sox10:lyn-tdTomato;entpd5a:kaede* double transgenic cartilages had much lower power output than the one used for the *col10a1a in situ* hybridizations. Though we increased ablation time to compensate for lower power output, we cannot rule out that we ablated less cells in double transgenic embryos since we could not assess the total number of ablated cells. Because of these reasons, we are unable to draw meaningful conclusions from this part of the study.

CHAPTER VI

Conclusions

Understanding how negative feedback loops form in signaling systems that pattern tissues during embryogenesis is a fundamental goal in developmental biology. In RD systems, a negative feedback loop forms between two signals: an activator that induces its own expression and that of an inhibitory signal that has longer range than the activator. The establishment of left-right asymmetry by Nodal and Lefty is an example of a negative feedback loop where the orientation of the loop is determined by the initial expression of Nodal, the activator signal, and the longer range of Lefty, the inhibitory signal (Tabin, 2006). In GPs of developing bones, *Ihh* and *Pthlh* also form a negative feedback loop that controls the rate and direction of endochondral ossification. *Ihh*, which promotes hypertrophic differentiation, activates itself and *Pthlh*. In turn, *Pthlh* has a longer range and represses *Ihh* expression elsewhere (Kronenberg, 2003). However, how HZs, which control the direction of the loop, are initially established is unclear. In Chapter II, using the ceratohyal cartilage, a rod-like cartilage that initially ossifies in its mid-region much like the long bones found in mice and chicks, I show that the *Pthlh* zebrafish orthologue *pthlha* is expressed in the distal parts of the cartilage, and that this expression is required to restrict HZ formation to the mid-region. Misexpression of *pthlha* in the cartilage can disrupt this pattern and lead to HZ formation in ectopic locations. Together these results suggest that *Pthlh* signaling determines where HZs initially form, thereby controlling the direction of the *Ihh/Pthlh* negative feedback loop. In Chapter III, I showed that chondrocytes require mechanical force for hypertrophic differentiation and proliferation, depending on their location within the cartilage.

Together, these results suggest that the direction of a negative feedback loop can be determined by the initial source of the inhibitory signal, unlike Nodal and Lefty in left-right asymmetry. In addition, these results support a model where chondrocytes respond to mechanical force by becoming hypertrophic in locations within the cartilage where Pthlh signaling is low.

Pthlh signaling establishes the feedback mechanisms that control GPs

Prior to this work, *Pthlh* signaling was known to maintain GP homeostasis by restricting hypertrophy-inducing *Ihh* expression to the HZ in a negative feedback loop (Chung et al., 1998; Mak et al., 2008; Vortkamp et al., 1996; Weir et al., 1996). Whether *Pthlh* was required for the initial patterning of HZs in embryonic cartilages was unknown. My results suggest that *pthlha* expression domains on the distal ends of the cartilage determine the position of the developing HZ by restricting hypertrophic differentiation to the mid-region of the embryonic cartilage element (Chapter II). Furthermore, chondrocytes misexpressing *pthlha* inhibit bone collar formation as a function of the number of cells that express it and their proximity to the bone collar, suggesting that Pthlha protein forms a gradient (Chapter II). My work also demonstrates that *pthlha* misexpression can lead to HZs forming in different locations within the cartilage, suggesting that *Pthlh* signaling not only restricts HZ expansion, but that it also determines where HZs form within the cartilage. These observations agree with known functions for *Pthlh* in GPs, but differ from the results of previous manipulations of *Pthlh* signaling that failed to change the locations where HZs formed within cartilages (Chung et al., 1998; Weir et al., 1996). This discrepancy likely reflects both the larger size of mouse and chick cartilages compared with zebrafish and the preference of

chondrocytes to respond to mosaic *Pthlh* manipulations by proliferation. My results provide novel evidence to suggest that *Pthlh* is the early signal that determines the locations of *Ihh* expression domains within cartilages, thereby establishing both the future locations of GPs and the orientation of the *Pthlh/Ihh* negative feedback loop.

In addition, my studies suggest that the *Ihh/Pthlh* negative feedback loop is active very early in ossifying zebrafish cartilages. HZs produce *Ihh* to promote hypertrophic differentiation in adjacent chondrocytes and induce osteoblast formation in adjacent perichondrium (Felber et al., 2011; Mak et al., 2008; St-Jacques et al., 1999). I have shown that developing HZs expand along the length of the cartilage in *pthlha* mutants, suggesting that *Pthlh* signaling also restricts the size of HZs (Chapter II). Since *pthlha* expression encompasses most of the cartilage after HZ formation (Yan et al., 2012), and *Ihh* is known to induce *Pthlh* expression (Vortkamp et al., 1996), I propose that *Ihh* from developing HZs induces *pthlha* expression in adjacent perichondrium, thereby generating the *pthlha* expression pattern observed in ossifying cartilages (Yan et al., 2012). In turn, this *pthlha* source would restrict HZ expansion. If true, this suggests that a version of the *Ihh/Pthlh* negative feedback loop, which was found in chick GPs (Vortkamp et al., 1996), is likely active very early in zebrafish ossifying cartilages. Future studies are needed to test this by examining *pthlha* expression in the absence of *Ihh* signaling.

Finally, my results suggest that another feedback mechanism controlling proliferation in GPs is active very early in zebrafish ossifying cartilages. Increased hypertrophic differentiation in HZs induces *Runx2* expression in ossifying perichondrium (Eames et al., 2011). This leads to *Fgf18* upregulation in the perichondrium adjacent to

the PZ, which in turn represses chondrocyte proliferation. This reduces the rate of PZ expansion, thereby reducing the number of PCs transitioning into the HZ (Hinoi et al., 2006; Ohbayashi et al., 2002). I have shown that, in addition to HZ size, *pthlha* CRISPR mutants had severely decreased proliferation rates. Hence, it is possible that the *Fgf18/Runx2* feedback mechanism is active in early zebrafish ossifying cartilages. Future studies are needed to test this by examining *Fgf18* expression in *pthlha* mutants.

Integration of Pthlh signaling and mechanical force

Mechanotransduction has been shown to be required in differentiating chondrocytes, but a role in direct regulation of chondrocyte hypertrophy is unknown. Muscle contraction is required for normal chondrocyte proliferation in the PZ (Germiller and Goldstein, 1997), and *Trpv4* mechanosensory channel activity is required for *Sox9* expression in chondrocytes (Nilius et al., 2004). Previous studies have suggested that mechanical force promotes hypertrophic differentiation (Hu and Albertson, 2017; Saitoh et al., 2000), but this could be an indirect effect of changes in chondrocyte proliferation. My results show that mechanical force is required for HZ development in the embryonic cartilages of zebrafish, and that this occurs at the same time *Pthlh* patterns HZs (Chapter III). How are these two signals, force and Pthlh, integrated during HZ development? One clue may be found in the way chondrocytes respond to mechanical force depending on their position within the cartilage. While HZs develop in the mid-region of the ceratohyal (ch) cartilage, my studies show that the bulk of chondrocyte proliferation occurs outside of developing HZs (Chapter III). Since *pthlha* expression domains located in the distal edges of the cartilage are responsible for restricting HZs to the mid region (Chapter II), it is possible that *Pthlh* signaling modulates chondrocyte

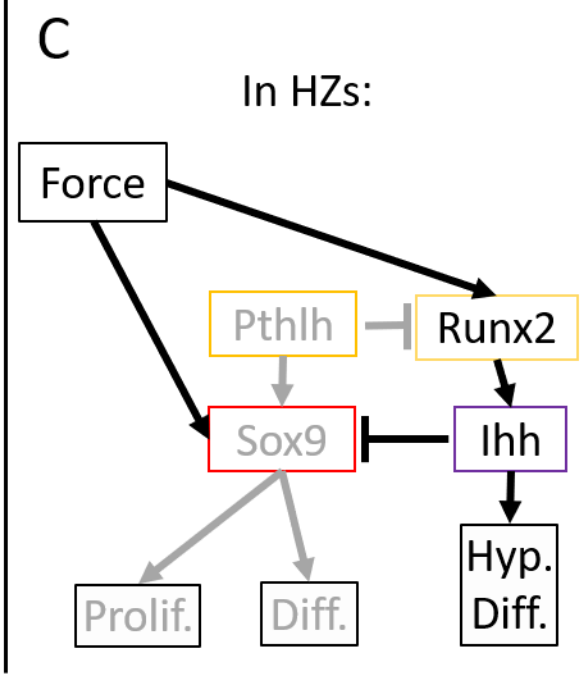
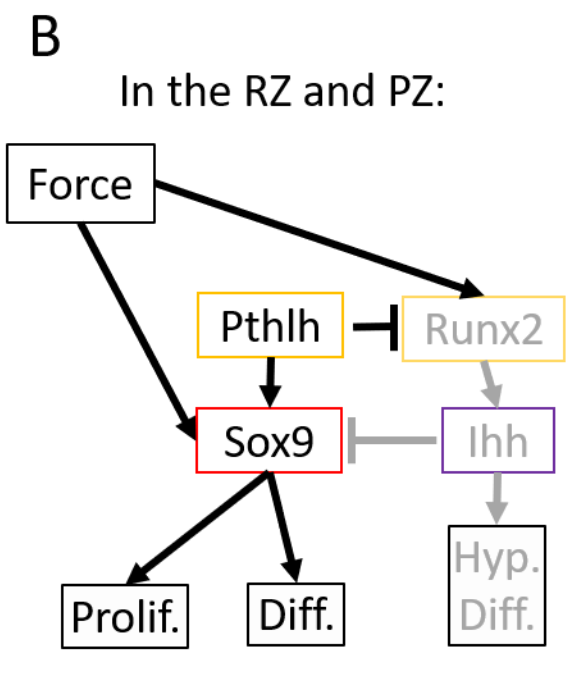
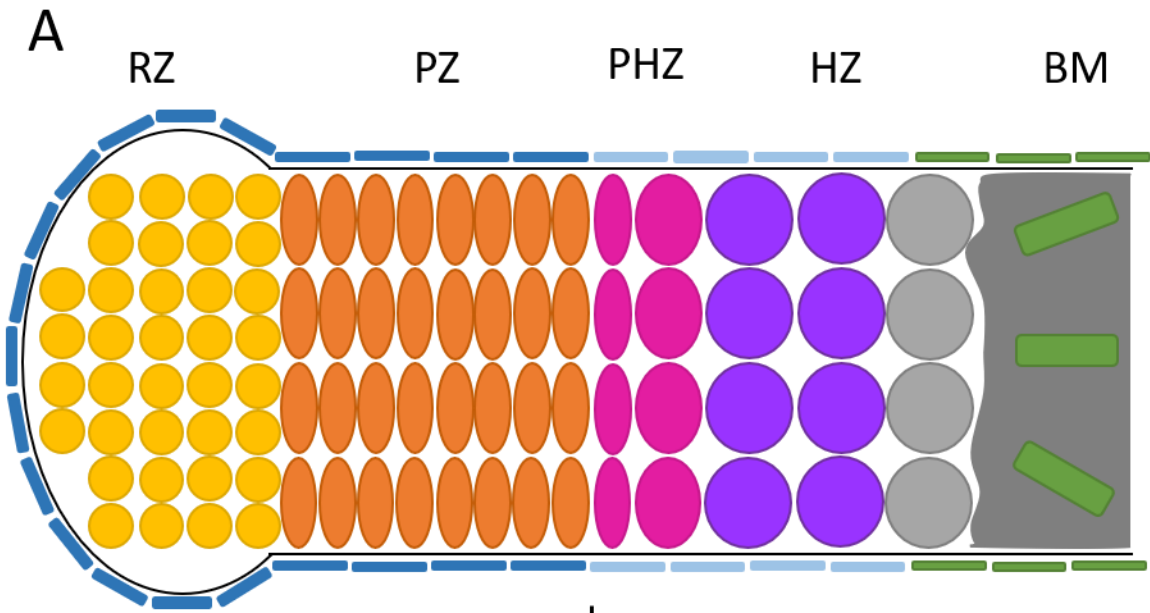


Figure 6.1: Model for the integration of mechanical force and Pthlh signaling in GPs. (A) Representation of a mammalian GP depicting the resting zone (RZ), proliferation zone (PZ), pre-hypertrophic zone (PHZ), hypertrophic zone (HZ), and bone marrow (BM). (B, C) In my model, mechanical force can promote chondrocyte hypertrophy through *Runx2* and *Ihh* and maintain differentiating chondrocytes and their proliferation through *Sox9*. (B) In the RZ and PZ, which are made of differentiating chondrocytes, Pthlh signaling represses *Runx2* expression, blocking the pathway for mechanical force to promote hypertrophy. (C) In contrast, in the HZ, Pthlh signaling is too low. This leads to upregulation of *Ihh*, which represses *Sox9* expression, thereby blocking the pathway for mechanical force to maintain differentiating chondrocytes and their proliferation.

responses to mechanotransduction (Figure 6.1). For instance, chondrocytes under the influence of *Pthlh* are unable to express *Runx2* or *Ihh* (Li et al., 2004; Yoshida et al., 2004). Hence, mechanotransduction maintains differentiating chondrocytes via upregulation of *Sox9* at these locations (Bi et al., 1999; Muramatsu et al., 2007) (Figure 6.1B). In contrast, chondrocytes outside the influence of *Pthlh* may respond to mechanotransduction by upregulating *Runx2* through an unknown mechanism (Figure 6.1C). Future studies are needed to test this model, such as determining if *Runx2* and/or *Ihh* in developing HZs respond to mechanical force. In addition, if this model is correct, paralysis should prevent HZ formation even in absence of *Pthlh* signaling. In conclusion, mechanotransduction induces HZ development, and *Pthlh* restricts their locations.

Could *Pthlh* signaling contribute to tendon attachment zone formation?

Using mosaic *crabp2bL:eGFP-Ntr* transgenic embryos that mark the perichondrium, my work has shown that the tenogenic marker *scxa:mCherry* is expressed in the perichondrium of musculoskeletal attachment zones, or entheses. This *scxa:mCherry* expression is restricted to perichondrial cells that are not ossifying. In fact, *scxa:mCherry* is expressed in most of the palatoquadrate (pq) cartilage perichondrium, except in the zone next to the mandibular joint (Chapter IV), which is where the pq begins ossifying (Brinkley et al., 2016). Studies in mouse long bones have shown that entheses form from cells on the edge of the cartilage co-expressing *Scx* and *Sox9*, and that loss of *Sox9* expression prevents enthesis formation (Blitz et al., 2013). Furthermore, Fibroblast Growth Factor 2 (*Fgf2*) expression in the mouse jaw condyle is required for *Scx* expression in cells of the same region (Roberts et al., 2019). In turn,

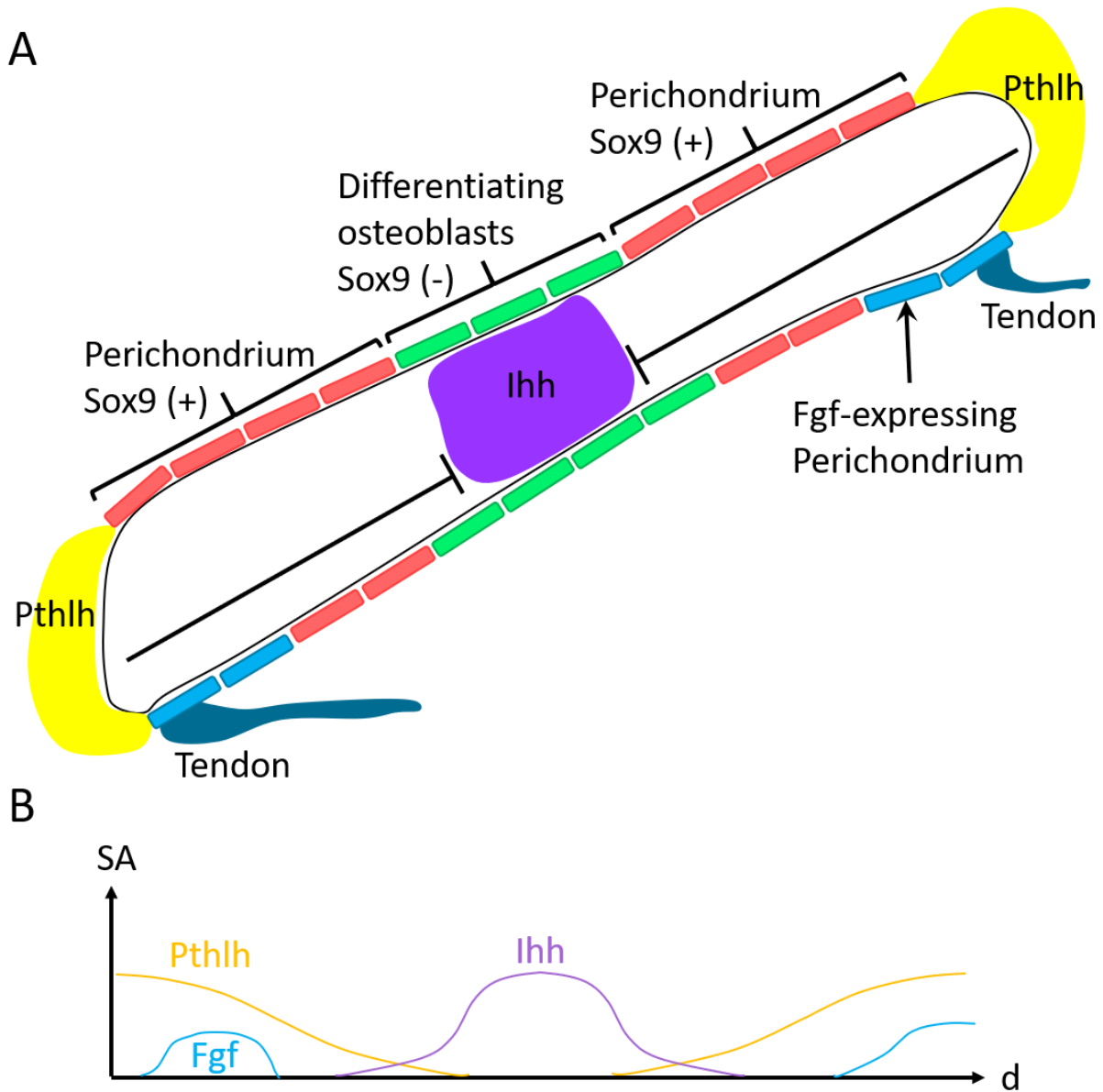


Figure 6.2: Tentative model for the formation of tendon attachment zones in developing cartilages. (A) Representation of a zebrafish ch cartilage at the onset of endochondral ossification. Briefly, *Pthlh* is expressed at the distal ends of the cartilage, restricting HZ formation to the mid-region. *Ihh* from the forming HZ signals to adjacent perichondrium to begin differentiating into osteoblasts and repress *Sox9* (green). However, this activity is contained by a gradient of *Pthlh*, allowing perichondrial cells elsewhere to express *Sox9* (red). Concurrently, tendons attach to the perichondrium in discrete distal domains in the cartilage that express *Fgfs* (blue). (B) Representation of signaling activities (SA) along the length (d) of the ch cartilage. *Fgf* signaling domains occur in zones of high *Pthlh* and low *Ihh* signaling.

Scx activates *Bmp4* expression, which promotes *Sox9* expression in these cells (Blitz et al., 2013; Blitz et al., 2009). The mouse jaw condyle is analogous to the edge of the mouse long bone where *Scx/Sox9* double positive cells are found, suggesting that *Fgf2* plays a role in maintaining *Scx/Sox9* double positive cells at developing entheses. Incidentally, entheses form on the distal regions of the ch cartilage (Subramanian et al., 2018), which is where *pthlha* expression is detected (Chapter II). Whether or not *Fgfs* play a similar role in zebrafish entheses has not been determined, but there appears to be a correlation between *pthlha* expression and entheses formation domains in the ch cartilage. Since osteoblast formation in the perichondrium requires *Sox9* repression by *Ihh* from the HZ (Hojo et al., 2013; Leung et al., 2011), it is possible that *Pthlh* signaling protects *Sox9* expression by repressing hedgehog signaling in the perichondrium where entheses form (Figure 6.2). However no evidence for a potential *Pthlh* role in entheses formation has been previously found, likely because *Pthlh* mutations are postnatally lethal, so tendon attachments in *Pthlh* deficiency models have never been examined (Karaplis et al., 1994; Schipani et al., 1997). Future studies examining *scxa:mCherry* in *pthlha* CRISPR F0 mutants are needed to test if *Pthlh* signaling plays a role in entheses formation.

Could dorsal-ventral (D-V) jaw patterning influence endochondral ossification?

One big question in developmental biology is how early patterning events lead to segmentation and compartmentalization of the embryo. In the introduction, I discussed the possibility that D-V patterning of the craniofacial cartilages results in the formation of expression domains of *Pthlh* that pattern the formation of HZs in endochondral bones. My work confirms that *Pthlh* expression domains are necessary and sufficient to pattern

HZs in embryonic cartilages. Though there is no evidence to connect *Pthlh* expression domains to earlier patterning events in the craniofacial skeleton, my work contributes to a growing body of evidence that indicates that early patterning events during embryogenesis can influence the outcome of later events via subcompartmentalization of previously specified domains in various systems.

One such system is the patterning of connective tissues in the limb. The Homeobox (*Hox*) genes are a group of very conserved genes that pattern the anterior-posterior axis of embryos ranging from insects to humans. During the evolution of species, these set of genes duplicated to generate four *Hox* clusters in mammals: *HoxA*, *HoxB*, *HoxC*, and *HoxD*, each containing up to 13 genes. Within a cluster, genes are expressed along the anterior-posterior axis in roughly the same order as their locations in the cluster from 3' to 5', such that *Hox1* genes pattern the most anterior part of the embryo and *Hox13* genes pattern the posterior part of the embryo (Wellik, 2007). In contrast, vertebrate limbs are patterned by the most 5' *Hox* genes in the cluster (*Hox 9-13*). The limb can be subdivided into the proximal stylopod, which corresponds to the humerus and femur, the medial zeugopod, which corresponds to the radius/ulna and tibia/fibula, and the distal autopod, which corresponds to hand and foot bones. Their segmental information is required prior to differentiation of any tissues in the limb. *Hoxa9* and *Hoxd9* contribute to patterning of the proximal joint of the stylopod (Fromental-Ramain et al., 1996a). *Hoxa10*, *Hoxc10*, and *Hoxd10* are all required for the formation of the stylopod (Wellik and Capecchi, 2003). *Hoxa11*, *Hoxc11*, and *Hoxd11* are required for zeugopod formation (Boulet and Capecchi, 2004; Wellik and Capecchi, 2003). Finally, *Hoxa13* and *Hoxd13* are required for proper patterning of the autopod

(Fromental-Ramain et al., 1996b). Interestingly, the expression of Hox11 genes is maintained in the zeugopod as limb skeletal tissues differentiate but becomes restricted to the perichondrium and mesenchymal precursors of connective tissues of the limb. Loss of Hox11 gene function lead to myotendinous junction patterning defects without disrupting cartilage-tendon junctions, highlighting how subdomains within a segment of the limb require the function of genes that specify whole segment identity (Swinehart et al., 2013). Since *Fgf2* expression domains are required to specify cartilage-tendon junction progenitors in the perichondrium of the developing mouse jaw, one potential mechanism for the specification of tendon attachment zones may be that genes such as Hox11 become progressively restricted and define domains of morphogen expression that are required to specify cell types that will make tendon attachment zones. Although these findings require much more investigation, they hint towards a model where perichondrial and mesenchymal progenitors contain subsegmental information to encode tendon attachment zones.

The formation of vertebral segments represents another example of perichondrial and mesenchymal tissues carrying pre-patterned segmental information. Segmentation of the axial skeleton of vertebrates relies on an oscillatory mechanism whereby the timing of Notch signaling turning on and off as it moves along the anterior-posterior axis determines somite boundaries (Saga and Takeda, 2001). Manipulations that accelerate this clock generate more somites, and correspondingly increase the number of vertebrae (Harima et al., 2013). In contrast, manipulations that decrease the clock speed generate fewer vertebrae (Schroter and Oates, 2010). A recent report revealed that the axial skeleton segmentation clock is not required for segmental patterning of the

notochord. Though it does not identify the signals that produce this pattern, the study proposes a reaction-diffusion model where the interplay between inhibitory and activator signals form Turing waves across the notochord to define the positions for each vertebra, and that the information to produce these waves is pre-patterned in the notochord sheath cells (Lleras Forero et al., 2018). Interestingly, the *pthlha* expression pattern I have shown in the ch cartilage appears to be, at least partially, in the perichondrium and surrounding tissues, prompting the question of whether the cartilage perichondrium plays a similar role by determining the zones where *pthlha* is expressed, thereby patterning hypertrophic differentiation of chondrocytes.

Finally, a model for subcompartmentalization of the zebrafish jaw cartilages emerges when considering all previous examples of pre-patterning. For instance, my work confirms that chondrocyte polarity (see Chapter V), which depends on the graded expression of certain components known to control PCP in *Drosophila* (Ambegaonkar et al., 2012; Simon, 2004; Strutt and Strutt, 2008; Yang et al., 2002; Zeidler et al., 1999), correlates with zones of endochondral ossification. Since I have shown that *pthlha* determines zones of ossification in cartilage, this correlation could reflect subcompartmentalization of the dorsal, intermediate, and ventral domains such that morphogens required to pattern the expression of PCP components as well as *pthlha* are expressed from specific subcompartments. For instance, Dlx genes, which define the intermediate domain of PAs, are initially expressed in a broad transitional ventral-intermediate domain, but their expression becomes restricted to the intermediate domain as *Hand2* expression activates in the ventral part of the this broad domain due to Dlx gene network activity and BMP signaling (Alexander et al., 2011; Barron et al.,

2011; Meinecke et al., 2018; Talbot et al., 2010; Zuniga et al., 2011; Zuniga et al., 2010). However, whether this transcriptional cascade results in subcompartmentalized expression of downstream transcription factors later in development has not been addressed. Therefore, the presence of such subcompartments is currently speculative.

Future studies tracing cells in the PAs are needed to investigate the potential role of D-V patterning in the specification of *pthlha* expression domains in the craniofacial cartilages. Given the complexity of this process and the time gap with endochondral ossification, identifying specific genes that may play a role in the formation of *pthlha* expression domains will be challenging. However, it is possible to permanently label individual cells in the PAs and trace them to cartilages that are beginning to ossify. The permanent labelling of NCCs has been done previously (Rodrigues et al., 2012). Using this technique in combination with the generation of mosaic transgenic embryos via NCC transplantation, as done recently in our lab (Le Pabic et al., 2014), would allow us to trace individual groups of cells in the PAs to their final position in endochondral cartilages and their surrounding mesenchyme. With this information, we can then identify subsets of cells in the PAs that eventually express *pthlha* around cartilages with the goal of determining their gene expression signatures and testing requirements for genes and in establishing endochondral patterns and *pthlha* expression.

Could some aspects of the *lhh*/*Pthlh* negative feedback loop fit the RD model?

In the introduction, we briefly discussed the RD Model, which differs from classic Morphogen gradient models in that RD models include negative feedback mechanisms that allow systems to form patterns while regulating themselves. In particular, the formation of a Turing pattern relies on two signals, one activator and one inhibitor,

where the activator induces its own expression and that of the inhibitor, which has longer range and represses the expression of the activator (Gierer and Meinhardt, 1972; Turing, 1990). The *Ihh/Pthlh* negative feedback loop is not often understood as fitting the RD model. However, mosaic mice with *Pth1r*^{-/-} mutant cells embedded in the PZ of their GPs have longer PZ, presumably due to induction of *Pthlh* expression around the *Pth1r*^{-/-} mutant cells (Chung et al., 1998). In this case, it is likely that a secondary *Pthlh* gradient is formed from the mutant cells. This resembles the interactions between *Nodal* and *Lefty* in the specification of left-right asymmetry of the vertebrate body axis, which fits the RD Model (Muller et al., 2012). Since expression of the *Pthlh* zebrafish orthologue *pthlha* appears to be initially restricted in the ch cartilage primordium but becomes more widespread as endochondral ossification proceeds (Yan et al., 2012), I speculate that *Ihh* from the developing HZ in the ch may induce *pthlha* expression around it in order to prevent premature expansion of the HZ during the early stages of endochondral ossification (See Figure 1.6). Though other models are possible, my results in Chapter II hint that this is the case in the forming GP. First, the HZ expands very rapidly along the cartilage in *pthlha* mutants. When considering that mosaic expression of *pthlha* in the cartilage only disrupts HZ or bone collar formation when the cells expressing it are in relative close proximity, this would support the hypothesis that *pthlha* expression in the distal edges of the ch cartilage is insufficient to contain this expansion, and that the additional induction of *pthlha* expression near the HZ by *Ihh* may be a requirement, hence the change in *pthlha* expression pattern at 6 days (Yan et al., 2012). Even if the interactions between *Ihh* and *Pthlh* in the GP, a stage in which ossification patterning has already occurred, do not fit the RD Model, if my hypothesis

could be confirmed, it would suggest that *Ihh* and *Pthlh* interact via RD during to pattern the early HZ domains in the cartilage, thereby shaping where GPs will form. Finally, unlike the case of Nodal and Lefty in the specification of left-right asymmetry in vertebrates where the shape of the system is determined by the initial expression of Nodal, the activator (Tabin, 2006), my proposed model for the early patterning of HZs in cartilage represents a system where expression of the repressor precedes that of the activator and determines the shape and direction of the system. Altogether, this work establishes endochondral ossification of the early zebrafish jaw cartilage as a useful model for understanding the general principles of formation of negative feedback loops, and their establishment in signaling networks. Thus, it has broad implications for the control mechanisms underlying pattern formation in many different tissues and organs.

REFERENCES

- Aday, A.W., Zhu, L.J., Lakshmanan, A., Wang, J., Lawson, N.D., 2011. Identification of cis regulatory features in the embryonic zebrafish genome through large-scale profiling of H3K4me1 and H3K4me3 binding sites. *Developmental biology* 357, 450-462.
- Adler, P.N., Krasnow, R.E., Liu, J., 1997. Tissue polarity points from cells that have higher Frizzled levels towards cells that have lower Frizzled levels. *Curr Biol* 7, 940-949.
- Afzal, A.R., Rajab, A., Fenske, C.D., Oldridge, M., Elanko, N., Ternes-Pereira, E., Tuysuz, B., Murday, V.A., Patton, M.A., Wilkie, A.O., Jeffery, S., 2000. Recessive Robinow syndrome, allelic to dominant brachydactyly type B, is caused by mutation of ROR2. *Nat Genet* 25, 419-422.
- Aguirre, J.I., Plotkin, L.I., Stewart, S.A., Weinstein, R.S., Parfitt, A.M., Manolagas, S.C., Bellido, T., 2006. Osteocyte apoptosis is induced by weightlessness in mice and precedes osteoclast recruitment and bone loss. *J Bone Miner Res* 21, 605-615.
- Akiyama, H., Lyons, J.P., Mori-Akiyama, Y., Yang, X., Zhang, R., Zhang, Z., Deng, J.M., Taketo, M.M., Nakamura, T., Behringer, R.R., McCrea, P.D., de Crombrughe, B., 2004. Interactions between Sox9 and beta-catenin control chondrocyte differentiation. *Genes & development* 18, 1072-1087.
- Ala-Kokko, L., Baldwin, C.T., Moskowitz, R.W., Prockop, D.J., 1990. Single base mutation in the type II procollagen gene (COL2A1) as a cause of primary osteoarthritis associated with a mild chondrodysplasia. *Proc Natl Acad Sci U S A* 87, 6565-6568.
- Alexander, C., Zuniga, E., Blitz, I.L., Wada, N., Le Pabic, P., Javidan, Y., Zhang, T., Cho, K.W., Crump, J.G., Schilling, T.F., 2011. Combinatorial roles for BMPs and Endothelin 1 in patterning the dorsal-ventral axis of the craniofacial skeleton. *Development* 138, 5135-5146.
- Alvarez, J., Sohn, P., Zeng, X., Doetschman, T., Robbins, D.J., Serra, R., 2002. TGFbeta2 mediates the effects of hedgehog on hypertrophic differentiation and PTHrP expression. *Development* 129, 1913-1924.
- Ambegaonkar, A.A., Pan, G., Mani, M., Feng, Y., Irvine, K.D., 2012. Propagation of Dachsous-Fat planar cell polarity. *Curr Biol* 22, 1302-1308.
- Andrade, A.C., Nilsson, O., Barnes, K.M., Baron, J., 2007. Wnt gene expression in the post-natal growth plate: regulation with chondrocyte differentiation. *Bone* 40, 1361-1369.
- Avaron, F., Hoffman, L., Guay, D., Akimenko, M.A., 2006. Characterization of two new zebrafish members of the hedgehog family: atypical expression of a zebrafish indian hedgehog gene in skeletal elements of both endochondral and dermal origins. *Developmental dynamics : an official publication of the American Association of Anatomists* 235, 478-489.
- Axelrod, J.D., 2001. Unipolar membrane association of Dishevelled mediates Frizzled planar cell polarity signaling. *Genes & development* 15, 1182-1187.
- Bairati, A., Comazzi, M., Gioria, M., 1996. An ultrastructural study of the perichondrium in cartilages of the chick embryo. *Anat Embryol (Berl)* 194, 155-167.
- Bandyopadhyay, A., Kubilus, J.K., Crochiere, M.L., Linsenmayer, T.F., Tabin, C.J., 2008. Identification of unique molecular subdomains in the perichondrium and periosteum and their role in regulating gene expression in the underlying chondrocytes. *Developmental biology* 321, 162-174.
- Barbieri, O., Astigiano, S., Morini, M., Tavella, S., Schito, A., Corsi, A., Di Martino, D., Bianco, P., Cancedda, R., Garofalo, S., 2003. Depletion of cartilage collagen fibrils in mice carrying a dominant negative Col2a1 transgene affects chondrocyte differentiation. *Am J Physiol Cell Physiol* 285, C1504-1512.
- Barron, F., Woods, C., Kuhn, K., Bishop, J., Howard, M.J., Clouthier, D.E., 2011. Downregulation of Dlx5 and Dlx6 expression by Hand2 is essential for initiation of tongue morphogenesis. *Development* 138, 2249-2259.

Bastida, M.F., Sheth, R., Ros, M.A., 2009. A BMP-Shh negative-feedback loop restricts Shh expression during limb development. *Development* 136, 3779-3789.

Bell, D.M., Leung, K.K., Wheatley, S.C., Ng, L.J., Zhou, S., Ling, K.W., Sham, M.H., Koopman, P., Tam, P.P., Cheah, K.S., 1997. SOX9 directly regulates the type-II collagen gene. *Nat Genet* 16, 174-178.

Bi, W., Deng, J.M., Zhang, Z., Behringer, R.R., de Crombrughe, B., 1999. Sox9 is required for cartilage formation. *Nat Genet* 22, 85-89.

Bi, W., Huang, W., Whitworth, D.J., Deng, J.M., Zhang, Z., Behringer, R.R., de Crombrughe, B., 2001. Haploinsufficiency of Sox9 results in defective cartilage primordia and premature skeletal mineralization. *Proc Natl Acad Sci U S A* 98, 6698-6703.

Bijakowski, C., Vadon-Le Goff, S., Delolme, F., Bourhis, J.M., Lecorche, P., Ruggiero, F., Becker-Pauly, C., Yiallourou, I., Stocker, W., Dive, V., Hulmes, D.J., Moali, C., 2012. Sizzled is unique among secreted frizzled-related proteins for its ability to specifically inhibit bone morphogenetic protein-1 (BMP-1)/tolloid-like proteinases. *J Biol Chem* 287, 33581-33593.

Blitz, E., Sharir, A., Akiyama, H., Zelzer, E., 2013. Tendon-bone attachment unit is formed modularly by a distinct pool of Scx- and Sox9-positive progenitors. *Development* 140, 2680-2690.

Blitz, E., Viukov, S., Sharir, A., Shwartz, Y., Galloway, J.L., Pryce, B.A., Johnson, R.L., Tabin, C.J., Schweitzer, R., Zelzer, E., 2009. Bone ridge patterning during musculoskeletal assembly is mediated through SCX regulation of Bmp4 at the tendon-skeleton junction. *Dev Cell* 17, 861-873.

Bosveld, F., Bonnet, I., Guirao, B., Tlili, S., Wang, Z., Pétalot, A., Marchand, R., Bardet, P.L., Marcq, P., Graner, F., Bellaiche, Y., 2012. Mechanical control of morphogenesis by Fat/Dachsous/Four-jointed planar cell polarity pathway. *Science* 336, 724-727.

Boulet, A.M., Capecchi, M.R., 2004. Multiple roles of Hoxa11 and Hoxd11 in the formation of the mammalian forelimb zeugopod. *Development* 131, 299-309.

Brinkley, J.F., Fisher, S., Harris, M.P., Holmes, G., Hooper, J.E., Jabs, E.W., Jones, K.L., Kesselman, C., Klein, O.D., Maas, R.L., Marazita, M.L., Selleri, L., Spritz, R.A., van Bakel, H., Visel, A., Williams, T.J., Wysocka, J., FaceBase, C., Chai, Y., 2016. The FaceBase Consortium: a comprehensive resource for craniofacial researchers. *Development* 143, 2677-2688.

Brittle, A., Thomas, C., Strutt, D., 2012. Planar polarity specification through asymmetric subcellular localization of Fat and Dachsous. *Curr Biol* 22, 907-914.

Buckland, R.A., Collinson, J.M., Graham, E., Davidson, D.R., Hill, R.E., 1998. Antagonistic effects of FGF4 on BMP induction of apoptosis and chondrogenesis in the chick limb bud. *Mechanisms of development* 71, 143-150.

Buxton, P., Edwards, C., Archer, C.W., Francis-West, P., 2001. Growth/differentiation factor-5 (GDF-5) and skeletal development. *J Bone Joint Surg Am* 83-A Suppl 1, S23-30.

Cai, A.Q., Radtke, K., Linville, A., Lander, A.D., Nie, Q., Schilling, T.F., 2012. Cellular retinoic acid-binding proteins are essential for hindbrain patterning and signal robustness in zebrafish. *Development* 139, 2150-2155.

Chan, D., Cole, W.G., Chow, C.W., Mundlos, S., Bateman, J.F., 1995. A COL2A1 mutation in achondrogenesis type II results in the replacement of type II collagen by type I and III collagens in cartilage. *J Biol Chem* 270, 1747-1753.

Chen, H., Capellini, T.D., Schoor, M., Mortlock, D.P., Reddi, A.H., Kingsley, D.M., 2016. Heads, Shoulders, Elbows, Knees, and Toes: Modular Gdf5 Enhancers Control Different Joints in the Vertebrate Skeleton. *PLoS genetics* 12, e1006454.

Chen, W.S., Antic, D., Matis, M., Logan, C.Y., Povelones, M., Anderson, G.A., Nusse, R., Axelrod, J.D., 2008. Asymmetric homotypic interactions of the atypical cadherin flamingo mediate intercellular polarity signaling. *Cell* 133, 1093-1105.

Cheung, M., Briscoe, J., 2003. Neural crest development is regulated by the transcription factor Sox9. *Development* 130, 5681-5693.

Chung, U.I., Lanske, B., Lee, K., Li, E., Kronenberg, H., 1998. The parathyroid hormone/parathyroid hormone-related peptide receptor coordinates endochondral bone development by directly controlling chondrocyte differentiation. *Proc Natl Acad Sci U S A* 95, 13030-13035.

Chung, U.I., Schipani, E., McMahon, A.P., Kronenberg, H.M., 2001. Indian hedgehog couples chondrogenesis to osteogenesis in endochondral bone development. *The Journal of clinical investigation* 107, 295-304.

Clouthier, D.E., Garcia, E., Schilling, T.F., 2010. Regulation of facial morphogenesis by endothelin signaling: insights from mice and fish. *American journal of medical genetics. Part A* 152A, 2962-2973.

Clouthier, D.E., Hosoda, K., Richardson, J.A., Williams, S.C., Yanagisawa, H., Kuwaki, T., Kumada, M., Hammer, R.E., Yanagisawa, M., 1998. Cranial and cardiac neural crest defects in endothelin-A receptor-deficient mice. *Development* 125, 813-824.

Collavin, L., Kirschner, M.W., 2003. The secreted Frizzled-related protein Sizzled functions as a negative feedback regulator of extreme ventral mesoderm. *Development* 130, 805-816.

Curado, S., Stainier, D.Y., Anderson, R.M., 2008. Nitroreductase-mediated cell/tissue ablation in zebrafish: a spatially and temporally controlled ablation method with applications in developmental and regeneration studies. *Nature protocols* 3, 948-954.

Dale, R.M., Topczewski, J., 2011. Identification of an evolutionarily conserved regulatory element of the zebrafish *col2a1a* gene. *Developmental biology* 357, 518-531.

Das, G., Jenny, A., Klein, T.J., Eaton, S., Mlodzik, M., 2004. Diego interacts with Prickle and Strabismus/Van Gogh to localize planar cell polarity complexes. *Development* 131, 4467-4476.

Davey, C.F., Moens, C.B., 2017. Planar cell polarity in moving cells: think globally, act locally. *Development* 144, 187-200.

De Robertis, E.M., 2006. Spemann's organizer and self-regulation in amphibian embryos. *Nat Rev Mol Cell Biol* 7, 296-302.

De Robertis, E.M., Kuroda, H., 2004. Dorsal-ventral patterning and neural induction in *Xenopus* embryos. *Annual review of cell and developmental biology* 20, 285-308.

Dentice, M., Bandyopadhyay, A., Gereben, B., Callebaut, I., Christoffolete, M.A., Kim, B.W., Nissim, S., Moron, J.P., Zavacki, A.M., Zeold, A., Capelo, L.P., Curcio-Morelli, C., Ribeiro, R., Harney, J.W., Tabin, C.J., Bianco, A.C., 2005. The Hedgehog-inducible ubiquitin ligase subunit WSB-1 modulates thyroid hormone activation and PTHrP secretion in the developing growth plate. *Nat Cell Biol* 7, 698-705.

Dranow, D.B., Hu, K., Bird, A.M., Lawry, S.T., Adams, M.T., Sanchez, A., Amatruda, J.F., Draper, B.W., 2016. Bmp15 Is an Oocyte-Produced Signal Required for Maintenance of the Adult Female Sexual Phenotype in Zebrafish. *PLoS genetics* 12, e1006323.

Eames, B.F., Yan, Y.L., Swartz, M.E., Levic, D.S., Knapik, E.W., Postlethwait, J.H., Kimmel, C.B., 2011. Mutations in *fam20b* and *xylt1* reveal that cartilage matrix controls timing of endochondral ossification by inhibiting chondrocyte maturation. *PLoS genetics* 7, e1002246.

Fanto, M., Clayton, L., Meredith, J., Hardiman, K., Charroux, B., Kerridge, S., McNeill, H., 2003. The tumor-suppressor and cell adhesion molecule Fat controls planar polarity via physical interactions with Atrophin, a transcriptional co-repressor. *Development* 130, 763-774.

Feiguin, F., Hannus, M., Mlodzik, M., Eaton, S., 2001. The ankyrin repeat protein Diego mediates Frizzled-dependent planar polarization. *Dev Cell* 1, 93-101.

Felber, K., Croucher, P., Roehl, H.H., 2011. Hedgehog signalling is required for perichondral osteoblast differentiation in zebrafish. *Mechanisms of development* 128, 141-152.

Fisher, S., Grice, E.A., Vinton, R.M., Bessling, S.L., McCallion, A.S., 2006. Conservation of RET regulatory function from human to zebrafish without sequence similarity. *Science* 312, 276-279.

Foster, J.W., Dominguez-Steglich, M.A., Guioli, S., Kwok, C., Weller, P.A., Stevanovic, M., Weissenbach, J., Mansour, S., Young, I.D., Goodfellow, P.N., et al., 1994. Campomelic dysplasia and autosomal sex reversal caused by mutations in an SRY-related gene. *Nature* 372, 525-530.

Francis-West, P.H., Abdelfattah, A., Chen, P., Allen, C., Parish, J., Ladher, R., Allen, S., MacPherson, S., Luyten, F.P., Archer, C.W., 1999. Mechanisms of GDF-5 action during skeletal development. *Development* 126, 1305-1315.

Fromental-Ramain, C., Warot, X., Lakkaraju, S., Favier, B., Haack, H., Birling, C., Dierich, A., Dollé, P., Chambon, P., 1996a. Specific and redundant functions of the paralogous *Hoxa-9* and *Hoxd-9* genes in forelimb and axial skeleton patterning. *Development* 122, 461-472.

Fromental-Ramain, C., Warot, X., Messadecq, N., LeMeur, M., Dollé, P., Chambon, P., 1996b. *Hoxa-13* and *Hoxd-13* play a crucial role in the patterning of the limb autopod. *Development* 122, 2997-3011.

Gao, B., Song, H., Bishop, K., Elliot, G., Garrett, L., English, M.A., Andre, P., Robinson, J., Sood, R., Minami, Y., Economides, A.N., Yang, Y., 2011. Wnt signaling gradients establish planar cell polarity by inducing Vangl2 phosphorylation through Ror2. *Dev Cell* 20, 163-176.

Garcia, S., Dirat, B., Tognacci, T., Rochet, N., Mouska, X., Bonnafous, S., Patouraux, S., Tran, A., Gual, P., Le Marchand-Brustel, Y., Gennero, I., Gouze, E., 2013. Postnatal soluble FGFR3 therapy rescues achondroplasia symptoms and restores bone growth in mice. *Science translational medicine* 5, 203ra124.

Gawantka, V., Delius, H., Hirschfeld, K., Blumenstock, C., Niehrs, C., 1995. Antagonizing the Spemann organizer: role of the homeobox gene *Xvent-1*. *EMBO J* 14, 6268-6279.

Gendron-Maguire, M., Mallo, M., Zhang, M., Gridley, T., 1993. *Hoxa-2* mutant mice exhibit homeotic transformation of skeletal elements derived from cranial neural crest. *Cell* 75, 1317-1331.

Germiller, J.A., Goldstein, S.A., 1997. Structure and function of embryonic growth plate in the absence of functioning skeletal muscle. *J Orthop Res* 15, 362-370.

Geurtzen, K., Knopf, F., Wehner, D., Huitema, L.F., Schulte-Merker, S., Weidinger, G., 2014. Mature osteoblasts dedifferentiate in response to traumatic bone injury in the zebrafish fin and skull. *Development* 141, 2225-2234.

Gibson, D.G., Young, L., Chuang, R.Y., Venter, J.C., Hutchison, C.A., 3rd, Smith, H.O., 2009. Enzymatic assembly of DNA molecules up to several hundred kilobases. *Nat Methods* 6, 343-345.

Gierer, A., Meinhardt, H., 1972. A theory of biological pattern formation. *Kybernetik* 12, 30-39.

Giovannone, D., Paul, S., Schindler, S., Arata, C., Farmer, D.T., Patel, P., Smeeton, J., Crump, J.G., 2019. Programmed conversion of hypertrophic chondrocytes into osteoblasts and marrow adipocytes within zebrafish bones. *eLife* 8.

Girkontaite, I., Frischholz, S., Lammi, P., Wagner, K., Swoboda, B., Aigner, T., Von der Mark, K., 1996. Immunolocalization of type X collagen in normal fetal and adult osteoarthritic cartilage with monoclonal antibodies. *Matrix biology : journal of the International Society for Matrix Biology* 15, 231-238.

Goodrich, L.V., Strutt, D., 2011. Principles of planar polarity in animal development. *Development* 138, 1877-1892.

Gudipaty, S.A., Lindblom, J., Loftus, P.D., Redd, M.J., Edes, K., Davey, C.F., Krishnegowda, V., Rosenblatt, J., 2017. Mechanical stretch triggers rapid epithelial cell division through Piezo1. *Nature* 543, 118-121.

Hall, B.K., Herring, S.W., 1990. Paralysis and growth of the musculoskeletal system in the embryonic chick. *J Morphol* 206, 45-56.

Hamada, H., 2015. Role of physical forces in embryonic development. *Semin Cell Dev Biol* 47-48, 88-91.

Hammond, C.L., Schulte-Merker, S., 2009. Two populations of endochondral osteoblasts with differential sensitivity to Hedgehog signalling. *Development* 136, 3991-4000.

Harima, Y., Takashima, Y., Ueda, Y., Ohtsuka, T., Kageyama, R., 2013. Accelerating the tempo of the segmentation clock by reducing the number of introns in the *Hes7* gene. *Cell reports* 3, 1-7.

Hatakeyama, Y., Tuan, R.S., Shum, L., 2004. Distinct functions of BMP4 and GDF5 in the regulation of chondrogenesis. *Journal of cellular biochemistry* 91, 1204-1217.

Hattori, T., Muller, C., Gebhard, S., Bauer, E., Pausch, F., Schlund, B., Bosl, M.R., Hess, A., Surmann-Schmitt, C., von der Mark, H., de Crombrughe, B., von der Mark, K., 2010. *SOX9* is a major negative

regulator of cartilage vascularization, bone marrow formation and endochondral ossification. *Development* 137, 901-911.

Healy, C., Uwanogho, D., Sharpe, P.T., 1999. Regulation and role of Sox9 in cartilage formation. *Developmental dynamics : an official publication of the American Association of Anatomists* 215, 69-78.

Heberlein, U., Wolff, T., Rubin, G.M., 1993. The TGF beta homolog dpp and the segment polarity gene hedgehog are required for propagation of a morphogenetic wave in the Drosophila retina. *Cell* 75, 913-926.

Hinoi, E., Bialek, P., Chen, Y.T., Rached, M.T., Groner, Y., Behringer, R.R., Ornitz, D.M., Karsenty, G., 2006. Runx2 inhibits chondrocyte proliferation and hypertrophy through its expression in the perichondrium. *Genes & development* 20, 2937-2942.

Hojo, H., Ohba, S., Taniguchi, K., Shirai, M., Yano, F., Saito, T., Ikeda, T., Nakajima, K., Komiyama, Y., Nakagata, N., Suzuki, K., Mishina, Y., Yamada, M., Konno, T., Takato, T., Kawaguchi, H., Kambara, H., Chung, U.I., 2013. Hedgehog-Gli activators direct osteo-chondrogenic function of bone morphogenetic protein toward osteogenesis in the perichondrium. *J Biol Chem* 288, 9924-9932.

Hosseini, A., Hogg, D.A., 1991. The Effects of Paralysis on Skeletal Development in the Chick-Embryo .2. Effects on Histogenesis of the Tibia. *Journal of anatomy* 177, 169-178.

Hu, Y., Albertson, R.C., 2017. Baby fish working out: an epigenetic source of adaptive variation in the cichlid jaw. *Proc Biol Sci* 284.

Huang, W., Chung, U.I., Kronenberg, H.M., de Crombrughe, B., 2001. The chondrogenic transcription factor Sox9 is a target of signaling by the parathyroid hormone-related peptide in the growth plate of endochondral bones. *Proc Natl Acad Sci U S A* 98, 160-165.

Huang, W., Zhou, X., Lefebvre, V., de Crombrughe, B., 2000. Phosphorylation of SOX9 by cyclic AMP-dependent protein kinase A enhances SOX9's ability to transactivate a Col2a1 chondrocyte-specific enhancer. *Mol Cell Biol* 20, 4149-4158.

Huebner, R.J., Wallingford, J.B., 2018. Coming to Consensus: A Unifying Model Emerges for Convergent Extension. *Dev Cell* 46, 389-396.

Huitema, L.F., Apschner, A., Logister, I., Spoorendonk, K.M., Bussmann, J., Hammond, C.L., Schulte-Merker, S., 2012. Entpd5 is essential for skeletal mineralization and regulates phosphate homeostasis in zebrafish. *Proc Natl Acad Sci U S A* 109, 21372-21377.

Hunter, M.P., Prince, V.E., 2002. Zebrafish hox paralogue group 2 genes function redundantly as selector genes to pattern the second pharyngeal arch. *Developmental biology* 247, 367-389.

Jee, Y.H., Wang, J., Yue, S., Jennings, M., Clokie, S.J., Nilsson, O., Lui, J.C., Baron, J., 2018. mir-374-5p, mir-379-5p, and mir-503-5p Regulate Proliferation and Hypertrophic Differentiation of Growth Plate Chondrocytes in Male Rats. *Endocrinology* 159, 1469-1478.

Joly, J.S., Joly, C., Schulte-Merker, S., Boulekbache, H., Condamine, H., 1993. The ventral and posterior expression of the zebrafish homeobox gene eve1 is perturbed in dorsalized and mutant embryos. *Development* 119, 1261-1275.

Karaplis, A.C., Luz, A., Glowacki, J., Bronson, R.T., Tybulewicz, V.L., Kronenberg, H.M., Mulligan, R.C., 1994. Lethal skeletal dysplasia from targeted disruption of the parathyroid hormone-related peptide gene. *Genes & development* 8, 277-289.

Karp, S.J., Schipani, E., St-Jacques, B., Hunzelman, J., Kronenberg, H., McMahon, A.P., 2000. Indian hedgehog coordinates endochondral bone growth and morphogenesis via parathyroid hormone related-protein-dependent and -independent pathways. *Development* 127, 543-548.

Kawahara, A., Wilm, T., Solnica-Krezel, L., Dawid, I.B., 2000. Functional interaction of vega2 and gooseoid homeobox genes in zebrafish. *Genesis* 28, 58-67.

Kawakami, K., Shima, A., 1999. Identification of the Tol2 transposase of the medaka fish *Oryzias latipes* that catalyzes excision of a nonautonomous Tol2 element in zebrafish *Danio rerio*. *Gene* 240, 239-244.

Kempf, H., Linares, C., Corvol, P., Gasc, J.M., 1998. Pharmacological inactivation of the endothelin type A receptor in the early chick embryo: a model of mispatterning of the branchial arch derivatives. *Development* 125, 4931-4941.

Kent, J., Wheatley, S.C., Andrews, J.E., Sinclair, A.H., Koopman, P., 1996. A male-specific role for SOX9 in vertebrate sex determination. *Development* 122, 2813-2822.

Kimmel, C.B., Ballard, W.W., Kimmel, S.R., Ullmann, B., Schilling, T.F., 1995. Stages of embryonic development of the zebrafish. *Developmental dynamics : an official publication of the American Association of Anatomists* 203, 253-310.

Kimmel, C.B., Miller, C.T., Kruze, G., Ullmann, B., BreMiller, R.A., Larison, K.D., Snyder, H.C., 1998. The shaping of pharyngeal cartilages during early development of the zebrafish. *Developmental biology* 203, 245-263.

Kimmel, C.B., Ullmann, B., Walker, M., Miller, C.T., Crump, J.G., 2003. Endothelin 1-mediated regulation of pharyngeal bone development in zebrafish. *Development* 130, 1339-1351.

Korkko, J., Cohn, D.H., Ala-Kokko, L., Krakow, D., Prockop, D.J., 2000. Widely distributed mutations in the COL2A1 gene produce achondrogenesis type II/hypochondrogenesis. *American journal of medical genetics* 92, 95-100.

Kronenberg, H.M., 2003. Developmental regulation of the growth plate. *Nature* 423, 332-336.

Kwan, K.M., Fujimoto, E., Grabher, C., Mangum, B.D., Hardy, M.E., Campbell, D.S., Parant, J.M., Yost, H.J., Kanki, J.P., Chien, C.B., 2007. The Tol2kit: a multisite gateway-based construction kit for Tol2 transposon transgenesis constructs. *Developmental dynamics : an official publication of the American Association of Anatomists* 236, 3088-3099.

Laue, K., Janicke, M., Plaster, N., Sonntag, C., Hammerschmidt, M., 2008. Restriction of retinoic acid activity by Cyp26b1 is required for proper timing and patterning of osteogenesis during zebrafish development. *Development* 135, 3775-3787.

Lawrence, K.M., Jones, R.C., Jackson, T.R., Baylie, R.L., Abbott, B., Bruhn-Olszewska, B., Board, T.N., Locke, I.C., Richardson, S.M., Townsend, P.A., 2017. Chondroprotection by urocortin involves blockade of the mechanosensitive ion channel Piezo1. *Scientific reports* 7, 5147.

Lawrence, P.A., Casal, J., Struhl, G., 2002. Towards a model of the organisation of planar polarity and pattern in the *Drosophila* abdomen. *Development* 129, 2749-2760.

Le Douarin, N.M., 1980. The ontogeny of the neural crest in avian embryo chimaeras. *Nature* 286, 663-669.

Le Pabic, P., Ng, C., Schilling, T.F., 2014. Fat-Dachsous signaling coordinates cartilage differentiation and polarity during craniofacial development. *PLoS genetics* 10, e1004726.

LeClair, E.E., Mui, S.R., Huang, A., Topczewska, J.M., Topczewski, J., 2009. Craniofacial skeletal defects of adult zebrafish Glypican 4 (knypek) mutants. *Developmental dynamics : an official publication of the American Association of Anatomists* 238, 2550-2563.

Lee, H.X., Ambrosio, A.L., Reversade, B., De Robertis, E.M., 2006. Embryonic dorsal-ventral signaling: secreted frizzled-related proteins as inhibitors of tolloid proteinases. *Cell* 124, 147-159.

Lee, W., Leddy, H.A., Chen, Y., Lee, S.H., Zelenski, N.A., McNulty, A.L., Wu, J., Beicker, K.N., Coles, J., Zauscher, S., Grandl, J., Sachs, F., Guilak, F., Liedtke, W.B., 2014. Synergy between Piezo1 and Piezo2 channels confers high-strain mechanosensitivity to articular cartilage. *Proc Natl Acad Sci U S A* 111, E5114-5122.

Leung, V.Y., Gao, B., Leung, K.K., Melhado, I.G., Wynn, S.L., Au, T.Y., Dung, N.W., Lau, J.Y., Mak, A.C., Chan, D., Cheah, K.S., 2011. SOX9 governs differentiation stage-specific gene expression in growth plate chondrocytes via direct concomitant transactivation and repression. *PLoS genetics* 7, e1002356.

Li, T.F., Dong, Y., Ionescu, A.M., Rosier, R.N., Zuscik, M.J., Schwarz, E.M., O'Keefe, R.J., Drissi, H., 2004. Parathyroid hormone-related peptide (PTHrP) inhibits Runx2 expression through the PKA signaling pathway. *Exp Cell Res* 299, 128-136.

Liu, R.Z., Sharma, M.K., Sun, Q., Thisse, C., Thisse, B., Denovan-Wright, E.M., Wright, J.M., 2005a. Retention of the duplicated cellular retinoic acid-binding protein 1 genes (*crabp1a* and *crabp1b*) in the zebrafish genome by subfunctionalization of tissue-specific expression. *The FEBS journal* 272, 3561-3571.

Liu, W., Selever, J., Murali, D., Sun, X., Brugger, S.M., Ma, L., Schwartz, R.J., Maxson, R., Furuta, Y., Martin, J.F., 2005b. Threshold-specific requirements for *Bmp4* in mandibular development. *Developmental biology* 283, 282-293.

Liu, W., Selever, J., Wang, D., Lu, M.F., Moses, K.A., Schwartz, R.J., Martin, J.F., 2004. *Bmp4* signaling is required for outflow-tract septation and branchial-arch artery remodeling. *Proc Natl Acad Sci U S A* 101, 4489-4494.

Liu, Z., Xu, J., Colvin, J.S., Ornitz, D.M., 2002. Coordination of chondrogenesis and osteogenesis by fibroblast growth factor 18. *Genes & development* 16, 859-869.

Lleras Forero, L., Narayanan, R., Huitema, L.F., VanBergen, M., Apschner, A., Peterson-Maduro, J., Logister, I., Valentin, G., Morelli, L.G., Oates, A.C., Schulte-Merker, S., 2018. Segmentation of the zebrafish axial skeleton relies on notochord sheath cells and not on the segmentation clock. *eLife* 7.

Long, F., Zhang, X.M., Karp, S., Yang, Y., McMahon, A.P., 2001. Genetic manipulation of hedgehog signaling in the endochondral skeleton reveals a direct role in the regulation of chondrocyte proliferation. *Development* 128, 5099-5108.

Lopez-Baez, J.C., Simpson, D.J., L, L.L.F., Zeng, Z., Brunson, H., Salzano, A., Brombin, A., Wyatt, C., Rybski, W., Huitema, L.F.A., Dale, R.M., Kawakami, K., Englert, C., Chandra, T., Schulte-Merker, S., Hastie, N.D., Patton, E.E., 2018. *Wilms Tumor 1b* defines a wound-specific sheath cell subpopulation associated with notochord repair. *eLife* 7.

Mak, K.K., Kronenberg, H.M., Chuang, P.T., Mackem, S., Yang, Y., 2008. Indian hedgehog signals independently of PTHrP to promote chondrocyte hypertrophy. *Development* 135, 1947-1956.

Mao, Y., Tournier, A.L., Bates, P.A., Gale, J.E., Tapon, N., Thompson, B.J., 2011. Planar polarization of the atypical myosin *Dachs* orients cell divisions in *Drosophila*. *Genes & development* 25, 131-136.

Matakatsu, H., Blair, S.S., 2004. Interactions between *Fat* and *Dachsous* and the regulation of planar cell polarity in the *Drosophila* wing. *Development* 131, 3785-3794.

McGurk, P.D., Swartz, M.E., Chen, J.W., Galloway, J.L., Eberhart, J.K., 2017. In vivo zebrafish morphogenesis shows *Cyp26b1* promotes tendon condensation and musculoskeletal patterning in the embryonic jaw. *PLoS genetics* 13, e1007112.

Meinecke, L., Sharma, P.P., Du, H., Zhang, L., Nie, Q., Schilling, T.F., 2018. Modeling craniofacial development reveals spatiotemporal constraints on robust patterning of the mandibular arch. *PLoS Comput Biol* 14, e1006569.

Merino, R., Macias, D., Ganan, Y., Economides, A.N., Wang, X., Wu, Q., Stahl, N., Sampath, K.T., Varona, P., Hurle, J.M., 1999. Expression and function of *Gdf-5* during digit skeletogenesis in the embryonic chick leg bud. *Developmental biology* 206, 33-45.

Miller, C.T., Maves, L., Kimmel, C.B., 2004. *moz* regulates *Hox* expression and pharyngeal segmental identity in zebrafish. *Development* 131, 2443-2461.

Miller, C.T., Schilling, T.F., Lee, K., Parker, J., Kimmel, C.B., 2000. *sucker* encodes a zebrafish Endothelin-1 required for ventral pharyngeal arch development. *Development* 127, 3815-3828.

Minoux, M., Rijli, F.M., 2010. Molecular mechanisms of cranial neural crest cell migration and patterning in craniofacial development. *Development* 137, 2605-2621.

Mitchell, R.E., Huitema, L.F., Skinner, R.E., Brunt, L.H., Severn, C., Schulte-Merker, S., Hammond, C.L., 2013. New tools for studying osteoarthritis genetics in zebrafish. *Osteoarthritis Cartilage* 21, 269-278.

Monson-Orran, E., Adar, R., Feferman, T., Segev, O., Yaron, A., 2000. The transmembrane mutation G380R in fibroblast growth factor receptor 3 uncouples ligand-mediated receptor activation from down-regulation. *Mol Cell Biol* 20, 516-522.

Morais da Silva, S., Hacker, A., Harley, V., Goodfellow, P., Swain, A., Lovell-Badge, R., 1996. Sox9 expression during gonadal development implies a conserved role for the gene in testis differentiation in mammals and birds. *Nat Genet* 14, 62-68.

Mork, L., Crump, G., 2015. Zebrafish Craniofacial Development: A Window into Early Patterning. *Current topics in developmental biology* 115, 235-269.

Mosimann, C., Kaufman, C.K., Li, P., Pugach, E.K., Tamplin, O.J., Zon, L.I., 2011. Ubiquitous transgene expression and Cre-based recombination driven by the ubiquitin promoter in zebrafish. *Development* 138, 169-177.

Muller, P., Rogers, K.W., Jordan, B.M., Lee, J.S., Robson, D., Ramanathan, S., Schier, A.F., 2012. Differential diffusivity of Nodal and Lefty underlies a reaction-diffusion patterning system. *Science* 336, 721-724.

Muramatsu, S., Wakabayashi, M., Ohno, T., Amano, K., Ooishi, R., Sugahara, T., Shiojiri, S., Tashiro, K., Suzuki, Y., Nishimura, R., Kuhara, S., Sugano, S., Yoneda, T., Matsuda, A., 2007. Functional gene screening system identified TRPV4 as a regulator of chondrogenic differentiation. *J Biol Chem* 282, 32158-32167.

Myers, D.C., Sepich, D.S., Solnica-Krezel, L., 2002. Bmp activity gradient regulates convergent extension during zebrafish gastrulation. *Developmental biology* 243, 81-98.

Nakamura, T., Mine, N., Nakaguchi, E., Mochizuki, A., Yamamoto, M., Yashiro, K., Meno, C., Hamada, H., 2006. Generation of robust left-right asymmetry in the mouse embryo requires a self-enhancement and lateral-inhibition system. *Dev Cell* 11, 495-504.

Nakashima, K., Zhou, X., Kunkel, G., Zhang, Z., Deng, J.M., Behringer, R.R., de Crombrughe, B., 2002. The novel zinc finger-containing transcription factor osterix is required for osteoblast differentiation and bone formation. *Cell* 108, 17-29.

Ng, L.J., Wheatley, S., Muscat, G.E., Conway-Campbell, J., Bowles, J., Wright, E., Bell, D.M., Tam, P.P., Cheah, K.S., Koopman, P., 1997. SOX9 binds DNA, activates transcription, and coexpresses with type II collagen during chondrogenesis in the mouse. *Developmental biology* 183, 108-121.

Nilius, B., Vriens, J., Prenen, J., Droogmans, G., Voets, T., 2004. TRPV4 calcium entry channel: a paradigm for gating diversity. *Am J Physiol Cell Physiol* 286, C195-205.

Noble, B.S., Peet, N., Stevens, H.Y., Brabbs, A., Mosley, J.R., Reilly, G.C., Reeve, J., Skerry, T.M., Lanyon, L.E., 2003. Mechanical loading: biphasic osteocyte survival and targeting of osteoclasts for bone destruction in rat cortical bone. *Am J Physiol Cell Physiol* 284, C934-943.

Noden, D.M., 1988. Interactions and fates of avian craniofacial mesenchyme. *Development* 103 Suppl, 121-140.

Nonaka, S., Tanaka, Y., Okada, Y., Takeda, S., Harada, A., Kanai, Y., Kido, M., Hirokawa, N., 1998. Randomization of left-right asymmetry due to loss of nodal cilia generating leftward flow of extraembryonic fluid in mice lacking KIF3B motor protein. *Cell* 95, 829-837.

O'Connor, C.J., Leddy, H.A., Benefield, H.C., Liedtke, W.B., Guilak, F., 2014. TRPV4-mediated mechanotransduction regulates the metabolic response of chondrocytes to dynamic loading. *Proc Natl Acad Sci U S A* 111, 1316-1321.

Oberlander, S.A., Tuan, R.S., 1994. Expression and functional involvement of N-cadherin in embryonic limb chondrogenesis. *Development* 120, 177-187.

Ohbayashi, N., Shibayama, M., Kurotaki, Y., Imanishi, M., Fujimori, T., Itoh, N., Takada, S., 2002. FGF18 is required for normal cell proliferation and differentiation during osteogenesis and chondrogenesis. *Genes & development* 16, 870-879.

Oishi, I., Suzuki, H., Onishi, N., Takada, R., Kani, S., Ohkawara, B., Koshida, I., Suzuki, K., Yamada, G., Schwabe, G.C., Mundlos, S., Shibuya, H., Takada, S., Minami, Y., 2003. The receptor tyrosine kinase Ror2 is involved in non-canonical Wnt5a/JNK signalling pathway. *Genes to cells : devoted to molecular & cellular mechanisms* 8, 645-654.

Olofsson, J., Sharp, K.A., Matis, M., Cho, B., Axelrod, J.D., 2014. Prickle/spiny-legs isoforms control the polarity of the apical microtubule network in planar cell polarity. *Development* 141, 2866-2874.

Pathi, S., Rutenberg, J.B., Johnson, R.L., Vortkamp, A., 1999. Interaction of Ihh and BMP/Noggin signaling during cartilage differentiation. *Developmental biology* 209, 239-253.

Person, A.D., Beiraghi, S., Sieben, C.M., Hermanson, S., Neumann, A.N., Robu, M.E., Schleiffarth, J.R., Billington, C.J., Jr., van Bokhoven, H., Hoogeboom, J.M., Mazzeu, J.F., Petryk, A., Schimmenti, L.A., Brunner, H.G., Ekker, S.C., Lohr, J.L., 2010. WNT5A mutations in patients with autosomal dominant Robinow syndrome. *Developmental dynamics : an official publication of the American Association of Anatomists* 239, 327-337.

Piccolo, S., Sasai, Y., Lu, B., De Robertis, E.M., 1996. Dorsal-ventral patterning in *Xenopus*: inhibition of ventral signals by direct binding of chordin to BMP-4. *Cell* 86, 589-598.

Pizette, S., Niswander, L., 2000. BMPs are required at two steps of limb chondrogenesis: formation of prechondrogenic condensations and their differentiation into chondrocytes. *Developmental biology* 219, 237-249.

Ploper, D., Lee, H.X., De Robertis, E.M., 2011. Dorsal-ventral patterning: Crescent is a dorsally secreted Frizzled-related protein that competitively inhibits Tolloid proteases. *Developmental biology* 352, 317-328.

Plotkin, L.I., Mathov, I., Aguirre, J.I., Parfitt, A.M., Manolagas, S.C., Bellido, T., 2005. Mechanical stimulation prevents osteocyte apoptosis: requirement of integrins, Src kinases, and ERKs. *Am J Physiol Cell Physiol* 289, C633-643.

Qian, D., Jones, C., Rzadzinska, A., Mark, S., Zhang, X., Steel, K.P., Dai, X., Chen, P., 2007. Wnt5a functions in planar cell polarity regulation in mice. *Developmental biology* 306, 121-133.

Rauch, G.J., Lyons, D.A., I., M., Friedlander, B., Arana, N., Reyes, T., Talbot, W.S., 2003. Submission and Curation of Gene Expression Data, ZFIN Direct Data Submission.

Reed, N.P., Mortlock, D.P., 2010. Identification of a distant cis-regulatory element controlling pharyngeal arch-specific expression of zebrafish *gdf6a/radar*. *Developmental dynamics : an official publication of the American Association of Anatomists* 239, 1047-1060.

Riddle, R.D., Johnson, R.L., Laufer, E., Tabin, C., 1993. Sonic hedgehog mediates the polarizing activity of the ZPA. *Cell* 75, 1401-1416.

Rijli, F.M., Mark, M., Lakkaraju, S., Dierich, A., Dolle, P., Chambon, P., 1993. A homeotic transformation is generated in the rostral branchial region of the head by disruption of *Hoxa-2*, which acts as a selector gene. *Cell* 75, 1333-1349.

Roberts, R.R., Bobzin, L., Teng, C.S., Pal, D., Tuzon, C.T., Schweitzer, R., Merrill, A.E., 2019. FGF signaling patterns cell fate at the interface between tendon and bone. *Development* 146.

Rodrigues, F.S., Doughton, G., Yang, B., Kelsh, R.N., 2012. A novel transgenic line using the Cre-lox system to allow permanent lineage-labeling of the zebrafish neural crest. *Genesis* 50, 750-757.

Rousseau, F., Bonaventure, J., Legeai-Mallet, L., Pelet, A., Rozet, J.M., Maroteaux, P., Le Merrer, M., Munnich, A., 1994. Mutations in the gene encoding fibroblast growth factor receptor-3 in achondroplasia. *Nature* 371, 252-254.

Rubin, D.A., Juppner, H., 1999. Zebrafish express the common parathyroid hormone/parathyroid hormone-related peptide receptor (PTH1R) and a novel receptor (PTH3R) that is preferentially activated by mammalian and fugu fish parathyroid hormone-related peptide. *J Biol Chem* 274, 28185-28190.

Saga, Y., Takeda, H., 2001. The making of the somite: molecular events in vertebrate segmentation. *Nat Rev Genet* 2, 835-845.

Saijoh, Y., Adachi, H., Sakuma, R., Yeo, C.Y., Yashiro, K., Watanabe, M., Hashiguchi, H., Mochida, K., Ohishi, S., Kawabata, M., Miyazono, K., Whitman, M., Hamada, H., 2000. Left-right asymmetric expression of *lefty2* and *nodal* is induced by a signaling pathway that includes the transcription factor FAST2. *Mol Cell* 5, 35-47.

Saitoh, S., Takahashi, I., Mizoguchi, I., Sasano, Y., Kagayama, M., Mitani, H., 2000. Compressive force promotes chondrogenic differentiation and hypertrophy in midpalatal suture cartilage in growing rats. *Anat Rec* 260, 392-401.

Sakuma, R., Ohnishi Yi, Y., Meno, C., Fujii, H., Juan, H., Takeuchi, J., Ogura, T., Li, E., Miyazono, K., Hamada, H., 2002. Inhibition of Nodal signalling by Lefty mediated through interaction with common receptors and efficient diffusion. *Genes to cells : devoted to molecular & cellular mechanisms* 7, 401-412.

Sato, T., Kurihara, Y., Asai, R., Kawamura, Y., Tonami, K., Uchijima, Y., Heude, E., Ekker, M., Levi, G., Kurihara, H., 2008. An endothelin-1 switch specifies maxillomandibular identity. *Proc Natl Acad Sci U S A* 105, 18806-18811.

Scemama, J.L., Hunter, M., McCallum, J., Prince, V., Stellwag, E., 2002. Evolutionary divergence of vertebrate Hoxb2 expression patterns and transcriptional regulatory loci. *J Exp Zool* 294, 285-299.

Schilling, T.F., Kimmel, C.B., 1994. Segment and cell type lineage restrictions during pharyngeal arch development in the zebrafish embryo. *Development* 120, 483-494.

Schilling, T.F., Kimmel, C.B., 1997. Musculoskeletal patterning in the pharyngeal segments of the zebrafish embryo. *Development* 124, 2945-2960.

Schilling, T.F., Le Pabic, P., Hoffman, T.L., 2010. Using transgenic zebrafish (*Danio rerio*) to study development of the craniofacial skeleton. *Journal of Applied Ichthyology* 26, 183-186.

Schipani, E., Lanske, B., Hunzelman, J., Luz, A., Kovacs, C.S., Lee, K., Pirro, A., Kronenberg, H.M., Juppner, H., 1997. Targeted expression of constitutively active receptors for parathyroid hormone and parathyroid hormone-related peptide delays endochondral bone formation and rescues mice that lack parathyroid hormone-related peptide. *Proc Natl Acad Sci U S A* 94, 13689-13694.

Schroter, C., Oates, A.C., 2010. Segment number and axial identity in a segmentation clock period mutant. *Curr Biol* 20, 1254-1258.

Scott-Savage, P., Hall, B.K., 1980. Differentiative ability of the tibial periosteum for the embryonic chick. *Acta Anat (Basel)* 106, 129-140.

Servin-Vences, M.R., Moroni, M., Lewin, G.R., Poole, K., 2017. Direct measurement of TRPV4 and PIEZO1 activity reveals multiple mechanotransduction pathways in chondrocytes. *eLife* 6.

Sharma, M.K., Saxena, V., Liu, R.Z., Thisse, C., Thisse, B., Denovan-Wright, E.M., Wright, J.M., 2005. Differential expression of the duplicated cellular retinoic acid-binding protein 2 genes (*crabp2a* and *crabp2b*) during zebrafish embryonic development. *Gene expression patterns : GEP* 5, 371-379.

Sharma, P., McNeill, H., 2013. Regulation of long-range planar cell polarity by Fat-Dachsous signaling. *Development* 140, 3869-3881.

Sharp, K.A., Axelrod, J.D., 2016. Prickle isoforms control the direction of tissue polarity by microtubule independent and dependent mechanisms. *Biol Open* 5, 229-236.

Shimada, Y., Usui, T., Yanagawa, S., Takeichi, M., Uemura, T., 2001. Asymmetric colocalization of Flamingo, a seven-pass transmembrane cadherin, and Dishevelled in planar cell polarization. *Curr Biol* 11, 859-863.

Shwartz, Y., Farkas, Z., Stern, T., Aszodi, A., Zelzer, E., 2012. Muscle contraction controls skeletal morphogenesis through regulation of chondrocyte convergent extension. *Developmental biology* 370, 154-163.

Sienknecht, U.J., 2015. Current concepts of hair cell differentiation and planar cell polarity in inner ear sensory organs. *Cell and tissue research* 361, 25-32.

Simon, M.A., 2004. Planar cell polarity in the *Drosophila* eye is directed by graded Four-jointed and Dachsous expression. *Development* 131, 6175-6184.

Sisson, B.E., Dale, R.M., Mui, S.R., Topczewska, J.M., Topczewski, J., 2015. A role of glypican4 and *wnt5b* in chondrocyte stacking underlying craniofacial cartilage morphogenesis. *Mechanisms of development* 138 Pt 3, 279-290.

Spemann, H., Mangold, H., 1924. Induction of Embryonic Primordia by Implantation of Organizers from a Different Species. *Roux's Arch. Entw. Mech.* 100, 599-638.

St-Jacques, B., Hammerschmidt, M., McMahon, A.P., 1999. Indian hedgehog signaling regulates proliferation and differentiation of chondrocytes and is essential for bone formation. *Genes & development* 13, 2072-2086.

Stangroom, J., 2018. One-Way ANOVA Calculator.

Strutt, H., Mundy, J., Hofstra, K., Strutt, D., 2004. Cleavage and secretion is not required for Four-jointed function in *Drosophila* patterning. *Development* 131, 881-890.

Strutt, H., Strutt, D., 2008. Differential stability of flamingo protein complexes underlies the establishment of planar polarity. *Curr Biol* 18, 1555-1564.

Suarez-Bregua, P., Torres-Nunez, E., Saxena, A., Guerreiro, P., Braasch, I., Prober, D.A., Moran, P., Cerda-Reverter, J.M., Du, S.J., Adrio, F., Power, D.M., Canario, A.V., Postlethwait, J.H., Bronner, M.E., Canestro, C., Rotllant, J., 2017. Pth4, an ancient parathyroid hormone lost in eutherian mammals, reveals a new brain-to-bone signaling pathway. *FASEB J* 31, 569-583.

Subramanian, A., Kanzaki, L.F., Galloway, J.L., Schilling, T.F., 2018. Mechanical force regulates tendon extracellular matrix organization and tenocyte morphogenesis through TGFbeta signaling. *eLife* 7.

Suster, M.L., Abe, G., Schouw, A., Kawakami, K., 2011. Transposon-mediated BAC transgenesis in zebrafish. *Nature protocols* 6, 1998-2021.

Swinehart, I.T., Schlientz, A.J., Quintanilla, C.A., Mortlock, D.P., Wellik, D.M., 2013. Hox11 genes are required for regional patterning and integration of muscle, tendon and bone. *Development* 140, 4574-4582.

Tabin, C.J., 2006. The key to left-right asymmetry. *Cell* 127, 27-32.

Talbot, J.C., Johnson, S.L., Kimmel, C.B., 2010. hand2 and Dlx genes specify dorsal, intermediate and ventral domains within zebrafish pharyngeal arches. *Development* 137, 2507-2517.

Thijssen, V.L., Postel, R., Brandwijk, R.J., Dings, R.P., Nesmelova, I., Satijn, S., Verhofstad, N., Nakabeppu, Y., Baum, L.G., Bakkers, J., Mayo, K.H., Poirier, F., Griffioen, A.W., 2006. Galectin-1 is essential in tumor angiogenesis and is a target for antiangiogenesis therapy. *Proc Natl Acad Sci U S A* 103, 15975-15980.

Thisse, B., Pflumio, S., Fürthauer, M., Loppin, B., Heyer, V., Degraeve, A., Woehl, R., Lux, A., Steffan, T., Charbonnier, X. Q. and Thisse, C., 2001. Expression of the zebrafish genome during embryogenesis (NIH R01 RR15402), ZFIN Direct Data Submission.

Thisse, B., Thisse, C., 2004. Fast Release Clones: A High Throughput Expression Analysis, ZFIN Direct Data Submission.

Thisse, C., Thisse, B., Schilling, T.F., Postlethwait, J.H., 1993. Structure of the zebrafish snail1 gene and its expression in wild-type, spadetail and no tail mutant embryos. *Development* 119, 1203-1215.

Toro, S., Wegner, J., Muller, M., Westerfield, M., Varga, Z.M., 2009. Identification of differentially expressed genes in the zebrafish hypothalamic-pituitary axis. *Gene expression patterns : GEP* 9, 200-208.

Tsumaki, N., Nakase, T., Miyaji, T., Kakiuchi, M., Kimura, T., Ochi, T., Yoshikawa, H., 2002. Bone morphogenetic protein signals are required for cartilage formation and differently regulate joint development during skeletogenesis. *J Bone Miner Res* 17, 898-906.

Turing, A.M., 1990. The chemical basis of morphogenesis. 1953. *Bull Math Biol* 52, 153-197; discussion 119-152.

van Bokhoven, H., Celli, J., Kayserili, H., van Beusekom, E., Balci, S., Brussel, W., Skovby, F., Kerr, B., Percin, E.F., Akarsu, N., Brunner, H.G., 2000. Mutation of the gene encoding the ROR2 tyrosine kinase causes autosomal recessive Robinow syndrome. *Nat Genet* 25, 423-426.

Vissing, H., D'Alessio, M., Lee, B., Ramirez, F., Godfrey, M., Hollister, D.W., 1989. Glycine to serine substitution in the triple helical domain of pro-alpha 1 (II) collagen results in a lethal perinatal form of short-limbed dwarfism. *J Biol Chem* 264, 18265-18267.

Vortkamp, A., Lee, K., Lanske, B., Segre, G.V., Kronenberg, H.M., Tabin, C.J., 1996. Regulation of rate of cartilage differentiation by Indian hedgehog and PTH-related protein. *Science* 273, 613-622.

Wada, N., Javidan, Y., Nelson, S., Carney, T.J., Kelsh, R.N., Schilling, T.F., 2005. Hedgehog signaling is required for cranial neural crest morphogenesis and chondrogenesis at the midline in the zebrafish skull. *Development* 132, 3977-3988.

Wagner, T., Wirth, J., Meyer, J., Zabel, B., Held, M., Zimmer, J., Pasantes, J., Bricarelli, F.D., Keutel, J., Hustert, E., Wolf, U., Tommerup, N., Schempp, W., Scherer, G., 1994. Autosomal sex reversal and campomelic dysplasia are caused by mutations in and around the SRY-related gene SOX9. *Cell* 79, 1111-1120.

Walker, M.B., Kimmel, C.B., 2007. A two-color acid-free cartilage and bone stain for zebrafish larvae. *Biotech Histochem* 82, 23-28.

Wang, X., Mao, J.J., 2002. Accelerated chondrogenesis of the rabbit cranial base growth plate by oscillatory mechanical stimuli. *J Bone Miner Res* 17, 1843-1850.

Weir, E.C., Philbrick, W.M., Amling, M., Neff, L.A., Baron, R., Broadus, A.E., 1996. Targeted overexpression of parathyroid hormone-related peptide in chondrocytes causes chondrodysplasia and delayed endochondral bone formation. *Proc Natl Acad Sci U S A* 93, 10240-10245.

Weirauch, M.T., Hughes, T.R., 2010. Conserved expression without conserved regulatory sequence: the more things change, the more they stay the same. *Trends Genet* 26, 66-74.

Wellik, D.M., 2007. Hox patterning of the vertebrate axial skeleton. *Developmental dynamics : an official publication of the American Association of Anatomists* 236, 2454-2463.

Wellik, D.M., Capecchi, M.R., 2003. Hox10 and Hox11 genes are required to globally pattern the mammalian skeleton. *Science* 301, 363-367.

Westerfield, M., 2000. *The zebrafish book. A guide for the laboratory use of zebrafish (Danio rerio)*. 4th ed. Univ. of Oregon Press, Eugene, Institute of Neuroscience, University of Oregon, Eugene, OR 97403.

Widelitz, R.B., Jiang, T.X., Murray, B.A., Chuong, C.M., 1993. Adhesion molecules in skeletogenesis: II. Neural cell adhesion molecules mediate precartilaginous mesenchymal condensations and enhance chondrogenesis. *Journal of cellular physiology* 156, 399-411.

Wolpert, L., 1969. Positional information and the spatial pattern of cellular differentiation. *J Theor Biol* 25, 1-47.

Wolpert, L., Beddington, R., Jessell, T., Lawrence, P., Meyerowitz, E., Smith, J., 2006. *Principles of Development*, Third Edition ed. Oxford University Press, New York.

Wong, L.L., Adler, P.N., 1993. Tissue polarity genes of *Drosophila* regulate the subcellular location for prehair initiation in pupal wing cells. *J Cell Biol* 123, 209-221.

Wopat, S., Bagwell, J., Sumigray, K.D., Dickson, A.L., Huitema, L.F.A., Poss, K.D., Schulte-Merker, S., Bagnat, M., 2018. Spine Patterning Is Guided by Segmentation of the Notochord Sheath. *Cell reports* 22, 2026-2038.

Wu, J., Lewis, A.H., Grandl, J., 2017. Touch, Tension, and Transduction - The Function and Regulation of Piezo Ion Channels. *Trends Biochem Sci* 42, 57-71.

Wu, J., Mlodzik, M., 2008. The frizzled extracellular domain is a ligand for Van Gogh/Stbm during nonautonomous planar cell polarity signaling. *Dev Cell* 15, 462-469.

Wu, R.S., Lam, H., Clay, H., Duong, D.N., Deo, R.C., Coughlin, S.R., 2018. A Rapid Method for Directed Gene Knockout for Screening in G0 Zebrafish. *Dev Cell* 46, 112-125 e114.

Yan, Y.L., Bhattacharya, P., He, X.J., Ponugoti, B., Marquardt, B., Layman, J., Grunloh, M., Postlethwait, J.H., Rubin, D.A., 2012. Duplicated zebrafish co-orthologs of parathyroid hormone-related peptide (PTHrP, Pthlh) play different roles in craniofacial skeletogenesis. *J Endocrinol* 214, 421-435.

Yan, Y.L., Miller, C.T., Nissen, R.M., Singer, A., Liu, D., Kirn, A., Draper, B., Willoughby, J., Morcos, P.A., Amsterdam, A., Chung, B.C., Westerfield, M., Haffter, P., Hopkins, N., Kimmel, C., Postlethwait, J.H., 2002. A zebrafish *sox9* gene required for cartilage morphogenesis. *Development* 129, 5065-5079.

Yan, Y.L., Willoughby, J., Liu, D., Crump, J.G., Wilson, C., Miller, C.T., Singer, A., Kimmel, C., Westerfield, M., Postlethwait, J.H., 2005. A pair of Sox: distinct and overlapping functions of zebrafish sox9 co-orthologs in craniofacial and pectoral fin development. *Development* 132, 1069-1083.

Yang, C.H., Axelrod, J.D., Simon, M.A., 2002. Regulation of Frizzled by fat-like cadherins during planar polarity signaling in the *Drosophila* compound eye. *Cell* 108, 675-688.

Yoshida, C.A., Yamamoto, H., Fujita, T., Furuichi, T., Ito, K., Inoue, K., Yamana, K., Zanma, A., Takada, K., Ito, Y., Komori, T., 2004. Runx2 and Runx3 are essential for chondrocyte maturation, and Runx2 regulates limb growth through induction of Indian hedgehog. *Genes & development* 18, 952-963.

Yu, T., Graf, M., Renn, J., Scharf, M., Larionova, D., Huysseune, A., Witten, P.E., Winkler, C., 2017. A vertebrate-specific and essential role for osterix in osteogenesis revealed by gene knockout in the teleost medaka. *Development* 144, 265-271.

Yukata, K., Kanchiku, T., Egawa, H., Nakamura, M., Nishida, N., Hashimoto, T., Ogasa, H., Taguchi, T., Yasui, N., 2018. Continuous infusion of PTH1-34 delayed fracture healing in mice. *Scientific reports* 8, 13175.

Zeidler, M.P., Perrimon, N., Strutt, D.I., 1999. The four-jointed gene is required in the *Drosophila* eye for ommatidial polarity specification. *Curr Biol* 9, 1363-1372.

Zhang, Y., Liu, T., Meyer, C.A., Eeckhoute, J., Johnson, D.S., Bernstein, B.E., Nusbaum, C., Myers, R.M., Brown, M., Li, W., Liu, X.S., 2008. Model-based analysis of ChIP-Seq (MACS). *Genome Biol* 9, R137.

Zhao, Q., Eberspaecher, H., Lefebvre, V., De Crombrughe, B., 1997. Parallel expression of Sox9 and Col2a1 in cells undergoing chondrogenesis. *Developmental dynamics : an official publication of the American Association of Anatomists* 209, 377-386.

Zimmerman, L.B., De Jesus-Escobar, J.M., Harland, R.M., 1996. The Spemann organizer signal noggin binds and inactivates bone morphogenetic protein 4. *Cell* 86, 599-606.

Zuniga, E., Rippen, M., Alexander, C., Schilling, T.F., Crump, J.G., 2011. Gremlin 2 regulates distinct roles of BMP and Endothelin 1 signaling in dorsoventral patterning of the facial skeleton. *Development* 138, 5147-5156.

Zuniga, E., Stellabotte, F., Crump, J.G., 2010. Jagged-Notch signaling ensures dorsal skeletal identity in the vertebrate face. *Development* 137, 1843-1852.